



UNIVERSITY OF MALAGA

PhD THESIS

Photovoltaic Lifetime Forecast: Models for long-term  
photovoltaic degradation prediction and forecast

Ismail Kaaya

Málaga, February, 2020



UNIVERSIDAD  
DE MÁLAGA

AUTOR: Ismail Kaaya

 <https://orcid.org/0000-0003-4524-0975>

EDITA: Publicaciones y Divulgación Científica. Universidad de Málaga



Esta obra está bajo una licencia de Creative Commons Reconocimiento-NoComercial-SinObraDerivada 4.0 Internacional:

<http://creativecommons.org/licenses/by-nc-nd/4.0/legalcode>

Cualquier parte de esta obra se puede reproducir sin autorización pero con el reconocimiento y atribución de los autores.

No se puede hacer uso comercial de la obra y no se puede alterar, transformar o hacer obras derivadas.

Esta Tesis Doctoral está depositada en el Repositorio Institucional de la Universidad de Málaga (RIUMA): [riuma.uma.es](http://riuma.uma.es)



PhD THESIS

Photovoltaic Lifetime Forecast: Models for long-term  
photovoltaic degradation prediction and forecast

Author:

Ismail Kaaya

Supervisors:

Mariano Sidrach de Cardona Ortín

Karl-Anders Weiss

PhD program:

Mechanical Engineering and Energy Efficiency

PhD thesis presented in the SCHOOL OF INDUSTRIAL ENGINEERING  
of MALAGA UNIVERSITY to obtain the Doctor Degree

Director:

Mariano Sidrach de Cardona Ortín

Málaga, February, 2020



## DECLARACIÓN DE AUTORÍA Y ORIGINALIDAD DE LA TESIS PRESENTADA PARA OBTENER EL TÍTULO DE DOCTOR

D./Dña ISMAIL KAAYA

Estudiante del programa de doctorado INGENIERÍA MECÁNICA Y EFICIENCIA ENERGÉTICA de la Universidad de Málaga, autor/a de la tesis, presentada para la obtención del título de doctor por la Universidad de Málaga, titulada: PHOTOVOLTAIC LIFETIME FORECAST: MODELS FOR LONG-TERM PHOTOVOLTAIC DEGRADATION PREDICTION AND FORECAST

Realizada bajo la tutorización de MARIANO SIDRACH DE CARDONA ORTÍN Y KARL-ANDERS WEISS y dirección de MARIANO SIDRACH DE CARDONA ORTÍN (si tuviera varios directores deberá hacer constar el nombre de todos)

### DECLARO QUE:

La tesis presentada es una obra original que no infringe los derechos de propiedad intelectual ni los derechos de propiedad industrial u otros, conforme al ordenamiento jurídico vigente (Real Decreto Legislativo 1/1996, de 12 de abril, por el que se aprueba el texto refundido de la Ley de Propiedad Intelectual, regularizando, aclarando y armonizando las disposiciones legales vigentes sobre la materia), modificado por la Ley 2/2019, de 1 de marzo.

Igualmente asumo, ante a la Universidad de Málaga y ante cualquier otra instancia, la responsabilidad que pudiera derivarse en caso de plagio de contenidos en la tesis presentada, conforme al ordenamiento jurídico vigente.

En Málaga, a 1 de FEBRERO de 2020

Fdo.: ISMAIL KAAYA

Dr. Mariano Sidrach de Cardona Ortín, Professor in the Applied Physics department at the University of Málaga and Dr. Karl-Anders Weiss head of service life analysis in the Fraunhofer Institut of Solar Energy as Directors of the Doctoral Thesis: Photovoltaic Lifetime Forecast: Models for long-term photovoltaic degradation prediction and forecast, presented by Mr. Ismail Kaaya in the School of Industrial Engineering of the University of Málaga to obtain the Doctor Degree.

They state that this thesis is supported by the following research articles:

Paper 1. I. Kaaya, M. Koehl, A.P. Mehili, S. de Cardona Mariano, & K.A. Weiss, "Modeling Outdoor Service Lifetime Prediction of PV Modules: Effects of Combined Climatic Stressors on PV Module Power Degradation". IEEE Journal of Photovoltaics, vol. 9, no. 4, pp. 1105–1112, May. 2019.

This paper is reprinted from the Open Access publication available at <https://ieeexplore.ieee.org/document/8720037>. All rights remain with the authors and editors.

Impact factor: 3.398

Paper 2. S. Lindig, I. Kaaya, K.A. Weiss, D. Moser, and M. Topic, "Review of statistical and analytical degradation models for photovoltaic modules and systems as well as related improvements," IEEE J. Photovoltaic., vol. 8, no. 6, pp. 1773–1786, Nov. 2018.

This paper is reprinted from the Open Access publication available at <https://ieeexplore.ieee.org/document/8472886>. All rights remain with the authors and editors.

Impact factor: 3.398

Paper 3. J. A-Vásquez, I. Kaaya, K. Brecla, K-A. Weiss and M.Topic, "Global climate data processing and mapping of degradation mechanisms and degradation rates of PV modules". energies MDPI ,vol. 12, no. 4749 Dec 2019.

This paper is reprinted from the Open Access publication available at <https://www.mdpi.com/1996-1073/12/24/4749/htm>. All rights remain with the authors and editors. Impact factor: 2.707

We would like also to note that the thesis contains some work accepted for publication in the journal of progress in Photovoltaics: Research and application: Article title, Photovoltaic lifetime forecast model based on degradation patterns; DOI:10.1002/pip.3280.

Málaga, April, 2020

Signed:

Mariano Sidrach de Cardona Ortín

Karl-Anders Weiss

## Acknowledgements

The author has carried out a big part of the research reported in this thesis at Fraunhofer Institute of Solar Energy (ISE), Freiburg, Germany, in the research group Service Life Analysis and Material Characterization. This research has received funding from the European Unions Horizon 2020 research and innovation program under the Marie Skłodowska-Curie grant agreement No 721452-Project Solar-Train.

Firstly, I would like to thank both my research supervisors: Dr. Mariano Sidrach de Ortin of the University of Malaga and Dr. Karl-Anders Weiss of Fraunhofer ISE, for their insight and mentorship, and for creating a collaborative and congenial working atmosphere for me during the process of my research.

Secondly, I would like to acknowledge the different sources of data used in this research as: Fraunhofer Institute of solar energy for sharing the module data from Negev, Gran Canaria and Zugspitze as well as indoor test data, the Scuola universitaria professionale della Svizzera italiana (SUPSI) for sharing the TISO plant data, the Institute for Renewable Energy, EURAC Research for sharing the Bolzano system data and the Desert Knowledge Australia Solar Centre (DKA Solar Centre) for the continuous effort to provide free access photovoltaic systems data. These data sources are properly referenced in the notes and bibliography.

Special thanks go to Micheal Koehl of Fraunhofer ISE, Lindig Sascha and David Moser of EURAC Research, Julián Ascencio-Vásquez of University of Ljubljana and Alessandro Virtuani of École Polytechnique Fédérale de Lausanne (EPFL) for their fruitful discussions and collaboration during different stages of my research. I cannot forget to thank my wife Sophie Marchand of Fraunhofer ISE for her continuous support and encouragements throughout the entire research period. I could not have done it smoothly without you. I also thank my daddy Mr.Nsubuga Med and my siblings for their support in my entire academic career. Lastly I extend my gratitude to the entire Solar-Train project team for the wonderful discussions, training and informal meetings. It has been grateful to work with and learn from everyone, indeed, it has been a time of tremendous learning and growth for me both scientifically and personally.



# Resumen

A medida que la proporción de energía solar fotovoltaica en la producción de energía eléctrica mundial sigue aumentando, se vuelve cada vez más interesante e urgente, estudiar y evaluar cómo el rendimiento general de los sistemas fotovoltaicos y de los módulos fotovoltaicos, en particular disminuye con el tiempo. Esto no solo es importante por razones financieras, sino también técnicamente, porque es crucial comprender los efectos del clima local en la degradación del rendimiento de los módulos. Se han propuesto muchos métodos para evaluar las tasas de degradación de los módulos y sistemas fotovoltaicos a partir de datos de su rendimiento en exteriores. Sin embargo, la mayoría de estos métodos se basan en datos registrados a través de la vida útil de los módulos, lo que significa que las tasas de degradación se evalúan a partir de los datos de rendimiento monitoreados sin comprender ni las rutas de degradación ni las variables ambientales que influyen en este proceso. Por lo tanto, en la primera parte de esta investigación, se propone un modelo físico para determinar las tasas de degradación de los módulos fotovoltaicos basados en variables climáticas. A través de él, se cuantifica el impacto de las cargas climáticas combinadas en la potencia máxima generada por el módulo. Se supone que son necesarias tres reacciones precursoras de la degradación, a saber, hidrólisis, fotodegradación y degradación termomecánica, para la predicción de la vida útil. Para cada reacción, se propone un modelo cinético empírico y se valida con mediciones realizadas en interiores. Se propone un modelo generalizado para cuantificar los efectos de las cargas climáticas combinadas para aplicaciones en exteriores. El modelo generalizado se calibra y valida utilizando datos experimentales de tres módulos de silicio monocristalino idénticos instalados en tres climas distintos de evaluación comparativa: clima marítimo (Gran Canaria, España), clima árido (Negev, Israel) y clima alpino (Zugspitze, Alemania). Luego, el modelo se extiende para simular y mapear las tasas de degradación global y se identifican las áreas de riesgo. Para validar los modelos seleccionados o propuestos, se utilizan datos experimentales de pruebas de envejecimiento acelerado. De los tres modelos se deriva un modelo generalizado para cuantificar los efectos de las cargas climáticas combinadas para aplicaciones en exteriores. El modelo generalizado se calibra y valida utilizando datos experimentales al aire libre de tres módulos de silicio monocristalino idénticos instalados en tres climas de referencia: marítimo (Gran Canaria, España), árido (Negev, Israel) y alpino (Zugspitze, Alemania). Finalmente, utilizando la base de datos climática pública (ERA5), se procesan los datos climáticos para extraer los parámetros necesarios para el cálculo de la tasa de degradación. Estos parámetros se aplican luego para evaluar las tasas de degradación basadas en los tres mecanismos precursores y también para evaluar las tasas de degradación total. Por lo tanto, se proporcionan mapas de riesgo de degradación global basados en mecanismos precursores específicos, así como la tasa de degradación total. Creemos que estos mapas de riesgos son útiles para comprender los mecanismos dominantes de degradación de acuerdo con las ubicaciones geográficas y, por lo tanto, podrían usarse para desarrollar materiales fotovoltaicos dependiendo de las ubicaciones geográficas operativas. Otro desafío fundamental de los métodos disponibles

es su precisión cuando se necesitan pronósticos a largo plazo después de un corto tiempo de operación y con puntos de datos limitados. La segunda parte de esta investigación aborda este desafío en el que se propone un nuevo método basado en datos para mejorar la precisión de la predicción a largo plazo con un pequeño historial de degradación. El modelo depende de los patrones de degradación y se introduce un nuevo concepto de tasa de degradación dependiente del tiempo. El modelo ha sido calibrado y validado utilizando diferentes módulos fotovoltaicos y datos de sistemas con una exposición de campo entre 5 a 35 años. El nuevo modelo se compara con los métodos existentes basados en datos. El modelo propuesto redujo las incertidumbres de pronóstico a largo plazo cuando los pronósticos se hacen después de una pequeña degradación del rendimiento. A partir de estos resultados, se evalúan los efectos de la degradación a largo plazo en la predicción del rendimiento a lo largo de la vida del módulo. Se ha demostrado que utilizando el enfoque propuesto, las predicciones de rendimiento de por vida son más confiables debido a un pronóstico de degradación a largo plazo más preciso. Finalmente, los dos enfoques se combinan para formar un modelo híbrido basado tanto en los métodos físicos como en los basados en datos. De hecho, el modelo híbrido tenía como objetivo proporcionar un pronóstico de degradación a largo plazo más confiable, así como tener una comprensión física de los mecanismos de degradación dominantes que influyen en la degradación del rendimiento. Creemos que este modelo es útil para calcular el costo nivelado de energía más confiable y, por lo tanto, la viabilidad económica de la energía solar, así como para mejorar el desarrollo de nuevos materiales fotovoltaicos de acuerdo con las condiciones climáticas de funcionamiento.

# Abstract

As the share of photovoltaic keeps increasing in the global electricity mix, it becomes critical to assess how the overall system and module performance (power) decreases over time. This is not only important for financial reasons but also technically, because it is crucial to understand the effects of the local climate on the performance degradation. Although different models have been proposed to quantify the impact of climatic stresses on performance degradation based on indoor ageing tests, less has been done to quantify these effects in outdoor operations. The available methods for outdoor application are mainly data-driven, meaning that the performance losses are evaluated from monitored performance data without an understanding of the influencing environmental variables. Moreover, these models are suitable for performance loss rates and not for degradation rates evaluations.

Therefore, in the first part of this research, a physical model to determine the degradation rates of photovoltaic modules based on outdoor climatic variables is proposed. Through it, the impact of combined climatic loads on the module's maximum power output is quantified. In this approach, three degradation precursor mechanisms, namely, hydrolysis, photodegradation, and thermo-mechanical, are assumed to be necessary for service lifetime prediction. For each mechanism, an empirical model that describe well the physical/chemical kinetics is selected or proposed. To validate the selected or proposed models, experimental data from accelerated ageing tests are used. A generalized model to quantify the effects of combined climatic loads for outdoor applications is then derived from the three models. The generalized model is calibrated and validated using outdoor experimental data of three identical mono-crystalline silicon modules installed in three benchmarking climates: maritime (Gran Canaria, Spain), arid (Negev, Israel), and alpine (Zugspitze, Germany). Finally, using the public climate database (ERA5), climatic data is processed to extract the climatic stresses necessary for the calculation of the degradation rate. These stresses are then applied to evaluate the degradation rates based on the three precursor mechanisms and also to evaluate the total degradation rates. Therefore, global degradation risk maps based on specific precursor mechanisms as well as total degradation rate are provided. We believe that these risk maps are useful to understand the dominating degradation mechanisms according to geographical locations and hence could be used to develop photovoltaic materials depending on the operating geographical locations.

Other fundamental challenge of the available methods is their accuracy when long-term forecasts are needed after a short operation time and with limited data points. The second part of this research, addresses this challenge where a new data-driven method is proposed so as to improve the accuracy of long-term prediction with small degradation history. The model depends on the degradation patterns and a new concept of time dependent degradation rate is introduced. The model has been calibrated and validated using different

photovoltaic modules and systems data with 5 to 35 years of field exposure. The new model is benchmarked against existing data-driven methods. The proposed model lowered the long-term forecast uncertainties when forecasts are made after a small performance degradation. Through this, the effects of long-term degradation to lifetime yield prediction are assessed. It has been shown that using the proposed approach, the lifetime yield predictions are more reliable due to more accurate long-term degradation forecast.

Finally, the two approaches are combined to form a hybrid model based on both the physical and data-driven methods. Indeed, the hybrid model is aimed to provide more reliable long-term degradation forecast as well as having a physical understanding of the dominating degradation mechanisms influencing the performance degradation. We believe such a model is useful to calculate more reliable levelized cost of energy and thus the economic viability of solar energy as well as to improve the development of new PV materials according to the operating climatic conditions.

# Contents

Resumen	iii
Abstract	v
1 Introduction	1
2 Literature review	5
2.1 Photovoltaic degradation and degradation modes	5
2.2 Degradation models	6
2.3 A review of the available physical models	7
2.3.1 Degradation models for corrosion	8
2.3.2 Models for potential induced degradation	14
2.3.3 Models for ultraviolet irradiance degradation	16
2.3.4 Degradation models for delamination, fatigue solder failure and cell cracks	16
2.3.5 Physical models for combined degradation modes/stresses	17
2.4 Chapter Overview	19
3 Methodology	21
3.1 Methodology for the proposed physical model	22
3.1.1 Combined climatic stresses degradation rate model	22
3.1.2 Degradation indicator model	26
3.1.3 Experimental part	26
3.1.4 Global climate data processing	28
3.1.5 Statistical error analysis methods	31
3.2 Methodology for data-driven model	32
3.2.1 Background	32
3.2.2 Modelling assumptions	33
3.2.3 Modeling approach	35
3.2.4 Experimental	38
3.2.5 Statistical errors analysis	39
3.3 Methodology of a hybrid model	40
4 Results and Discussion	41
4.1 Results for the physical model	42
4.1.1 Properties of the proposed power degradation function	42
4.1.2 Calibration and validation of the specific degradation rate models	43
4.1.3 Calibration and validation of the combined degradation rate model	44
4.1.4 Degradation rates and lifetime prediction	45

4.1.5	Comparison of the proposed physical model with other physical model	46
4.1.6	Global degradation rates mapping: A global PV degradation risk analysis . . . . .	47
4.1.7	Uncertainties evaluation of the physical model . . . . .	50
4.2	Results for the data-driven model . . . . .	53
4.2.1	”Time and degradation pattern” dependent models as well as 3% degradation threshold . . . . .	53
4.2.2	Model calibration . . . . .	54
4.2.3	Validation . . . . .	55
4.2.4	Model application and comparison with statistical models . . . . .	56
4.2.5	Model limits and uncertainties . . . . .	59
4.2.6	Assessing the effects of PV modules long-term degradation on lifetime energy yield . . . . .	60
4.2.7	Simplified User Interface (PVLIFE Toolbox) . . . . .	62
4.3	Results for the hybrid model . . . . .	64
4.3.1	Application of the hybrid model . . . . .	64
5	Conclusion	65
	Appendix	77

# Chapter 1

## Introduction

PV modules as well as systems are affected by continuous cycles of temperature, humidity, irradiation, mechanical stress, and soiling. These environmental stresses cause different degradation modes that take place within a PV module and reduce the performance of the system. In order to accurately determine the degradation rates of PV modules and to understand the effects of the operating conditions, the evolution of power in real life operation must be monitored simultaneously with the local operating condition. However, this requires waiting a considerable amount of time and huge financial investments. In this case, two main approaches are currently used to mimic the outdoor degradation rates.

The first approach is using indoor accelerated ageing tests where modules are exposed to extreme controlled operating conditions in climatic chambers in order to degrade the modules within a short time. Although these tests are carried out based on the established International Electrotechnical Commission (IEC) standards [Wohlgemuth \(2012\)](#), an open question remains if they can really represent outdoor degradation.

The second approach is the utilization of mathematical models to determine the degradation rates in shorter periods and to predict the lifetime of PV modules. Two modelling techniques are commonly used; physical and data driven techniques. Physical models are developed to describe the link between the modules performance degradation to environmental variables [Bala Subramaniyan et al. \(2018\)](#). Data-driven techniques utilize monitored operational data related to system's performance to evaluate the degradation rate [Meyers et al. \(2019\)](#). The biggest challenge of mathematical models is the reliability of the predicted results [Jordan et al. \(2020\)](#). Usually, to valid degradation models, one needs to have enough degradation data available, which is not always the case.

On one hand, according to the state-of-the-art of degradation models, most physical models are developed for accelerated indoor ageing application. Physical models to quantify the effects of outdoor climatic stresses are very helpful to understand the correlation of the different local climates with the degradation processes. This understanding is useful to develop new materials based on the operation local climates. However, such models have received relatively little attention in the industry. According to our knowledge, it is of recent that, [Bala Subramaniyan et al. \(2018\)](#) proposed a model to link the module performance degradation to environmental variables for outdoor application. They applied their model to predict the degradation rates of a mono-crystalline silicon module in different climatic locations. However, since PV modules are characterized by numerous degradation modes [Köntges et al. \(2017\)](#) and that PV modules are of different technologies, further developments for a model that take into account multiple climatic factors are still needed. Moreover, degradation models are developed on basic assumptions as well as simplifica-

tions based on the available or known degradation patterns, this makes generalization of a given model a challenge. In this case, it is important to develop different models using different assumptions describing different degradation patterns. Therefore, in the first part of research, a new physical model to quantify the effects of combined climatic stresses is proposed as a contribution to this challenge.

The new model is based on the assumptions that, three major degradation mechanisms; hydrolysis, photo-degradation and thermo-mechanical degradation are necessary for lifetime prediction. Empirical models are proposed to describe the kinetics of these three mechanism and hence to calculate the degradation rates. Through accelerated ageing tests, these mechanisms are reproduced and hence the models are validated. A model to evaluate the impacts of the combined climatic stresses is then derived from the three mechanisms. The derived model is calibrated and validated using identical mono-crystalline silicon modules installed in three different climates: maritime (Gran Canaria, Spain), arid (Negev, Israel), and alpine (Zugspitze, Germany) using real monitored meteorological data. To extend the analysis on a global scale, global climate reanalysis data is used to extract the model's climatic input variables. The extracted variables are then applied to simulate maps of degradation rates based on specific degradation mechanisms as well as the total degradation rates.

On the other hand, data-driven techniques [Phinikarides et al. \(2014\)](#), [Meyers et al. \(2019\)](#) that utilize monitored operational data related to system's are commonly used especially to evaluate the degradation rates as well as the performance loss rates of PV systems in outdoor performance. Generally, in spite of the wide application and the recognized potential of the data-driven techniques, limitations still exist for their use in PV degradation analysis. The lack of a systematic and flexible approach to select parameters of these models and their black-box character limit their understanding. Moreover, data-driven techniques for lifetime forecast are based on fitting the available systems degradation data by regression models and then extrapolating the evolution up to the time of failure. However, in practice, the system's degradation history available may be short and incomplete, and a simple extrapolation may lead to large uncertainties. Also, one other serious challenge is the accuracy of the models when applied after a shorter time interval. Data-driven models usually require enough degradation history for their training. When applied to forecast long-term degradation using a short degradation history, they often provide unrealistic degradation scenarios. For example, Taylor and Letham [Taylor and Letham \(2018\)](#) performed a comparison of the forecasting accuracy of different statistical models at different time horizons. In their study, most models displayed large uncertainties when applied after shorter time interval. To address these challenges, a new data-driven model is proposed specifically for long-term degradation forecast. The proposed model is aimed at improving the long-term forecasting accuracy for a shorter operation time. To achieve this, time dependent degradation factors are assumed instead of a constant one. To further improve the accuracy, different degradation factor models are proposed based on the degradation patterns. Moreover, the model has been calibrated and validated using degradation data from different sources and of different PV technologies both on module and system level.

One other drawback of the data-driven methods is the lack of a correlation of the evaluated rates with the triggering degradation mechanisms. To solve this problem, we combine both the physical and the data-driven approaches proposed in this research into a hybrid model. The hybrid model will aid to have more reliable long-term degradation forecast as

well as having a physical understanding of the dominating degradation mechanisms influencing the performance degradation. We believe such a model is useful to calculate more reliable levelized cost of energy and thus the economic viability of solar energy as well as to improve the PV materials according to the operating conditions.

The structure of the thesis is as follows:

- Chapter 1. Introduction of the research, the novelty of the research work is introduced with regard to the start-of-the-art.
- Chapter 2. The available physical models are reviewed and Where possible a comparison of the performance of the different models is carried out using experimental data from indoor tests. At the end of the chapter the gaps for improvements are identified.
- Chapter 3. In this chapter, the methodologies of the proposed models are presented. The chapter contains three major sections corresponding to methodologies for a physical, data-driven and hybrid models respectively. In the first two sections, the experimental data used for model calibration and validation are also described.
- Chapter 4. Here, the results are presented and discussed in order of the sections in chapter 3.
- Chapter 5. Summarises the main conclusions of the research. The references follows the chapter and the annex with the copies of the published articles that supports the research are attached after the references.



# Chapter 2

## Literature review

Table 2.1: Chapter Nomenclatures

Symbols	
$E_a$	activation energy [eV]
$I$	Intensity
$I_{SC}$	short circuit current [A]
$k_B$	Boltzmann constant ( $8.62 \times 10^{-5}$ eV/K)
$P_{max}$	power at maximum power point [W]
$R_D$	degradation rate [%/hour]
$T_{max}$	maximum temperature [K]
$T_{min}$	minimum temperature [K]
$R_s$	Series resistance [ $\Omega$ ]
$R_{sh}$	Shunt resistance [ $\Omega$ ]
$U$	voltage [volt]
$\Delta T$	temperature cycles [K]
Abbreviations	
BoM	bill of materials
DH	damp heat
EVA	Vinyl-acetate monomers present in Ethylene-vinyl acetate
LID	light induced degradation
PID	potential induced degradation
PV	Photovoltaic
RH	relative humidity [%]
RMSE	root means square error
t	time
T	temperature [K]
TOW	Time of wetness
UV	Ultraviolet [ $W/m^2$ ]

### 2.1 Photovoltaic degradation and degradation modes

Photovoltaic degradation is the reduction in efficiency with which a PV module/system converts sunlight into electricity [Jordan and Kurtz \(2013\)](#). Degradation modes are effects that irreversibly degrade the performance of a PV module or of a system and cloud cause

safety problems [Köntges et al. \(2017\)](#). A great number of different degradation modes are observed in PV modules, both under outdoor operation and also using indoor accelerated ageing testing. The most commonly observed degradation modes include [Köntges et al. \(2017\)](#): LID, solder fatigue failure, silver grid finger delamination, bypass diode failure, delamination, cell cracks, corrosion, polymeric discoloration, UV degradation of the cell, polymeric mechanical failure, and PID. Each of these degradation modes has different causes and is triggered by various stress factors.

Apart from the modes listed, different technical risks, which affect the PV performance and the resulting costs, were found by [Moser et al. \(2017\)](#) as: glass breakage, snail track, defective backsheet, hotspot, soiling, overheating, and junction box failure. An occurring degradation mode can have an increasing impact on the PV performance over time. It can develop in isolation as well as in combination with other degradation modes or technical risks and might lead to the failure of a PV module. However, despite the definitions above, a clear understanding of the definition of a degradation mode is also still a challenge and stress should be put on common nomenclature to define a degradation mode with the same terminology.

## 2.2 Degradation models

In general terms, degradation models are used to relate a test item's estimated failure time with the wear and tear during its usage period. It is important to note that for a PV module, failure can be related to both performance degradation and safety issues. In this regard, it is a prerequisite to describe in which context it is being used. To add on, degradation models can either be developed to evaluate electrical performance or material degradation, it is also necessary to clarify the context in this regard. Therefore, in this section, the term failure (as used throughout the entire document) is defined only in terms of performance degradation. The described as well as the proposed models quantify the evolution of PV modules performance over time.

Two modeling approaches; physical and data-driven are commonly used to evaluate the degradation rates and lifetime of PV modules.

Data-driven models are often employed to estimate degradation rates based on analysis of given data sets. Data-driven techniques can be divided into two categories: statistical techniques (regression methods, ARMA models, etc.) and artificial intelligence (AI) techniques (neural networks (NNs), fuzzy systems (FSs), etc.) [Chen Xiongzi et al. \(2011\)](#). The goal of the statistical analysis is to calculate the trend of the PV performance time series and to translate the slope of the trend to an annual loss rate, in units of %/year [Phinikarides et al. \(2014\)](#). Although these models can provide consistent performance loss rates (PLRs), which are useful for data extrapolation and service life predictions, they do not directly provide evidence for the degradation modes taking place in the module. Other effects such as diffuse soiling, snow, shading or module mismatch have also a direct impact on the performance trend.

Physical models are based on the physical/chemical understanding and assumptions of a specific degradation mode. These models represent the mechanism involved in complex physical/chemical processes. For well-known PV module degradation modes, several analytical models to predict PV module degradation are available. All these models are based on the principle of understanding the underlying process, but they are still only heuristic

models, which do not include the influence of material parameters.

A significant part of the research is devoted to physical models, therefore, the literature discussion is inclined towards this directions. The statistical methods are also reviewed in the supporting article attached in the annex.

## 2.3 A review of the available physical models

On one hand, physical models are developed to explain experimental observations of different degradation modes and can also be used in experimental designs. A model can be applied to analyze the experimental observations by fitting experimental data to extract parameters that cannot be directly measured (e.g kinetic energy), used to study the sensitivity of performance degradation to climatic stress factors such as T, RH,  $\Delta T$ , UV and other influence factors.

On the other hand, models are also used to predictive or forecast future behavior. Models are used to predict in situations where a given module needs to be analyzed under different test conditions. In this case, the measurements of the module under a given condition can be applied to calibrate the degradation models and apply the calibrated model to predict the effects of other different test conditions as illustrated in 2.1. Degradation models are used as forecasting models to know the progress of degradation for an extended time horizon. In this case, the models are calibrated on experimental data after a shorter time and then applied to extrapolate the degradation for a longer time.

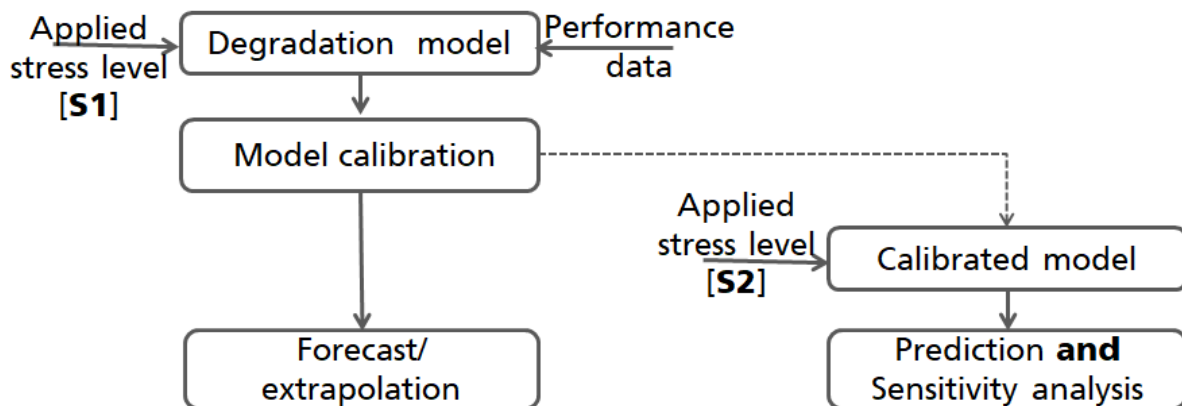


Figure 2.1: Schematic diagram showing the different applications of degradation models: forecasting, predictive, sensitivity analysis and experimental evaluation. S1 are the applied experimental stress conditions and S2 are the modeled stress conditions. At model calibration stage, the extracted parameters can be used for extrapolation, results assessment by correlating them to material properties or used as inputs to predict the degradation at different test condition as well as to perform a sensitivity analysis

Electrical parameters such as:  $P_{max}$ ,  $I_{SC}$ ,  $R_{sh}$  and  $R_s$  resistances are commonly modeled as degradation indicators. Hence, the environmental stresses and their interactions with the PV module components are assessed based on the reduction of the initial electrical parameter at time ( $t = 0$ ) before aging and at time ( $t = t$ ) after aging or in the field. The degradation models can be divided into two categories: models for the degradation indicators and models for the degradation rates. The degradation indicator models are

mathematical functions proposed to evaluate the degradation trends of a given degradation indicator over time. Since each degradation mode or technology under investigation can have a different degradation curve, different authors have proposed models to fit the observed degradation curves. On contrast, degradation rate models evaluate the rate of change of degradation indicators. They are function of the applied stress factors.

The structure of the review is as follows; models are discussed according to specific degradation modes, how they are applied and where necessary their performances are compared and discussed.

### 2.3.1 Degradation models for corrosion

Corrosion is one of the most occurring degradation modes in PV modules [Ndiaye et al. \(2013\)](#). Corrosion is caused by the presence of high temperature and high humidity in the module. Humidity can enter the module through the backsheet or the layers of the encapsulant and spread into the module [Park et al. \(2013\)](#). One hypothesis is that humidity leads to the formation of acetic acid through the hydrolysis of EVA [Kempe et al. \(2007\)](#); [Whitfield et al. \(2012\)](#); [Masuda et al. \(2015\)](#) resulting to corrosion. Corrosion attacks the metallic connections of PV cells and results in a loss of adhesive strength between the cells and the metallic frame, as well as an increased leakage current and therefore a loss in performance [Kempe et al. \(2007\)](#).

Degradation indicator models based on power at maximum power point and series resistance have been proposed to fit the degradation patterns for corrosion as:

- (1) Model of [Pan et al. \(2011\)](#)

$$\frac{P_{max}}{P_{max(0)}} = \exp(-R_D t^\beta) \quad (2.1)$$

- (2)  $P_{max}$  and  $R_s$  models according to [Braisaz et al. \(2014\)](#)

$$P_{max} = \frac{1 + \exp(-B)}{1 + \exp(R_D t - B)} \quad (2.2)$$

$$R_s = R_{S(0)} = \exp(R_D t - B) \quad (2.3)$$

where  $P_{max}$  [W] and  $R_s$  [ $\Omega$ ] are the output power and series resistance at time ( $t$ ),  $P_{max(0)}$  &  $R_{S(0)}$  are the power output and series resistance at time ( $t = 0$ ),  $\beta$  is the experimental parameter,  $B$  is a coefficient to be calibrated and  $R_D$  [%/hour] is the degradation rate.

These functions can be applied in two way; to extract the degradation rates and also for extrapolation. The first application is used to compare the degradation rates of a similar module but with different stress conditions or to analyze the impact of applied stresses to different BoM. In this case, different modules with different BoM are tested under similar conditions and the extracted degradation rates are compared. The second application is used to forecast the evolution of degradation at an extended time horizon.

#### A. Comparison of Pan and Braisaz Model

The two models are applied to fit time series datasets from DH ageing tests at different conditions: DH/75<sup>0</sup>C/85%RH, DH/90<sup>0</sup>C/50%RH and DH/90<sup>0</sup>C/70%RH. Since the loss in power could take different shapes as reported by [Köntges et al. \(2014\)](#), it is unlikely that a single degradation function can fit all the different shapes. Here we compare how well

the two function can fit three time series dataset from DH measurements with different degradation profiles as shown in figure 2.2. The fitting is done using the least squares fitting function inbuilt in Python. In both cases the derived degradation rates, the model parameters as well as the RMSE are presented in table 2.2 . The RMSE is calculated as:

$$RMSE = \sqrt{\frac{\sum_{j=1}^n (f_i - m_i)^2}{n}} \quad (2.4)$$

where, m is a measured value and f is the fit value, n are the number of observations.

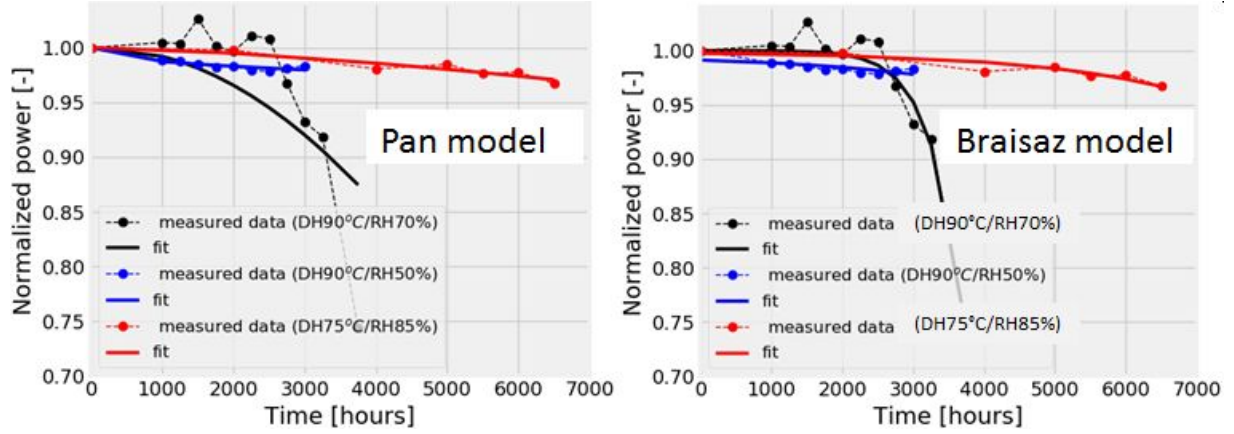


Figure 2.2: Pan and Braisaz model fit for different DH measurements, the dotted lines represent the experimental data and the thick lines are the corresponding models fit respectively. The colors represents the different experimental condition as well as the different failure profiles.

Table 2.2: Derived model parameters for different damp heat conditions

Experimental condition	$R_D$ [%/hour]	Model parameter ( $\beta$ )	model parameter (B)	RMSE [%]
Pan Model				
DH 75°C/85% <i>RH</i>	5.66e-8	1.50	-	0.35
DH 90°C/50% <i>RH</i>	6.40e-4	0.43	-	0.19
DH 90°C/70% <i>RH</i>	3.15e-9	2.13	-	4.99
Braisaz Model				
DH 75°C/85% <i>RH</i>	4.43e-4	-	6.34	0.39
DH 90°C/50% <i>RH</i>	4.66e-4	-	5.42	0.39
DH 90°C/70% <i>RH</i>	2.58e-3	-	10.75	1.33

Figure 2.2 shows the experimental data with the respective models fit. It is can be seen that, depending on the degradation shape, the fitting accuracy varies for both models. For example, the model of Pan was able to fit well the red and blue curves and could not provide perfect fitting of the black curve. On contrary, the model according to Braizas was able to perfectly fit the black curve but not the the blue curve. Overall the model according to Braizas is preferable to that of Pan since the extracted degradation rates are consistent with the applied stresses. However, a model that include a shape parameter that can perfectly fit/optimize, the different degradation shapes is still needed and will be

part of this research work.

Another application of degradation models, as mentioned before, is to extrapolate the measured performance degradation to longer time horizons. Therefore, the two models are calibrated on the same dataset (i.e. DH/75<sup>0</sup>C/85%RH) but only after 4000 hours. In each case the model parameters are extracted as in Table 2.3. Then the calibrated models are applied to forecast the power degradation from 4000 hours until 6500 hours. The results for all the three models are plotted with the extended measurements 2.3

Table 2.3: Model parameters for Pan and Braisaz model after 4000 hours of DH/75C/85%RH

Model	$R_D$ [%/hour]	Model parameter ( $\beta$ )	model parameter (B)	RMSE [%]
Pan Model				
Pan	6.44e-10	2.07	-	0.13
Braisaz	9.00e-4	-	7.56	0.10

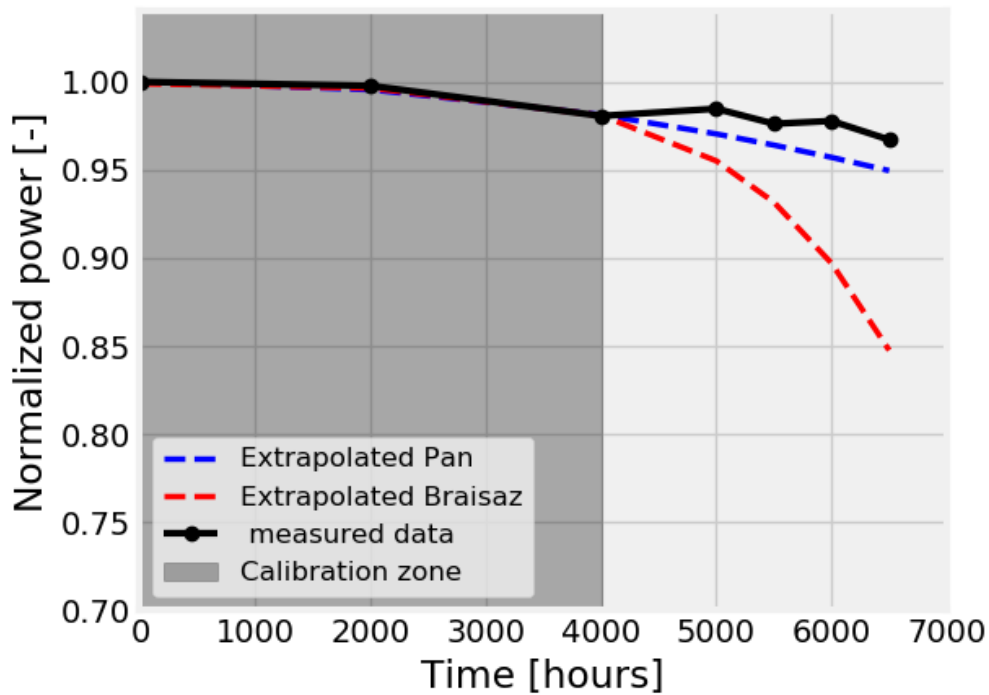


Figure 2.3: Extrapolation after 4000 hours of DH/75C/85%RH using Pan (blue) and Braisaz (red) models

Figure 2.3 shows the extrapolation of power degradation from 4000 hours to 6500 hours using of Pan and Braisaz models. Indeed, it is hard to conclude that a particular model is better than the other as this might highly depend on the degradation shape under evaluation. However, two main conclusions can be drawn:

- A perfectly fitting model does not guarantee good forecasting. This is visible for

the case of Braisaz's model, with small residual deviation but instead the model demonstrates the worst performance for this data set.

- Simple extrapolation after a given interval might not be reliable for longer time extrapolation. This is visible in all the models. Indeed, this can be influenced by measurement uncertainties, nature of the degradation pattern and many other factors. Although many researchers use this kind of extrapolation, the reliability of extrapolated performance is questionable and yet an unresolved challenge. Therefore, part of this research focuses on developing methods to improve long-term extrapolation accuracy.

The degradation rates of indicator models (equations 2.1, 2.2 and 2.3 can be calculated as functions of T and RH using three common kinetics models namely; the Peck's model, the Eyring model and the exponential model Escobar and Meeker (2007); Jordan and Kurtz (2010). These models are developed on the primary assumption that the rate of degradation is proportional to the concentration of water in PV modules and that the rate constant has Arrhenius temperature dependence. The models are written as:

(3) Peck's model

$$R_{D.Peck} = A \cdot \exp\left(-\frac{E_a}{k_B T}\right) RH^n \quad (2.5)$$

(4) Eyring Model

$$R_{D.Eyring} = A \cdot \exp\left(\frac{-E_a}{k_B T} - \frac{b}{RH}\right) \quad (2.6)$$

(5) Exponential model

$$R_{D.Exp} = A \cdot \exp\left(\frac{-E_a}{k_B T}\right) \cdot \exp(m \times RH) \quad (2.7)$$

where  $A$  and  $n$ ,  $b$  and  $m$  are model parameters. In order to obtain  $A$ ,  $E_a$ ,  $n$ ,  $b$  and  $m$  in the equations (2.5), (2.6) and (2.7), the equations can be fitted to experimental data or represented on a logarithmic scale by a straight line, using the following equations:

$$\ln(R_{D.Peck}) = \ln(A) - \left(\frac{E_a}{k_B T}\right) + n \times \ln(RH) \quad (2.8)$$

$$\ln(R_{D.Eyring}) = \ln(A) - \left(\frac{E_a}{k_B T}\right) - \frac{b}{RH} \quad (2.9)$$

$$\ln(R_{D.Exp}) = \ln(A) - \left(\frac{E_a}{k_B T}\right) + m \times RH \quad (2.10)$$

A plot of  $\ln(R_D)$  versus  $1/T(^{\circ}K)$  gives an Arrhenius plot with a slope  $E_a/k_B$  and an intercept  $\ln(A)$ .

## B. Comparison of Peck's, Eyring and Exponential models

Here we performed a sensitivity analysis of the degradation rate models 2.5, 2.6 and 2.7 to compare how the degradation rate varies with input climatic variables (temperature and humidity). To perform unbiased comparison, all the three models were fitted using the same dataset (in this case DH/75°C/85% RH). Also since the Braisaz model was found to have consistent results, it was selected for the calibration. For all the datasets, the model

parameter B was kept the same in order to evaluate the same degradation rate. Moreover since the activation energy should be the same in the physical point of view for a similar reaction, it was kept constant for the three models. This is also good for a comparison purpose, given that, this parameter is very sensitive. The extracted models parameters used in the sensitivity analysis simulations are presented in table 2.4.

Figures 2.4, 2.5 and 2.6 show the plots of the sensitivity analysis of the Pecks, Eyring and exponential models respectively. It is clearly visible that despite a uniform calibration procedure, the sensitivity of the model varies to a big extent. This can be explained by the assumptions taken during the models formulation. Although all the models have an Arrhenius temperature dependence, the formulation of the relative humidity contribution changes the variation of the degradation rate. For example, the exponential model, assumes an exponential dependence of the relative humidity and this explain why the model is too sensitive to relative humidity compared to the Pecks and Eyring model. This high sensitivity of relative humidity together with the Arrhenius temperature dependence could deteriorate the model if used for extrapolation. Overall, the Pecks model shows a good dependence of both temperature and relative humidity.

Table 2.4: Derived model parameters used in the sensitivity analysis

Model	A	Parameters (n,b & m)	( $E_a$ ) [eV]	RMSE [%]
Peck	9.46	2.07	0.57	0.39
Eyring	9.97e4	6.01	0.57	0.39
Exponential	3.64e-4	0.23	0.57	0.39

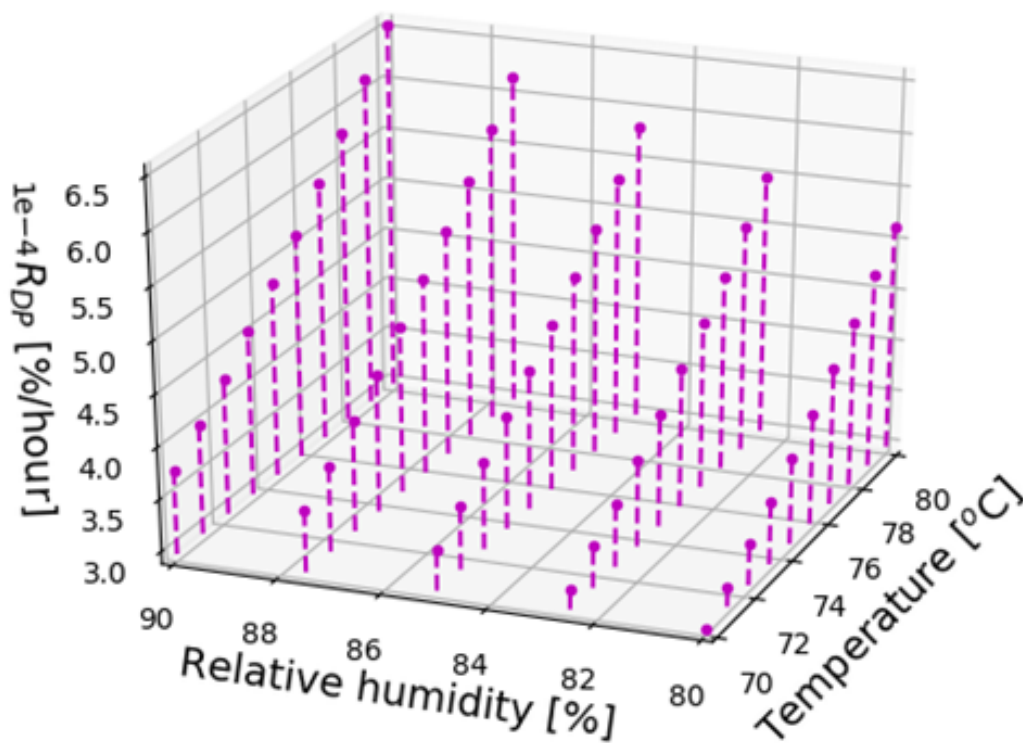


Figure 2.4: Sensitivity analysis plot of the degradation rate with relative humidity and temperature using the Pecks model (note the y axis in multiplied by 1e-4)

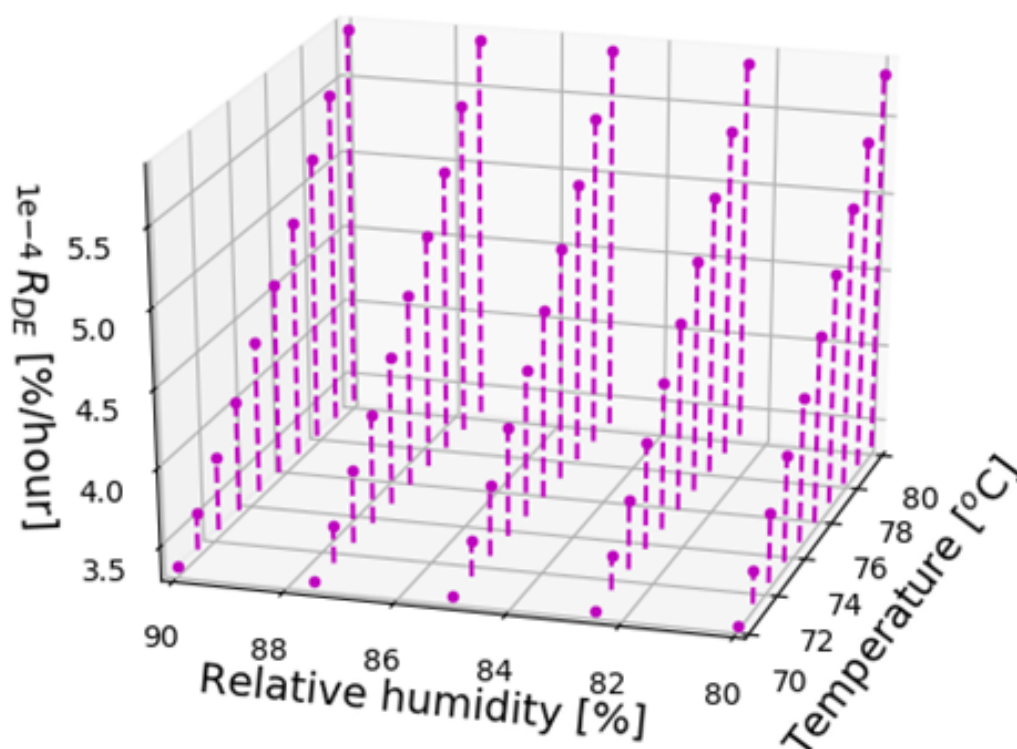


Figure 2.5: Sensitivity analysis plot of the degradation rate with relative humidity and temperature using the Eyring model (note the y axis in multiplied by  $1e-4$ )

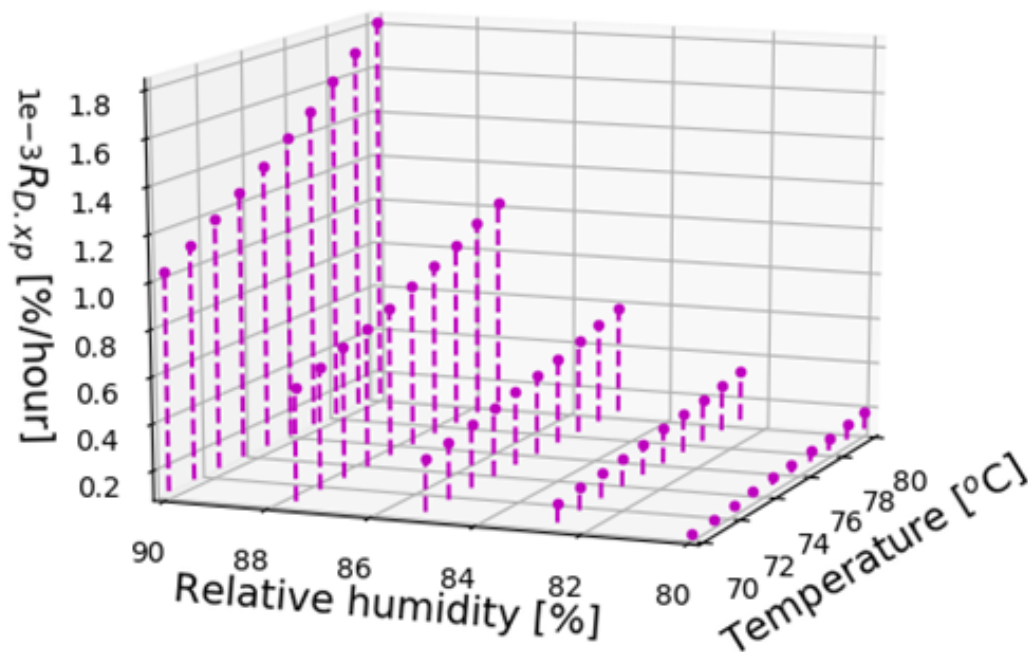


Figure 2.6: Sensitivity analysis plot of the degradation rate with relative humidity and temperature using the exponential model (note the y axis in multiplied by  $1e-3$ )

### 2.3.2 Models for potential induced degradation

Potential induced degradation (PID) has been observed in all PV technologies and in almost all operating climates. It does not occur so frequently, but if it does, its effect can lead to a dramatic performance loss within a short period [Moser et al. \(2017\)](#); [Hacke et al. \(2016, 2015\)](#); [Köntges et al. \(2014\)](#). In general terms, PID is caused by the difference in potential between the cells and the support structure of the module. This difference drives a leakage current that can lead to power degradation. Different types of PID occur depending on the module technology. For crystalline silicon PV, two degradation modes can be identified, PID-p (for polarisation or passivation) and PID-s (for shunting). PID-p is a temporary and reversible degradation of the passivation layer, which reduces the performance due to a surface recombination increase [Naumann et al. \(2014\)](#); [Halm et al. \(2015\)](#); [Swanson et al. \(2005\)](#). PID-s is due to a leakage current involving an ionic flow of sodium ions (Na+) from the glass, encapsulant or cell surface into the cell, diffusing into the silicon stacking faults and shunting the cell [Lausch et al. \(2014\)](#). The sodium incorporation in the silicon surface degrades primarily the fill factor (FF), the open circuit voltage ( $V_{oc}$ ), and lastly the short circuit current ( $I_{sc}$ ). The relevant stress factors for PID-s include [Köntges et al. \(2014\)](#): high temperature, relative humidity, system voltage, light, bias-junction potential and injected carriers.

Different authors [Braisaz et al. \(2014\)](#); [Hacke et al. \(2015\)](#); [Annigoni et al. \(2017\)](#); [Hacke et al. \(2016\)](#); [Hattendorf et al. \(2012\)](#); [Taubitz et al. \(2014\)](#) have proposed models to evaluate PID degradation patterns using different indicators as;

(6) PIDHACKE model

$$\frac{P_{max}}{P_{max(0)}} = 1 - A \cdot \exp\left(-\frac{E_a}{k_B T}\right) RH^n \times t^2 \quad (2.11)$$

A parabolic model was proposed by [Hacke et al. \(2015\)](#) to fit the power degradation of c-Si modules. The constants  $A$  and  $n$  are determined by fitting the equation to experimental results. The parameters have to be determined for each module type. This parabolic model is applicable to the beginning of the degradation phases of PID-s, as it can fit the beginning of a sigmoid and does not describe the stabilization phase of the sigmoidal curve.

(7) PID model according to [Annigoni et al. \(2017\)](#)

$$\frac{P_{max}}{P_{max(0)}} = 1 - A \cdot \exp\left(-\frac{E_a}{k_B T}\right) RH^n \times t^2 \times U \quad (2.12)$$

[Annigoni et al. \(2017\)](#) re-wrote the PIDHACKE model (2.11) including a voltage term ( $U$ ) (2.12) and used the indoor data to determine coefficients of the model for distinct aging contributions (temperature, relative humidity and time) and then applied the model (2.12) to outdoor PID degradation for different climates.

(8) Hattendorf model

$$P_{max}(U, T, RH, t) = P_{max(0)}(1 - P(t)) \quad (2.13)$$

$$P(t) = P_\infty \frac{1 - \exp\left(-\frac{t}{\tau_1}\right)}{1 - \exp\left(-\frac{t-t_0}{\tau_2}\right)} ; P(U) = \left(1 + \exp\left(\frac{U - U_0}{\Phi}\right)\right)^{-2} \quad (2.14)$$

$$t_0 = a \times b \times \hat{t}_0 ; \tau_1(T) = b^2 \times \hat{\tau}_1; \tau_2 = \hat{\tau}_2 \quad (2.15)$$

$$a(H) = \frac{H_0}{H} ; b(T) = \exp\left(\frac{T - T_0}{\phi}\right) \quad (2.16)$$

The model of [Hattendorf et al. \(2012\)](#) is based on a matrix of indoor experiments where modules are exposed to varying voltage, module temperature and ambient humidity. The conditions are varied to determine the model parameters for the module power. The model includes six adaptation parameters:  $\hat{t}_0$ ,  $U_0$ ,  $\hat{\tau}_1$ ,  $\hat{\tau}_2$ ,  $\Phi$  and  $\phi$ .  $H_0$  and  $T_0$  are scaling parameters. The function  $P(t)$  describes the power loss caused by degradation.  $P_\infty(U)$  is its limit for  $t \rightarrow \infty$ ,  $a(H)$  and  $b(T)$  are the acceleration functions of relative humidity and temperature. For  $T = 0$  and  $H = 0$ , they are equal to 1, therefore  $\hat{\tau}_1$ ,  $\hat{\tau}_2$  are the time constants under these conditions.  $\tau_2$  remains constant for a given module. To determine the model's parameter, the power degradation is measured as a function of time with the system voltage  $U$  as parameter and a fixed humidity  $H$  as well as temperature  $T$ . The saturating power  $P_\infty$  is extracted by fitting  $P(t)$  to the measured data.

(9) Taubitz model [Taubitz et al. \(2014\)](#)

Shunting phase

$$R_{sh}(t) = a_S \exp\left(\frac{-t}{b_S(t)}\right) \quad (2.17)$$

Regeneration phase

$$R_{sh}(t) = C_R + a_R \exp\left(\frac{t}{b_R(t)}\right) \quad (2.18)$$

Transition phase

$$R_{sh}(t) = a_T(T)(t + b_T(T))^2 + C_T \quad (2.19)$$

[Taubitz et al. \(2014\)](#) proposed a regeneration model for shunt resistance evolution over time due to PID degradation. The shunt resistance was modeled in three phases; shunting phase, regeneration phase and transition phase. Where  $a_S$ ,  $b_S$ ,  $C_T$ ,  $b_T$ ,  $a_T(T)$ ,  $b_S(T)$ ,  $b_T(T)$ ,  $C_R$  and  $a_R$  are constants and have to be determined for a specific module type. Some of them are dependent on the module temperature  $T$ . The constants are determined by measuring the times  $t_S$ ,  $t_T$ , and  $t_R$  for reaching certain target values.

(10) PID model according to [Braisaz et al. \(2014\)](#)

$$R_{sh}(t) = \frac{R_{sh(0)}}{1 + aR_D t} \quad (2.20)$$

$$R_D = A \times U \frac{B}{1 + \exp(-C(RH) + D)} \exp\left(-\frac{E_a}{k_B T}\right) \quad (2.21)$$

The model is based on shunt resistance  $R_{sh}$  degradation as an indicator, as it is the most important parameter for PID. The evolution of  $R_{sh}$  as a function of voltage, temperature and relative humidity was modeled as (2.20). Where  $R_{sh}$  is the shunt resistance at time ( $t$ ),  $R_{sh(0)}$  is the initial shunt resistance,  $A, B, C$  and  $D$  are model coefficients,  $U$  is the applied voltage and  $R_D$  is the degradation rate dependent on RH, U and T.

### 2.3.3 Models for ultraviolet irradiance degradation

Ultraviolet (UV) light exposure has been reported to cause PV module degradation in a number of ways. As an example, it could result in discoloration of the encapsulant material [Dunn et al. \(2013\)](#), delamination at the glass encapsulant or cell encapsulant interface [Munoz et al. \(2011\)](#). The parameter most impacted by UV exposure is the short circuit current ( $I_{sc}$ ). [Braisaz et al. \(2014\)](#) proposed a model for short circuit degradation due to UV exposure over time. They found that the degradation curve is not linear but an exponentially decreasing curve. The short circuit is modeled as a function of UV as:

(11) UV model according to [Braisaz et al. \(2014\)](#)

$$I_{sc}(t) = I_{sc(0)} - aD_{UV}(t) - b(1 - \exp(-CD_{UV})(t)) \quad (2.22)$$

$$D_{UV}(t) = \int_0^t E(u) \times 5.5\% du \quad (2.23)$$

Here,  $D_{UV}$  is the UV dose in in  $MJ/m^2$  or  $kWh/m^2$ ,  $I_{sc}$  is the short circuit current at time (t),  $I_{sc(0)}$  is the initial short circuit current and  $a$ ,  $b$  and  $C$  are model coefficients. The multiplication by 5.5% is due to the UV radiation between (280nm – 400nm) which is approximately 5.5% of the total light spectrum  $E(u)$  [Koehl et al. \(2009\)](#).

(12) The Schwarzschild Law

$$k = A(I)^p \quad (2.24)$$

The Schwarzschild law has been applied by [Gu et al. \(2015\)](#) to study the effect of intensity and wavelength of spectral UV light on discoloration of laminated glass/EVA/PPE PV modules. Here,  $k$  is a constant,  $I$  the intensity and  $p$  is the Schwarzschild coefficient. Recommendation: When applying this expression in performance (power) prediction models where other loads are also applied, the parameter  $p$  must be calibrated according to the knowledge of severity ranking [Jordan et al. \(2017a\)](#).

### 2.3.4 Degradation models for delamination, fatigue solder failure and cell cracks

(13) Coffin-Manson's equation

$$N = \frac{\sigma}{(\Delta T)^{\beta_1}} \quad (2.25)$$

The model is used to predict degradation modes caused by temperature cycling such as encapsulant delamination, fatigue solder failure and cell cracks. According to [Escobar and Meeker \(2007\)](#), the model describes the number of cycles to failure as (2.25), where  $\Delta T$  is the temperature range,  $\sigma$  and  $\beta_1$  are properties of the material and test setup. The cycles-to-failure distribution for temperature cycling can also depend on the cycling rate (e.g. due to heat buildup). An empirical extension of the Coffin-Manson relationship that describes such dependencies is [Escobar and Meeker \(2007\)](#):

$$N = \frac{\sigma}{(\Delta T)^{\beta_1}} \frac{1}{(freq)^{\beta_2}} \exp\left(\frac{E_a \times 11605}{T_{max}(K)}\right) \quad (2.26)$$

where  $freq$  is the cycling frequency and  $E_a$  is a quasi-activation energy.

(14) Crack propagation model

$$C_a(t) = C_a(t-1) + \frac{1}{x\left(\frac{125}{T_a}\right)^m} \quad (2.27)$$

The model was suggested by Braisaz et al. (2014) and it was applied to simulate the degradation of the short-circuit current  $I_{sc}$  due to the expansion of cell cracks caused by temperature.  $C_a(t)$  is the crack activation at time ( $t$ ),  $C_a(t-1)$  the crack activation at time ( $t-1$ ),  $T_a$  is the daily temperature amplitude,  $m$  a model parameter and  $x$  is the number of thermal cycles. The crack activation/propagation model is dependent on the daily temperature amplitude  $T_a$ .

(15) Damage accumulation model

$$D = C(\Delta T)^n (r(T))^m \cdot \exp\left(-\frac{Q}{k_B T_{max}}\right) \quad (2.28)$$

The model was used by Bosco et al. (2016) in order to calculate the solder fatigue damage in seven cities investigated in their study and compared to FEM simulated results. They found out that the model fits well to the simulated calculations. In this equation,  $\Delta T$  is the mean daily maximum cell temperature change,  $T_{max}$  the mean maximum daily temperature,  $C$  a scaling constant,  $Q$  the activation energy,  $k_B$  Boltzmann's constant,  $r(T)$  the number of times the temperature history increases or decreases across the reversal temperature,  $T$  the period of a year and  $n$  &  $m$  are model constants similar to those in the Coffin-Manson equation.

(16) Backsheet degradation rate model

$$R_D \approx I^X (b + m \times TOW) \times (T_f)^{\frac{T-T_0}{10}} \quad (2.29)$$

Here,  $I$  is the light intensity,  $X$ ,  $b$  and  $m$  are fit parameters,  $TOW$  is the time of wetness,  $T$  the temperature,  $T_0$  a reference temperature and  $T_f$  is a multiplier for the increase in degradation for a rise in temperature in 10 K steps.

The model is used to estimate a potential form of the degradation kinetics of the backsheet. This model was applied by Kempe (2014) to model the uncertainty in a 25 year equivalent test for module backside exposure to irradiance and temperatures in different climatic zones.

Recommendation: As also mentioned by Kempe, the parameter that describes the effect of time of wetness has very high uncertainties, we recommend careful comparison of the relative change in degradation rate with changes in TOW. In case one wants to extract thermal parameters such as activation energy, the multiplier term ( $T_f$ ) can be replaced by the Arrhenius term.

### 2.3.5 Physical models for combined degradation modes/stresses

Since degradation of PV modules in outdoor operation is influenced by multiple environmental stresses, models based on multiple stresses are viable for outdoor service lifetime prediction. In the literature, only a few authors Gaines et al. (1978); Bala Subramaniyan et al. (2018) have proposed models based on the combination of several stresses.

(17) Model of Gaines

$$\frac{P_{max}}{P_{max(0)}} = [1 - R_D t]^{\frac{1}{\beta}} \quad (2.30)$$

$$R_D = A f_T f_{RH} f_M f_G f_\omega \quad (2.31)$$

Gaines et al. (1978) proposed a model for power output degradation based on multiple accelerated environmental stresses (2.30). Where  $R_D$  is the degradation rate and the factors  $f_T$ ,  $f_{RH}$ ,  $f_M$ ,  $f_G$  and  $f_\omega$  are associated with a decrease in power output due to effects of temperature ( $T$ ), relative humidity ( $RH$ ), mechanical stresses (from temperature differences) ( $M$ ), gaseous concentration ( $G$ ) and the frequency of the temperature excursion ( $\omega$ ). The mathematical form of each factor is formulated to represent the underlying physical phenomena.

An Arrhenius form is used for temperature influenced effects:

$$f_T = \exp\left(-\frac{B}{T}\right) \quad (2.32)$$

$B$  denotes a constant parameter and  $T$  denotes temperature.

The effect of relative humidity  $f_{RH}$  is represented by:

$$f_{RH} = 1 + (RH)_0 \cdot \exp\left(C_0\left(\frac{1}{T_C} - \frac{1}{T_0}\right)\right)^{C-\frac{D}{T}} \quad (2.33)$$

the second term in the bracket corrects the relative humidity as a function of temperature, given a specified relative humidity at  $T_0$ .  $C$  and  $D$  are constant parameters.

The mechanical/temperature excursion factor  $f_M$  is represented by:

$$f_M = \left[ \frac{\exp\left(G_1\left(\frac{1}{T} - \frac{1}{T_b}\right)\right) + \exp\left(-G_2\left(\frac{1}{T} - \frac{1}{T_b}\right)\right)}{D_0} \right] \times \exp(J\Delta T) \quad (2.34)$$

the first term in the bracket reflects the stresses arising from differences in expansion coefficients of bonded materials. The constants  $G_1$ ,  $G_2$ ,  $D_0$  and  $T_b$  are chosen to represent the estimated magnitudes of these fatigue effects. The factor  $\exp(J\Delta T)$  estimates the magnitude of the temperature excursion  $\Delta T$ , where  $J$  is a constant.

The effect of gaseous concentration  $f_G$  is represented by:

$$f_G = \left[1 + \frac{G}{G_o}\right]^{E-\frac{F}{T}} \quad (2.35)$$

here,  $E$  and  $F$  denote constant parameters and  $T$  is the temperature.

The frequency of the temperature excursion  $f_\omega$  is represented by:

$$f_\omega = \left[1 + \frac{\omega}{\omega_o}\right]^{P-\frac{Q}{T}} \quad (2.36)$$

$\omega$  is the frequency and  $P$  as well as  $Q$  are constant parameter. In a constant temperature test,  $T$  is a constant and  $\omega$  is taken to be zero. In the cyclic temperature tests, reciprocal temperature is considered to be a sinusoidal function of time:

$$\frac{1}{T}(t) = \tau + \Delta\tau \sin(\omega t) \quad (2.37)$$

$$\tau = \frac{1}{2} \left[ \frac{1}{T_{min}} - \frac{1}{T_{max}} \right] \quad (2.38)$$

$T_{min}$  and  $T_{max}$  are the minimum and maximum temperatures associated with the temperature cycles.

Recommendation: The model of Gaines presents the previous approach on multiple stress modeling, however, the user should take caution that this model was developed and applied on PV modules that had a different construction from today's modules. Therefore, its application might need some modification to fit the current PV module construction types.

(18) Degradation rate model of Subramaniyan

$$Rate(T, \Delta T, UV, RH) = \beta_0 \cdot \exp\left(-\frac{\beta_1}{k_B T_{max}}\right) \times (\Delta T_{daily})^{\beta_2} \times (UV_{daily})^{\beta_3} \times (RH_{daily})^{\beta_4} \quad (2.39)$$

Another model to calculate the degradation rate due to combined environmental stresses has been proposed recently by [Bala Subramaniyan et al. \(2018\)](#). The model takes into account the effect of both static and cyclic temperature, ultraviolet radiation and relative humidity as (2.39). Where  $Rate(T, \Delta T, UV, RH)$  is the reaction rate,  $T_{max}$  the daily maximum temperature of the module [K],  $\Delta T_{daily}$  the daily cyclic temperature of the module [K],  $UV_{daily}$  the daily daytime average irradiance [W/m<sup>2</sup>],  $RH_{daily}$  the daily average relative humidity [%] and  $k$  is the Boltzmann constant. The model parameters  $\beta_0$ , which is the frequency factor [s<sup>-1</sup>];  $\beta_1$ , the activation energy [eV];  $\beta_2$ , the effect of cyclic temperature;  $\beta_3$ , the effect of UV radiation and  $\beta_4$ , the effect of RH, can be estimated from measured data through data fitting techniques. In their study, the model was calibrated using outdoor measurements and then applied to predict the degradation rates in four other climates.

## 2.4 Chapter Overview

Based on the reviewed literature, two main aspects/challenges have been identified as;

- Degradation indicator models are developed to fit specific degradation patterns based on a specific degradation mode. A generalized model that can optimize the different degradation patterns is still a challenge. Therefore, in this research we aim to propose a model that can be generalized for different degradation patterns.
- Although several degradation rate models are developed for specific degradation modes for indoor application, little advances are made to develop models for combined climatic stresses that can be used for outdoor prediction. It is clearly seen that the need for such a model dates back in the 1970's however since then it has been of recent that [Bala Subramaniyan et al. \(2018\)](#) added a contribution to this effort. Therefore, further developments for a model that take into account multiple environmental stress factors are proposed in this research.



# Chapter 3

## Methodology

Table 3.1: Chapter 3 Nomenclatures

Symbols	
$c_i$	clearness index
$E_a$	activation energy [eV]
$k$	degradation factor [1/year]
$k_B$	Boltzmann constant ( $8.62 \times 10^{-5}$ eV/K)
$P_{max}$	power at maximum power point [W]
$R_D$	degradation rate [%/hour]
$SD_{res}$	residual standard deviation
$T_{amb}$	ambient temperature [ $^{\circ}C$ ]
$T_{Dew}$	dew point temperature [ $^{\circ}C$ ]
$T_m$	module temperature [K]
Subscripts	
$cal$	calibration
$h$	hydrolysis
$p$	photo-degradation
$t$	thermo-mechanical
$T$	total
Abbreviations	
$\Delta T$	temperature cycles [K]
DH	damp heat
FT	failure time
GHI	global horizontal irradiance
MSEP	mean square error of prediction
NWP	Numerical Weather Predictions
RUL	remaining usefull lifetime
STC	standard test conditions
t	time
UV	Ultraviolet [ $W/m^2$ ]
WS	wind speed [m/s]
WVP	saturated water vapour pressure

In this chapter, the methodologies for the proposed physical, data-driven and hybrid models are described. The chapter is therefore, divided into three sections, 3.1, 3.2 and

**3.3.** In section 3.1, the physical model is described, the experimental data used for model calibration and validation as well as the methods used to process the climate data used to simulate the global degradation maps are described. In section 3.2, the data-driven approach is described as well as the experimental data used for model calibration and validation. In section 3.3, we describe how the two methods are linked into a hybrid model. For consistence and to allow the reader to follow, it is better to read section 3.1 with the corresponding results in section 4.1 and section 3.2 together with 4.2 respectively.

## 3.1 Methodology for the proposed physical model

In chapter 2 further development of a physical degradation rate model that take into account multiple climatic stress factors as well as a generalized degradation indicator model were identified. In this research, we contribute to these challenges by proposing a new model to quantify the impact of combined climatic stresses as well as a degradation indicator model that can optimize several degradation patterns.

### 3.1.1 Combined climatic stresses degradation rate model

Photovoltaic modules are exposed to a variety of climatic loads during outdoor operation. Over time, these loads trigger a number of degradation modes within the modules leading to performance loss. In section, an approach to develop a combined climatic stress degradation rate model is described.

#### A. Background and modelling assumptions

When developing a model for PV modules degradation prediction, three main aspects need to be considered:

- Impact of PV materials variations. New materials are proposed frequently to improve PV performance.
- The different operating climatic conditions. PV modules operate in different climates for example in arid, maritime, tropical climates.
- The different PV technologies, for example: crystalline silicon, thin films, and different module designs like bifacial, glass-glass or glass-backsheet.

However, a model that takes into account all the three aspects is rather complex and might require an extensive experimental campaign which in turn makes it expensive. Moreover the fact that, materials are changing frequently makes developing a generalized model a challenging problem. In this regard, several assumptions and simplification have to be used. In developing our model, the following assumptions are used.

- The degradation rates are assumed to be proportional to the applied stresses and to have an Arrhenius temperature dependence. Therefore, the material dependence of the model is evaluated through the activation energy.
- Three degradation processes are assumed to be necessary for service lifetime prediction as; hydrolysis, photodegradation, and thermomechanical degradation. The assumption is based on the ability to reproduce these degradation mechanism in the

laboratory using accelerated ageing tests and that, the underlying physical and(or) chemical degradation kinetics have been studied from different studies [Zhu et al. \(2016\)](#); [Kempe \(2006\)](#); [Sharma and Chandel \(2013\)](#); [Ndiaye et al. \(2013\)](#); [Gok et al. \(2017\)](#); [Jordan and Kurtz \(2013\)](#); [Marín et al. \(1996\)](#); [Park et al. \(2013\)](#); [Wu et al. \(2014\)](#); [Koehl et al. \(2017\)](#) .

Empirical kinetics models to evaluate the degradation rate constant are proposed or selected to describe the three degradation processes. These models are developed depending on the applied climatic stresses as illustrated using the general reaction equation below:

$$\mathit{Stress1} + \mathit{Stress2} + \dots \mathit{StressN} \rightarrow \mathit{Degradation\ precursor} \quad (3.1)$$

where  $\mathit{Stress1}$ ,  $\mathit{Stress2}$ ,  $\dots \mathit{StressN}$  are the (climatic) degradation factors triggering the degradation mechanism under evaluation. The kinetics of the dominating degradation process is quantified as the degradation rate ( $R_D$ ). The mathematical form of the degradation rates of the three degradation processes is described in the following sections.

- The three processes are described based on combinations of input climatic variables. The combinations are selected based on the current indoor testing procedures [Wohlgemuth \(2012\)](#) which aim to reproduce degradation modes according to three main processes. Therefore, the combination of the input stresses are assumed to be responsible for triggering a specific reaction that might induce specific degradation modes. Figure 3.1 summarizes the hypothesized degradation mechanisms that are known to be induced by the applied loads.
- The effects of the applied loads is quantified on how much they affect the power output of the module, hence power at maximum power point is used as a degradation indicator in this research.

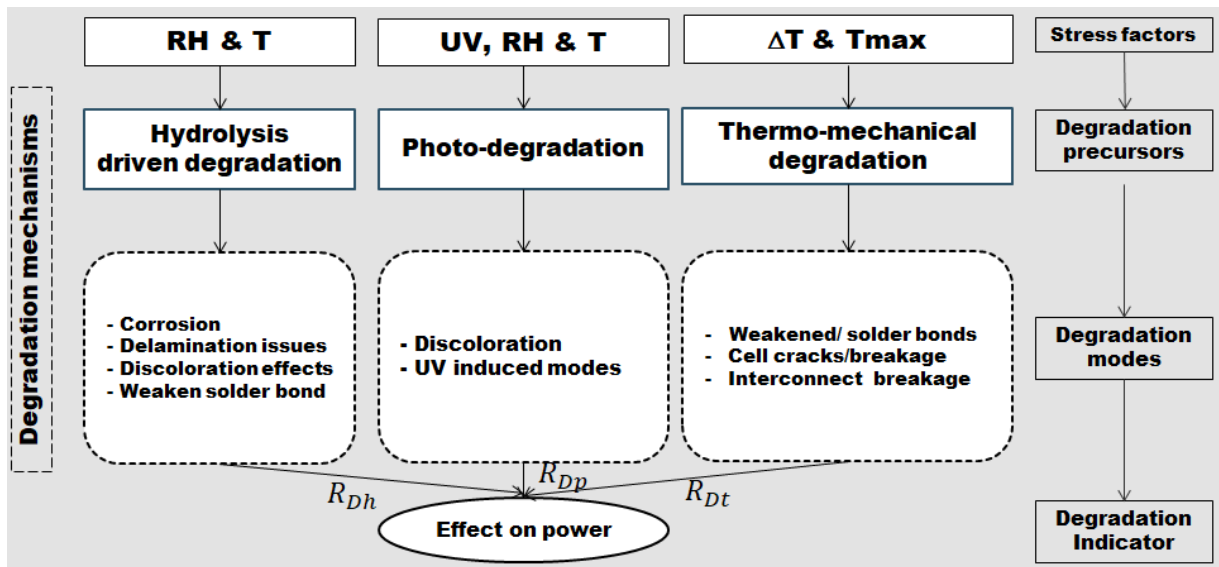


Figure 3.1: Schematic diagram of the modelling hypotheses. The combination of climatic stress triggers the three main precursor processes and the triggered processes are linked to different degradation modes

### B. Hydrolysis: Temperature and Relative humidity model

The Peck's model described in chapter 2 equation (2.5) is selected to model the effect of temperature and relative humidity based on the sensitivity analysis study in chapter 2, figure 2.4. The model shows a good dependence of both temperature and relative humidity. The models is hereby re-written as:

$$R_{Dh} = A_h \cdot rh_{eff}^n \cdot \exp\left(-\frac{E_{ah}}{k_B T_m}\right) \quad (3.2)$$

$$rh_{eff}(\%) = \frac{100}{1 + 98 \cdot \exp[-9.4 \times (RH(\%)/100)]} \quad (3.3)$$

where  $R_{Dh}$  is the degradation rate constant,  $k_B$  is the Boltzmann constant ( $8.62 \times 10^{-5} eV$ ),  $T_m$  is the module temperature (Kelvin),  $A_h$  is the pre-exponential constant,  $rh_{eff}$  (%) is the effective module relative humidity proposed by Koehl et al. (2012),  $n$  is a model parameter that indicates the impact of relative humidity on power degradation. In this context,  $E_{ah}$  is defined as the activation energy for power degradation due to hydrolysis process.

### C. Photo-degradation: UV, temperature and relative humidity model

The formulation of photo-degradation has been developed to take into account the combined effects of UV stress and moisture on PV modules. The baseline line assumption is that, UV stress alone would influence some degradation modes but also some modes might be influenced with a combined UV moisture stresses. For example, Ngo et al. (2016) has demonstrated that, UV irradiation plays a significant role in generating acetic acid with the presence of relative humidity that causes the power degradation of PV modules. Therefore to take into account the effect of UV alone and the combined UV-moisture contributions a model is proposed as:

$$R_{Dp} = A_h \cdot UV^X \cdot rh_{eff}^n \cdot \exp\left(-\frac{E_{ap}}{k_B T_m}\right) + A_h \cdot UV_{dose}^X \cdot \exp\left(-\frac{E_{ap}}{k_B T_m}\right) \quad (3.4)$$

OR

$$R_{Dp} = A_h \cdot UV^X (1 + rh_{eff}^n) \cdot \exp\left(-\frac{E_{ap}}{k_B T_m}\right) \quad (3.5)$$

where  $R_{Dp}$  is the rate due to photo-degradation processes,  $UV$  is the UV irradiance ( $W/m^2$ ),  $X$  is a model parameter that indicates the impact of UV on power degradation and  $E_{ap}$  is the activation energy for power degradation due to photo-degradation process.

### D. Thermo-mechanical degradation: $T_{max}$ , & $\Delta T$

The model used to quantify the effects of thermo-mechanical stresses is the modified Coffin-Mansion relationship that includes the effect of maximum temperature according to Escobar and Meeker (2007). The modified model is re-written as;

$$R_{Dt} = A_t \cdot C_N \cdot (273 + \Delta T)^\Theta \cdot \exp\left(-\frac{E_{at}}{k_B T_{max}}\right) \quad (3.6)$$

where  $\Delta T = (T_{max} - T_{min})$  is the temperature difference (Kelvin),  $C_N$  is the cycling rate,  $T_{max}$  and  $T_{min}$  are the module maximum and minimum temperatures,  $E_{at}$  the activation energy of power degradation due to thermo-mechanical process.

### E. Combined ( $RH$ , $T$ , $UV T_{max}$ & $\Delta T$ ) model

The transition from indoor degradation rate evaluation to outdoor is a challenging task as the interaction of different stresses and processes leading to PV degradation is not well known. The underlying assumption deployed in this research is that: some degradation processes might lead to specific degradation modes independent of the others and that some might have a synergistic nature as described in the schematic figure 3.2, which results in a variety of degradation modes.

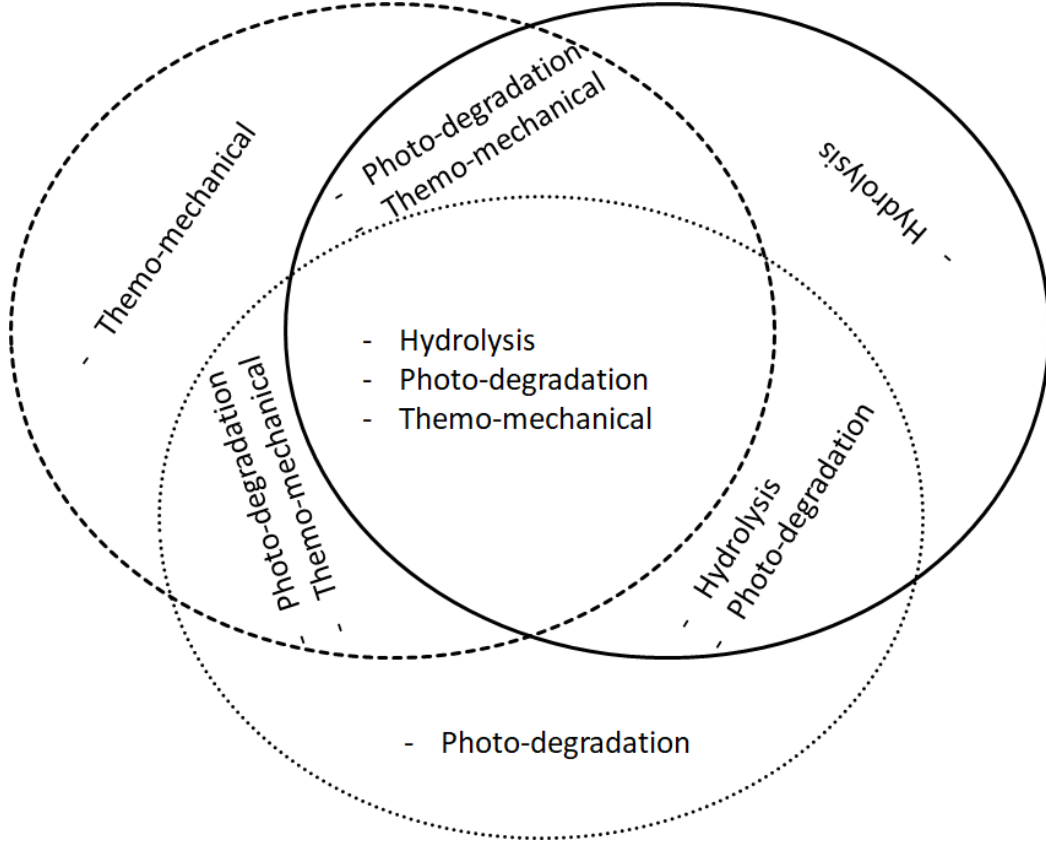


Figure 3.2: Schematic showing possible interactions of the three degradation processes

Hence, this assumption allows us to evaluate the total degradation rate as the sum of both independent and dependent processes. The mathematical form of the total rate is expressed as:

$$R_{DT} = A_N(R_{Dh} + R_{Dp} + R_{Dt} + R_{Dh} \cdot R_{Dp} + R_{Dh} \cdot R_{Dt} + R_{Dp} \cdot R_{Dp} + R_{Dh} \cdot R_{Dp} \cdot R_{Dt}) \quad (3.7)$$

OR

$$R_{DT} = A_N(1 + R_{Dh})(1 + R_{Dp})(1 + R_{Dt}) - 1 \quad (3.8)$$

OR

$$R_{DT} = A_N \cdot \prod_{i=1}^n (1 + R_{Di}) - 1 \quad (3.9)$$

where  $R_{DT}$  (%/year) is the total degradation rate,  $R_{Di}$  is the  $i^{th}$  rate constant and  $n$  is the total number of degradation processes.  $A_N$  is the normalization constant of the physical quantities, in this case it takes the units ( $year^{-2}\%$ ).

### 3.1.2 Degradation indicator model

As already mentioned in chapter 2, different electrical parameters such as:  $P_{max}$ ,  $I_{SC}$ ,  $R_{sh}$  and  $R_s$  are commonly modeled as degradation indicators to quantify the effects of the applied stresses. In this study,  $P_{max}$  is considered as the degradation indicator. The reasons to use  $P_{max}$  as an indicator are: it is easily calculated from the current-voltage (I-U) curves unlike  $R_{sh}$  and  $R_s$  that are derived from fitting procedure of the illuminated I-U curve with diode equations. Moreover, it's a parameter needed for energy yield evaluation and a metric used by manufacturers to give warranties.

#### A. Proposed power degradation model

Usually a linear-shaped power loss is assumed for outdoors degradation analysis and lifetime predictions. However, as reported by Jordan et al. (2017b), non-linearity of power loss is often observed in the field depending on the modules technologies or degradation modes. In their study, the effect of the different degradation curves, observed (approximately) in field performance on the levelized cost of energy (LCOE) was quantified using Monte Carlo simulation. Köntges et al. (2014) also reported that, the loss in power can take different shapes, for example the following categories: exponential-shaped, linear-shaped, steps degradation and saturating power loss over time. A simplified non-linear power degradation model that can optimize most these degradation shapes has been proposed as;

$$\frac{P(t=t)}{P_{Initial}} = 1 - \exp\left(-\left(\frac{\Gamma}{R_{Di}.t}\right)^\mu\right) \quad (3.10)$$

where  $P(t=t)$  and  $P_{Initial}$  are the module output power at time t and the initial output power, respectively.  $\Gamma$  is the power susceptibility, which is assumed to be a material property,  $\mu$  is the shape parameter and  $R_{Di}$  is the degradation rate constant of degradation process  $i$  or the total degradation rate.

#### B. Failure time function

The failure time (FT) is defined in this study as a 20% loss of the nominal power (common manufacturer's warranty). Using equations (3.8) and 3.10, the failure time can be derived as:

$$FT = \frac{\Gamma}{R_{DT} \cdot (|\log(0.2)|)^\frac{1}{\mu}} \quad (3.11)$$

### 3.1.3 Experimental part

In order to calibrate and valid the models, two sets of experiments where carried out; first using indoor accelerated ageing tests and second, using outdoor monitoring tests.

#### A. Experimental: Indoor accelerated aging

Distributed damp heat (DH), thermal cycling (TC) and combined DH-UV stress tests were carried out at different test conditions as shown in 3.2. The condition are varied because one set is used for model calibration and the other set is used for model validation. Table 3.3 shows the time steps and the measured power degradation at the different applied test conditions. The tested modules are from the same manufacturer with p-type homo-junction crystalline silicon (c-Si) cells, with a thermoplastic encapsulant material and no aluminum layer as additional moisture barrier.

Table 3.2: Experimental conditions for DH, combined UV/DH and TC tests

Test conditions		
Experimental	Test conditions for model calibration	Test conditions for model validation
DH	$75^{\circ}\text{C}/85\%RH$ (6500 hours)	$85^{\circ}\text{C}/85\%RH$ (6500 hours)
UV/DH	$180\text{W}/\text{m}^2/65^{\circ}\text{C}/55\%RH$ (4000 hours)	$180\text{W}/\text{m}^2/85^{\circ}\text{C}/55\%RH$ (4000 hours)
TC	$-40^{\circ}\text{C}/40^{\circ}\text{C}$ (3500 cycles)	$-40^{\circ}\text{C}/85^{\circ}\text{C}$ (1200 cycles)

Table 3.3: Time steps and measured power degradation at different test conditions

DH: $75^{\circ}\text{C}/85\%RH$										
Time steps[hours]	0	2000	4000	5000	5500	6000	6500			
Normalized power	1.000	0.991	0.967	0.993	0.986	0.990	0.987			
DH: $85^{\circ}\text{C}/85\%RH$										
Time steps[hours]	0	500	1000	1500	2000	2500	3000	3500	4000	
Normalized power	1.000	1.000	0.995	0.991	0.991	0.983	0.977	0.953	0.944	
UV/DH: $180\text{W}/\text{m}^2/65^{\circ}\text{C}/55\%RH$										
Time steps[hours]	0	2000	2500	3000	3500	4000				
Normalized power	1.00	0.976	0.972	0.964	0.953	0.945				
UV/DH: $180\text{W}/\text{m}^2/85^{\circ}\text{C}/55\%RH$										
Time steps[hours]	0	2000	2500	3000	3500	4000				
Normalized power	1.00	0.984	0.960	0.928	0.872	0.845				
TC: $-40^{\circ}\text{C}/40^{\circ}\text{C}$										
Cycle steps	0	2000	2010	2050	2100	2600	3000	3200	3400	3600
Normalized power	1.00	0.979	0.978	0.975	0.976	0.926	0.968	0.972	0.975	0.960
TC: $-40^{\circ}\text{C}/85^{\circ}\text{C}$										
Cycle steps	0	200	400	600	800	1000	1200			
Normalized power	1.00	0.965	0.957	0.941	0.937	0.920	0.888			

## B. Experimental: Outdoor monitoring

To clearly assess the effect of combined climatic stresses on performance degradation, three identical experimental mono-crystalline silicon (mc-Si) modules are exposed and under monitoring in three climatic zones, maritime in Gran Canaria, Spain; arid in Negev, Israel; and alpine in Zugspitze, Germany (see Figure 3.3). At each test site, the electrical performances and climatic conditions are under monitoring at high time-resolution. In Gran Canaria, the tilt angle is  $23^{\circ}$ , and the azimuth angle is  $169^{\circ}$  of PV modules. In the Negev the tilt angle is  $31^{\circ}$ , and the azimuth angle  $180^{\circ}$  for PV modules. The module in Gran Canaria has been exposed for over 7 years and the ones in Negev as well as in Zugspitze have been exposed over 5 years. A more detailed descriptions focusing on the test sites and categorization of weathering stresses for PV modules in Koehl et al. (2011, 2018). Apart from the electrical performance measurements, the modules temperatures are also recorded every 10 minutes. The sensors for measuring modules temperatures are located under one of the central cells. They are Pt100 sensors, which are attached from the back using adhesive aluminum tapes. Other meteorological data such as: relative humidity, global irradiation, UV irradiance and wind speed are also under monitoring in all the three zones with a one minute resolution. Figure 3.4 shows the temperature distribution



Figure 3.3: The outdoor test facilities: Alpine: Zugspitze, Germany; Desert: Negev, Israel; and Maritime: Gran Canaria, Spain.

in the three locations, the annual averages of UV dose and RH as well as the performance measurements of ( $P_{max}$ ).

### C. Data processing of the three location

An irradiance filter between ( $800-1200 \text{ W/m}^2$ ) is used for all locations and the power is corrected to standard test conditions (STC) of irradiance. The irradiance bin ensures that only clear sky conditions were considered in order to have irradiance conditions near to STC and to model a common situation for all the climates. The temperature filter applied varied from location to location depending on the most frequent temperature that a module experiences over its lifetime in each location (see figure 3.4). Foreexample a temperature filter between ( $30^{\circ}\text{C}-35^{\circ}\text{C}$ ) is used for Gran Canaria, ( $35^{\circ}\text{C}-45^{\circ}\text{C}$ ) for negev and ( $5^{\circ}\text{C}-25^{\circ}\text{C}$ ) for Zugspitze. To make sure that the power degradation observed for outdoor modules are not due to soiling effects, periodic cleaning of the modules is done. To avoid seasonal effects in climatic variables evaluation, five years data is averaged to calculate the models input values (see table 3.4). Indeed, this ensures that, the values used in degradation prediction correspond to what a module will experience during its lifetime. The mean value of the module minimum and maximum temperature has been computed considering upper and lower temperature bins as in figure 3.4 C. This also ensures that extreme values corresponding to measurement anomalies are not used in degradation rates calculations.

#### 3.1.4 Global climate data processing

The studies over large geographical regions can be made by processing global gridded data estimated from NWP including satellite or reanalysis models [Urraca et al. \(2018\)](#). Even

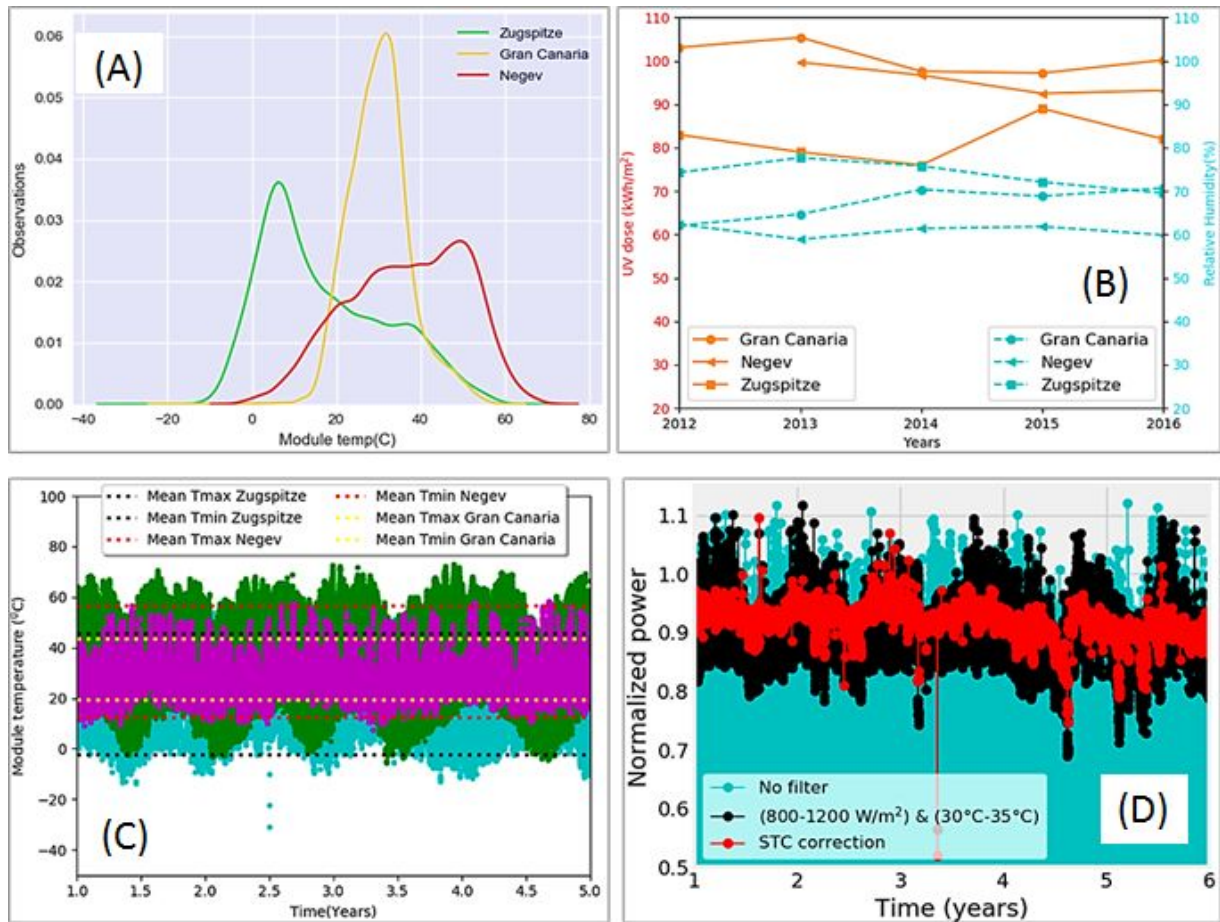


Figure 3.4: (A): Distribution of module temperature in the three climatic zones. (B): Total UV dose and average annual relative humidity for the three zones measured for 5 years. (C) : Ten minutes values of module temperature for 5 years. The dotted lines show the mean maximum and minimum temperatures. (D) : Raw and filtered power measurements in Gran Canaria, Spain. In cyan is the power raw data (before applying filters), in black is the data after applying the irradiance and temperature filters and in red is the data after STC correction.

Table 3.4: Summary of 5 years average climatic inputs used in simulation.

Input parameters						
Location	RH [%]	$T_m$ [°C]	UV [kWh/m <sup>2</sup> ]	$T_{max}$ [°C]	$T_{min}$ [°C]	
Negev	61.0	36.8	87.7	56.7	12.7	
Canaria	68.0	30.6	101.0	43.6	19.6	
Zugspitze	74.0	18.7	81.0	44.7	-2.30	

though satellite-based estimations can be more accurate than the reanalysis-based ones, the advantage of the second is the possibility to extract all the essential variables together in the same data-set, without gaps and identical timestamps.

In this research, the ERA5 climate reanalysis data-set (C3S) (2017) was processed to extract and model the climatic stresses necessary for the degradation rate evaluation. This dataset provides a spatial resolution of 31 km and temporal resolution of hourly data from 1979. The estimated climate data is compared and validated with real ground measure-

ments taken from the World Radiation Monitoring Centre - Baseline Surface Radiation Network (WRMC-BSRN) [Driemel et al. \(2018\)](#) (the validation procedure is described in the annex). Although not all variables required are directly available from the ERA5, we calculate the missing local climate variables, WS, RH and UV irradiance from existing models as described below. The derived maps are presented in the annex.

### A. Evaluation of relative humidity

The relative humidity is not extracted directly from ERA5, so it is estimated using equations 3.12 and 3.13. The saturation water vapour pressure (WVP) over water and ice is calculated using the Buck's formula [Buck \(1981\)](#) from the dew point temperature ( $T_{Dew}$ ) and ambient temperature ( $T_{amb}$ ):

$$WVP(T)[kpa] = \begin{cases} 0.61115 \cdot \exp\left(23.036 \frac{T}{333.70}\right) \cdot \left(\frac{T}{279.82+T}\right) & \text{for } T < 0 \\ 0.61115 \cdot \exp\left(18.678 \frac{T}{234.84}\right) \cdot \left(\frac{T}{257.14+T}\right) & \text{for } T \geq 0 \end{cases} \quad (3.12)$$

$$RH[\%] = \frac{WVP(T_{Dew})}{WVP(T_{amb})} \cdot 100[\%] \quad (3.13)$$

### B. Evaluation of UV

Regarding the UV irradiation, although this variable is included in the ERA5 dataset, it considers a wavelength-range up to 440 nm. In our case, the effective UV irradiance covers up to 400 nm, since that is a typical average value where encapsulates change the transmittance properties [Miller et al. \(2015\)](#). For this reason, we neglect the UV irradiance given by ERA5, and model it using a formula proposed by [Crommelynck and Joukoff \(1990\)](#) as expressed in equations 3.14-3.17. It is based on the clearness index ( $c_i$ ) and the global horizontal irradiance (GHI). The  $c_i$  is calculated by dividing the GHI and the top-of-atmosphere irradiance extracted from ERA5. Unfortunately, the lack of valid measurements disallows us to do a benchmarking of UV models.

$$c_i = \max(0.1, \min(c_i, 0.7)) \quad (3.14)$$

$$UV_B = (1.897 - 0.860 \cdot c_i) \cdot 1e^{-3} \cdot GHI \quad (3.15)$$

$$UV_A = (7.210 - 2.365 \cdot c_i) \cdot 1e^{-2} \cdot GHI \quad (3.16)$$

$$UV = UV_A + UV_B \quad (3.17)$$

### C. Evaluation of wind speed (WS)

The WS is a parameter of interest in this study because it is used to estimate the PV module temperature ( $T_m$ ) due to the related cooling effect of materials. The WS is calculated and height corrected according to equation 3.18 and equation 3.19 [Huld and Amillo \(2015\)](#), where  $\hat{u}_{wind}$  and  $\hat{v}_{wind}$  are the vector components of the wind,  $h_{ERA}$  is the height from ground which the wind is modelled in the ERA5 dataset, and  $h_{ERA}$  is the assumed height of the PV modules equal to 2 meters. The 2 meters height assumed are in accordance with

the height of modelled ambient temperature ( $T_{amb}$ ) and dew point temperature ( $T_{Dew}$ ) given by ECMWF.

$$WS_{ERA} = \sqrt{\hat{u}_{wind}^2 + \hat{v}_{wind}^2} \quad (3.18)$$

$$WS = \left(\frac{h_{mod}}{h_{ERA}}\right)^{0.2} \cdot WS_{ERA} \quad (3.19)$$

#### D. Modelling module temperature

The module temperature is the most effective parameter in degradation rate evaluation, since the rate models are built on the assumption that, the degradation follows an Arrhenius temperature dependence. In most cases, the module temperature is estimated from, ambient conditions of temperature, irradiance and wind speed using a number of different models proposed by Kratochvil et al. (2004), Segado et al. (2015), Faiman (2008). In this research the Faiman model (equation 3.20) is selected for module temperature evaluation because it has been reported that, it provides a good accuracy under different climate conditions for crystalline silicon PV modules Faiman (2008); Schwingshackl et al. (2013) The model estimate the PV module temperature as a function of the GHI, WS and  $T_{amb}$  as:

$$T_m = T_{amb} + \frac{GHI}{u_0 + u_1 \cdot WS} \quad (3.20)$$

where  $u_0$  is a coefficient describing the effect of the radiation on the module temperature ( $W^0Cm^2$ ) and  $u_1$  describes the cooling by the wind ( $Ws^0Cm^2$ ). In this research, the values of  $u_0 = 26.9$  ( $W^0Cm^2$ ) and  $u_1 = 6.2$  ( $Ws^0Cm^3$ ) according to Huld and Amillo (2015). The presented calculations consider an open-rack flat mounting configuration for the PV modules at all locations. However, the installation over rooftops or any other surface and the re-positioning can increase the thermal stress due to higher reception of photons from the sun or more circulation of air.

#### 3.1.5 Statistical error analysis methods

To analyse how well a set of data points fit with a given model, the residual standard deviation as a measure of a goodness-of-fit is used. Given that,

$$Residual = Y_m - Y_f \quad (3.21)$$

The residual standard deviation ( $SD_{res}$ ) is expressed as:

$$SD_{res} = \sqrt{\frac{\sum(Y_m - Y_f)^2}{n - 2}} \quad (3.22)$$

where  $Y_m$  measured value,  $Y_f$  fitted value and  $n$  number of data points.

To check the prediction accuracy and to evaluate the uncertainties of the model, the percentage mean square error of prediction (MSEP) is used according to McKay et al. (1999) as:

$$MSEP = 100 \times \left[ V[P_p] + (\mu_{pp} - \mu_{pm})^2 \right] \quad (3.23)$$

Where  $V[P_p]$  is the variance of predicted power,  $\mu_{pp}$  and  $\mu_{pm}$  are the mean of predicted and measured power respectively.

## 3.2 Methodology for data-driven model

Different from the physical model presented in the previous section, here a data-driven methodology for long-term degradation forecast is described. In this approach, the lifetime forecast is based on the existing degradation history observed in the field and not on the climatic stress factor. The schematic figure 3.5 summarises the methodology.

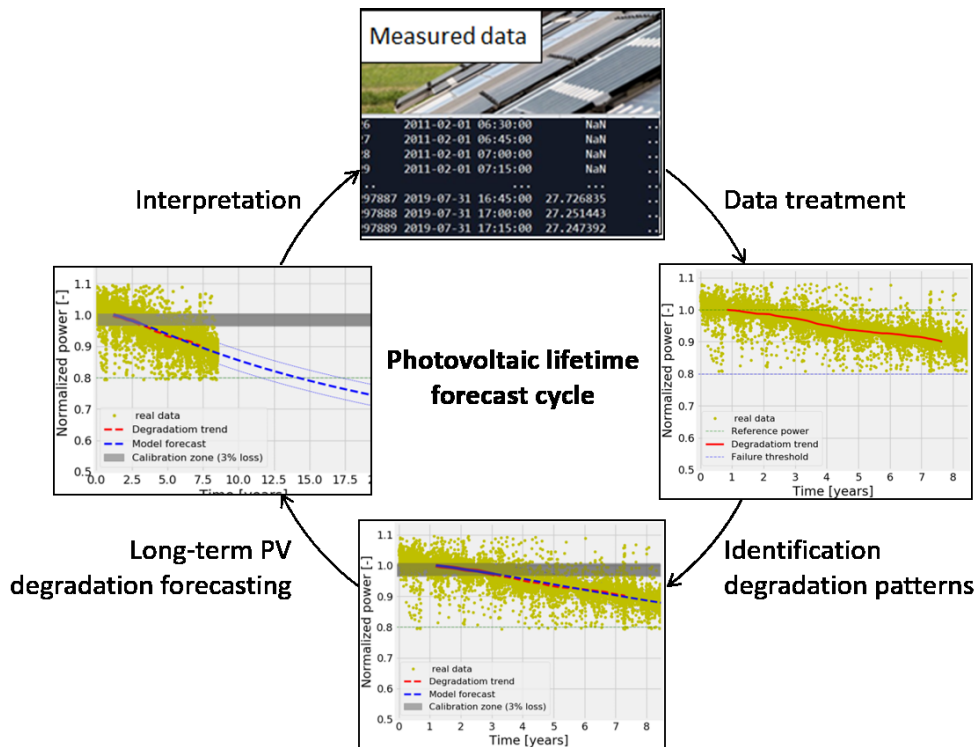


Figure 3.5: Illustration of the overall objective of the data-driven methodology. The major steps are; data treatment, identification of degradation pattern and selection of the best degradation model for long-term forecast

### 3.2.1 Background

The ever-growing secondary market of PV systems (that is, the transaction of solar plants ownership) calls for reliable and high quality long-term PV degradation forecasts to mitigate the financial risks. Data-driven techniques that utilize monitored operational data related to system's performance are used in many fields, for example in the aircraft industry [Zhang et al. \(2018\)](#); [Listou Ellefsen et al. \(2019\)](#) to forecast the future trend or the remaining useful lifetime. They are normally applied to complex systems where developing a physical model could be more complex and expensive.

For PV applications, a few authors have proposed data-driven prognosis models to evaluate the remaining useful lifetime of PV modules. For example, Laayouj et.al [Laayouj et al. \(2016\)](#) proposed a smart prognostic method for PV module health degradation and remaining useful lifetime prediction. The model is based on two approaches; the on-line diagnosis and data-driven prognosis. Also, Sheng et al [Sheng et al. \(2019\)](#) proposed an autoregressive moving average model-filtered hidden Markov model to predict the residual life for complex systems with multi-phase degradation. They applied the model to predict

the residual life of a specific PV module system. Although both methods are reported to provide good predictions, the biggest drawback of these methods is that their performances are not rigorously validated or analysed with different degradation datasets. Both methods are calibrated, validated and applied based on a single PV module or system dataset. Moreover, for the later, the methodology was applied to simulated performance measurements for its reliability evaluation and residual life prediction. PV modules can exhibit different degradation scenarios [Köntges et al. \(2014\)](#) especially due to different technologies, different failure modes as well as different operating local climates. Therefore, it is very unlikely that a model calibrated and validated on a single dataset can be generalized to apply to other degradation scenarios. In this regard, we propose a model based on a rigorous analysis of degradation data of several PV modules as well as systems of different technologies and installed in different locations. Hence the proposed model is aimed to be generalized to the different degradation scenarios. Also related work is that of [Rizzo et al. \(2018\)](#) where an algorithm for lifetime extrapolation, prediction, and estimation was proposed. However, their algorithm is proposed only for emerging PV technologies and for shorter time forecasts.

Generally, in spite of the recognized potential of empirical data-driven techniques for time series forecast, limitations still exist for their application in long-term PV degradation evaluation. Different factors such as outliers in the dataset, seasonal variations and many other reducing factors (e.g. soiling) should be separated from long-term non reversible degradation. The lack of a systematic and flexible approach to select parameters of these techniques and their black-box character limit the understanding and control of their performance. We address this issue by proposing a systematic and flexible approach with adjustable model parameters to evaluate the degradation trend based on the nature of the dataset under evaluation. The proposed method aims to evaluate the irreversible long-term degradation of PV modules as well as systems. To achieve this we propose an iterative algorithm for degradation trends evaluation that allows to separate seasonal variations and other reversible performance reducing effects from irreversible degradation.

Another drawback of the available data-driven techniques is their accuracy when long-term predictions are required after a short time interval and with limited data points. For example, [Taylor and Letham \(2018\)](#) performed a comparison of the forecasting accuracy of different statistical models at different time horizons. In their study, most models displayed large uncertainties when applied after shorter time interval. Indeed, the available techniques are based on fitting the available systems degradation data using regression models and then applying a simple extrapolation to forecast the lifetime. However, in practice, the system's degradation history available may be short and incomplete, and a simple extrapolation could lead to large uncertainties hence degrading the reliability of the forecasts. To address this challenge, the proposed model is aimed at improving the long-term forecasting accuracy using a small degradation history and few data points. To achieve this, we propose a new concept using time dependent degradation factor for degradation extrapolation instead of using a simple extrapolation for lifetime forecast. To further improve the accuracy and to have a generalized model, the concept of multiple degradation factor models dependent on degradation patterns is proposed.

### 3.2.2 Modelling assumptions

To begin with, the concept of the proposed data-driven model is based on the work reported by [Jordan et al. \(2017\)](#), that associating specific degradation and failure modes with specific time series behavior can aid in service life prediction. Based on

this understanding, our model is based on analysing time series degradation patterns to extracted different parameters (see Figure. 3.6).

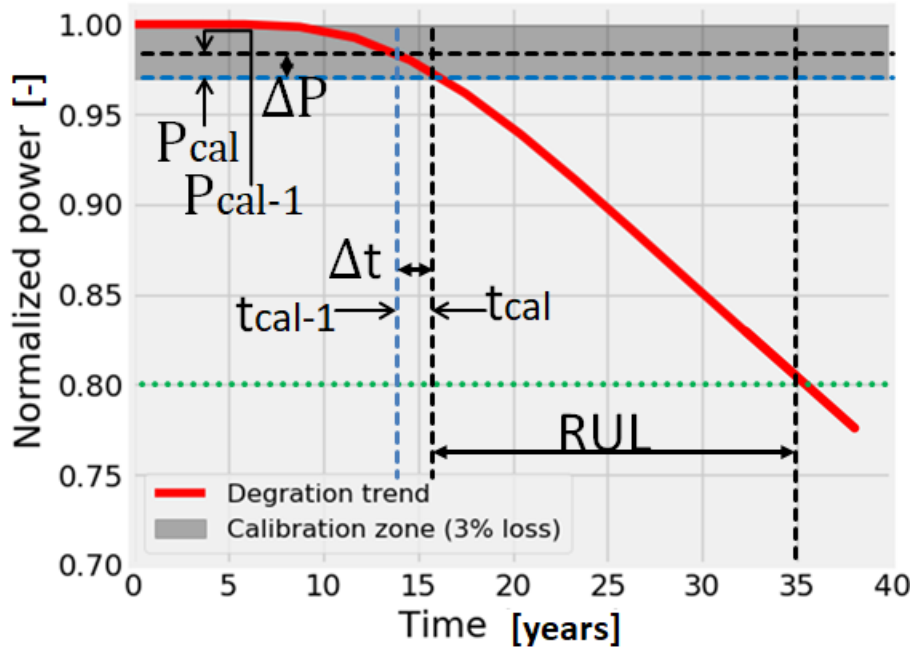


Figure 3.6: Illustration of the different degradation pattern parameters extracted during calibration and the remaining useful lifetime (RUL)

The extracted parameters are then used to formulate degradation rate functions. In developing the model, we also use the following assumptions:

- Different degradation modes might cause differences in degradation patterns meaning that it is unlikely that a single degradation function can represent all expected degradation patterns. Therefore the approach depends on multi-degradation rate functions.
- Some degradation modes might be triggered by other degradation modes and might appear at certain stages of a module's lifetime, meaning that using a constant degradation rate extracted at a given stage of PV operation to represent the entire lifetime could affect the forecast accuracy. Therefore, time dependent degradation rates are proposed. Moreover, the usage of degradation factor is preferable to degradation rate since we consider a non-linear degradation with a non-constant degradation rate.

### A. "Time and degradation pattern" dependent models

Taking the aforementioned assumptions into consideration, we propose different degradation factor models dependent on time and degradation pattern. The degradation factor models are expressed as:

$$k_1 = k_{cal} \left( 1 + A_1 \cdot k_{cal} \cdot \ln \left( \frac{1}{\Delta P} \right) \cdot \tau_1^{y_1} \cdot \tau_2^{x_1} \cdot \rho^{z_1} \cdot t \right) \quad (3.24)$$

$$k_2 = k_{cal} \left( 1 + A_2 \cdot k_{cal} \cdot \left( \frac{1}{\tau_1} \right) \cdot \rho^{z_1} \cdot t \right) \quad (3.25)$$

$$k_3 = k_{cal} \left( 1 + A_3 \cdot k_{cal} \cdot \ln \left( \frac{1}{\Delta P} \right) \cdot \left( \frac{1}{\tau_1} \right) \cdot \tau_2^{x_1} \cdot \rho^{z_1} \cdot t \right) \quad (3.26)$$

Table 3.5: Definition of coefficients and parameters

Coefficients and parameters	Definitions
$t_{cal}$	Time at calibration threshold
$P_{cal}$	Power at $t_{cal}$
$SD_{P_{cal}}$	Standard deviation of calibrated data
$\tau_1 = \sqrt{\max(t_{cal})}$	-
$\tau_2 =  \ln \Delta t  =  \ln(t_{cal} - t_{cal-1}) $	-
$\rho = \ln \left( \frac{1}{SD_{P_{cal}}} \right)$	-
$A_1$ [ $year^{-3/2}$ ], $A_2$ [ $year^{-1/2}$ ] and $A_3$ [ $year^{-1/2}$ ]	Proportionality constants
$y_1$ , $z_1$ and $x_1$	Optimization parameters

It should be noted that, these models are purely empirical without any physical implication, they are derived from degradation pattern parameters shown in figure 3.6 as they describe well the specific degradation patterns. It is also important to note that the model parameters are extracted after an initial 3% performance degradation threshold. The 3% optimization threshold is calculated from the degradation trend that excludes early degradation effects. The reasoning for using a 3% threshold are further described and demonstrated in the results section.

## B. Power degradation model

The power degradation function proposed in section 3.1, equation (3.10) is used to fit the degradation data also in this part. However, since the evaluation is independent of material properties evaluation or analysis, the model parameter  $\Gamma$  is fixed to one. Therefore, the power degradation function can be re-written as:

$$\frac{P(t=t)}{P_{Norm}} = 1 - \exp \left( - \left( \frac{1}{k_{cal} t} \right)^\mu \right) \quad (3.27)$$

where  $P_{Norm}$  is the maximum power of the degradation trend and  $k_{cal}$  is the degradation factor [ $a^{-1}$ ] at calibration. In this case the degradation factor is preferred for use instead of the degradation rate because of the non-linearity of the power degradation and non-constant degradation.

### 3.2.3 Modeling approach

#### A. Failure time and remaining useful lifetime definitions

Chen Xiongzi et al [Chen Xiongzi et al. \(2011\)](#) defined the RUL of a system or a component as the length from the current time to the end of its useful life. The question is how to define the "useful life". In this study the useful life is defined as the non-reversible performance loss such that the module or system power decreases by 20% of the "maximum stable power" measured in the field. The notion of a maximum stable power is introduced to separate long term degradation from early stage degradation events such as light induced degradation (LID) for p-type crystalline silicon modules [Köntges et al. \(2014\)](#) or light and

elevated temperature induced degradation (LeTID for multicrystalline silicon and modules with passivated emitter and rear cell (PERC) Kersten et al. (2017); Philipp et al. (2019). It also helps to separate other reversible effects reducing module performance such as soiling Zorrilla-Casanova et al. (2013) and seasonal variations Cañete et al. (2014). Moreover, due to these effects and variation of the outdoor conditions, the power printed on the PV module label substantially deviates from the initial PV module power outdoors. From our point of view, the maximum stable power can be easily compared among systems and is describing the system performance well which is not necessarily the case for the nominal power. The nominal power of a PV module/system may deviate substantially from the real power since it is recorded under STC. These well defined conditions of  $1000 \text{ W/m}^2$  and  $25^\circ\text{C}$  are almost never prevalent as shown in the histogram in figure 3.7b.

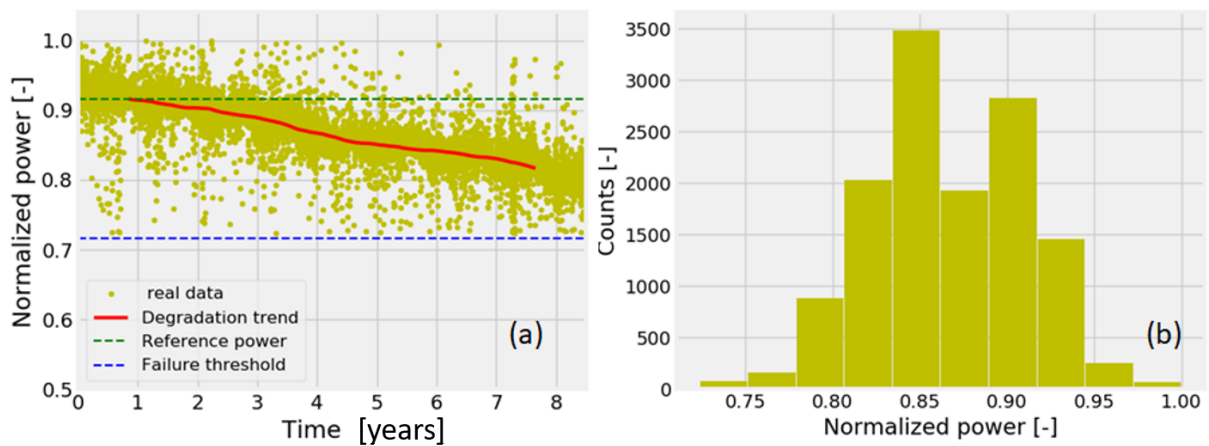


Figure 3.7: A, Illustration of the stable power (red line) used in this study, the green dotted line is "maximum stable power" (reference power) and the blue dotted is the failure time threshold. B, Histogram of the data distribution throughout the 8.5 years

Although, the term failure time has already been defined in subsection 3.1.2 it is re-defined here accordingly to the context. In this study, we therefore, define the FT as a reduction in the module or system performance by 20% of the maximum stable power (indicated by the green dotted line in figure 3.7). The 20% loss is purely arbitrary and it is used in this case because of its consistence with the warranties given by manufacturers. It might be interesting to predict the module or system performance for its entire lifetime (until the module stops working), however, such a prediction could be more unreliable and unrealistic since certain future events are unpredictable. Moreover, the longer a module stays in the field the more sensitive it becomes to different degradation modes. That might lead to a dramatic increase in the degradation rate which cannot be easily modeled. Therefore, according to FT definition, the RUL is the length between the current time (CT) to the FT and can be expressed as:

$$RUL = FT - CT \quad (3.28)$$

### 1. Data filtering

The first filter applied to the input dataset is an irradiance filter. The upper limit for irradiance was set and fixed at  $1200 \text{ W/m}^2$  and the lower limit was chosen flexible between  $600\text{-}900 \text{ W/m}^2$  depending on the location under evaluation. This clear sky filter is used as a way to separate low performances due to low irradiance from degradation. The filtered

power is then corrected to STC of irradiance by applying a linear correction of power to 1000 W/m<sup>2</sup> irradiance. The second step is to remove outliers. Because of the stochastic behavior of outdoor conditions and anomalies in the measuring equipment, data measured from outdoor PV modules as well as systems is usually subject to outliers. When not treated well, Outliers might lead to large uncertainties, especially in degradation trend evaluation. The outliers are removed by computing the standard deviation (SD) around the mean value of the entire dataset, whereby all points that are out of the range of ( $Mean \pm 2 \times SD$ ) are eliminated. For LID or LeTID sensitive systems, it is a crucial step to analyse the degradation pattern during the first year of operation. These degradation modes are characterized by strong non-linear trends in the initial phase which might either stabilize gradually or undergo a regeneration phase Kersten et al. (2017); Philipp et al. (2019). If the regeneration phase is detected, we recommend to eliminate the data until the onset of this phase.

## 2. Data decomposition

Time series data is characterized by four major components; level, trend, seasonality, and noise. There are two models that are used to model the effects of these components; additive (linear) and multiplicative (non-linear) Brownlee (2017). In our case a multiplicative model is used. The model suggests that the components are multiplied together as follows:

$$y(t) = Level \times Trend \times Seasonality \times Noise \quad (3.29)$$

This function is implemented and available for free use in the python library. The function uses a moving average (MA) method to extract a degradation trend in the time series data. The averaging depends on the required resolution (weekly, monthly or yearly) of one's interest and it determines the extracted degradation trend in this case.

In outdoor conditions seasonal and other different effects can reduce the performance of a PV module or system. For non-reversible performance degradation evaluation it is crucial to choose a good averaging temporal interval that eliminates seasonality and other reversible effects. It has been reported that reversible effects such as inverter failures and soiling of PV modules have a higher impact on performance loss rates than the actual performance degradation which is non-reversible Klünter et al. (2019). These effects could be module technology dependent, for example Virtuani et al. Virtuani et al. (2015) reported that amorphous silicon (a-Si) systems are more affected by variations in the incident spectrum than crystalline silicon (c-Si) systems because of their narrower spectral sensitivity. Therefore, it is important to separate these performance reducing effects from long term degradation by choosing a good averaging temporal interval. The selection of a good temporal interval could be very tedious if one has to do it manually. An iterative algorithm has been implemented to assist in determining a proper interval for degradation trend evaluation depending on the datasets being evaluated.

## 3. Iterative algorithm for degradation trend evaluation

One way to completely remove any variation in the degradation trend will be to apply a strict constraint, which removes the difference between each  $n^{th}$  and  $(n + 1)^{th}$  value of the trend that is greater or equal to zero, that is;  $trend[n - (n + 1)] \geq 0$ . However, according to the stochastic behavior of outdoor conditions, outdoor measurements usually contain unavoidable outliers which can appear even after applying certain filters. This implies that applying such a strict condition to outdoor datasets is quite unrealistic; in most cases this

condition is not fulfilled or might require a considerable amount of computation time to converge depending on the nature of the dataset. Therefore, a tolerance ( $tol$ ) is introduced and the condition is applied as:

$$trend \left[ \left| \frac{\max(dn) - \min(dn)}{\min(dn)} \right| \right] \leq toll, \text{ for: } dn = n - (n + 1) \quad (3.30)$$

The process begins by initialising the temporal interval by: initial temporal interval = 2% of the total length of the time series. Afterwards, the iterative loop is repeated until the condition in 3.30 is fulfilled. The tolerance depends on the nature of the dataset under investigation, for example it can be correlated with the resolution of the data or the magnitude of outliers in the datasets. This makes the process of temporal interval selection a quasi-automated process. By analyzing a number of datasets, a range of  $tol$  values can be set granting the flexibility for application on broad datasets of the different distributions.

### 3.2.4 Experimental

Different data-sets for PV modules as well as systems that have been exposed for quiet a long period of time with considerable degradation were used in this study. The data-sets are from three different sources:

1. The first set of data are those of the TICino SOLare (TISO)-10-kW PV plant in Lugano (Switzerland) [Virtuani et al. \(2019\)](#); [Annigoni et al. \(2019\)](#). The TISO-10 PV system has been connected to the grid since 1982, and is the oldest installation of this kind in Europe (We shall refer to them as "TISO-Modules" here after). The performance (i.e. current-voltage curves) of 18 selected reference modules were measured at regular intervals between 1982 and 2017. After 35 years in the field, these modules show a degradation rate ranging from -0.2 to -0.7%/year considering a  $\pm 3\%$  measurement uncertainty. In this study 10 of the 18 modules with a considerable degradation have been used in module calibration and validation stages.
2. Another source of data is a PV plant installed at the airport of Bolzano/Italy (position ca. 46.46 N, 11.33 E, elevation: 262 m) including 11 experimental PV systems, which are in operation for 8.5 years and covering the time period from 01 February 2011 until 31 July 2019. They are referred to as "Bolzano systems". Most major PV system technologies are included, namely one and three junction amorphous silicon (a-Si), cadmium telluride (CdTe), CIGS, silicon solar cells made out of a heterojunction with an intrinsic thin layer (HIT), mono-crystalline silicon (mc-Si), poly-crystalline silicon (pc-Si) and poly-crystalline silicon string ribbon (ribbon). All systems are part of one experimental PV plant, they are ground mounted with an orientation of  $8.5^{\circ}$  west of south and a fixed tilt of  $30^{\circ}$ . The installed nominal power for the systems range from 1 to 4 kWp per individual installation. According to a new PV sensitive climate classification, proposed by Ascencio-Vázquez et al. [Ascencio-Vázquez et al. \(2019\)](#), the climate in Bolzano is categorized as a temperature climate with medium irradiation. The irradiance is measured with a Kipp & Zonen CMP11 pyranometer. Calibrations are performed in regular intervals and the measurement uncertainty is between 2% and 4%. Additionally, climate data are taken from a ground based meteo-station installed in close proximity to the test side.
3. Finally, data from the Desert Knowledge Australia Solar Centre (DKA Solar Centre) [DKASC \(2019\)](#), named hereafter as "DKA systems", are used. The data can

be downloaded through <sup>1</sup>. The data sets used in this study are given as monthly yield in kWh of three different systems; Kyocera-5.4kW-Poly-Si Dual (2008), eco-Kinetics-26.5kW-mono-Si-Dual (2010) and trina-23.4kw-mono-dual (2009). For the first system (Kyocera), data from 01 January 2009 to 01 December 2018 was used in the analysis, for the eco-Kinetics system from 01 January 2011 to 01 December 2018 and for the Trina system, data from 01 January 2014 to 01 June 2019. More information about these systems and datasets are available on the DKA Solar Centre website. It should be noted that the data plotted here have been normalized to the maximum power and were subject to the outlier filters described in the previous section.

### 3.2.5 Statistical errors analysis

The error measurement employed for the performance evaluation of the proposed forecasting method is the root mean square error (RMSE). Given a measured ( $m$ ) and a predicted ( $p$ ) value, respectively, for a given quantity and number of observations ( $n$ ), the RMSE is expressed as.

$$RMSE = \sqrt{\frac{\sum_{j=1}^n (p_i - m_i)^2}{n}} \quad (3.31)$$

The metric deployed to compare the performance of the proposed method with other methods is the relative difference. This is a relative comparison of the failure time forecasted after a 3% interval and on the full dataset. It is expressed as,

$$Rel_{diff} = \frac{|FT_{3\%} - FT_{full}|}{\max(|FT_{3\%}|, |FT_{full}|)} \quad (3.32)$$

where,  $Rel_{diff}$  the relative difference is,  $FT_{3\%}$  and  $FT_{full}$  are the failure time evaluated after a 3% degradation and using the entire dataset respectively.

<sup>1</sup>DKA data download: <http://dkasolarcentre.com.au/locations/alice-springs/graphs?sources=91>

### 3.3 Methodology of a hybrid model

The described physical models is very useful when one need to correlate the predicted lifetime to the influencing climatic factors as well as dominating degradation mechanisms. However, one draw back is on the accuracy when it comes to long-term degradation prediction. And also, the described data-driven model could help to improve the long-term prediction accuracy, however, it provides no information about the influencing degradation mechanisms. A model that can provide more accurate long-term predictions as well as information of the dominating degradation mechanism is of great importance for financial evaluation as well as material development. In this regard, the two approaches are combined into a hybrid model to achieve these two aspects. The combination of the two approaches is illustrated in the schematic diagram (figure 3.8)

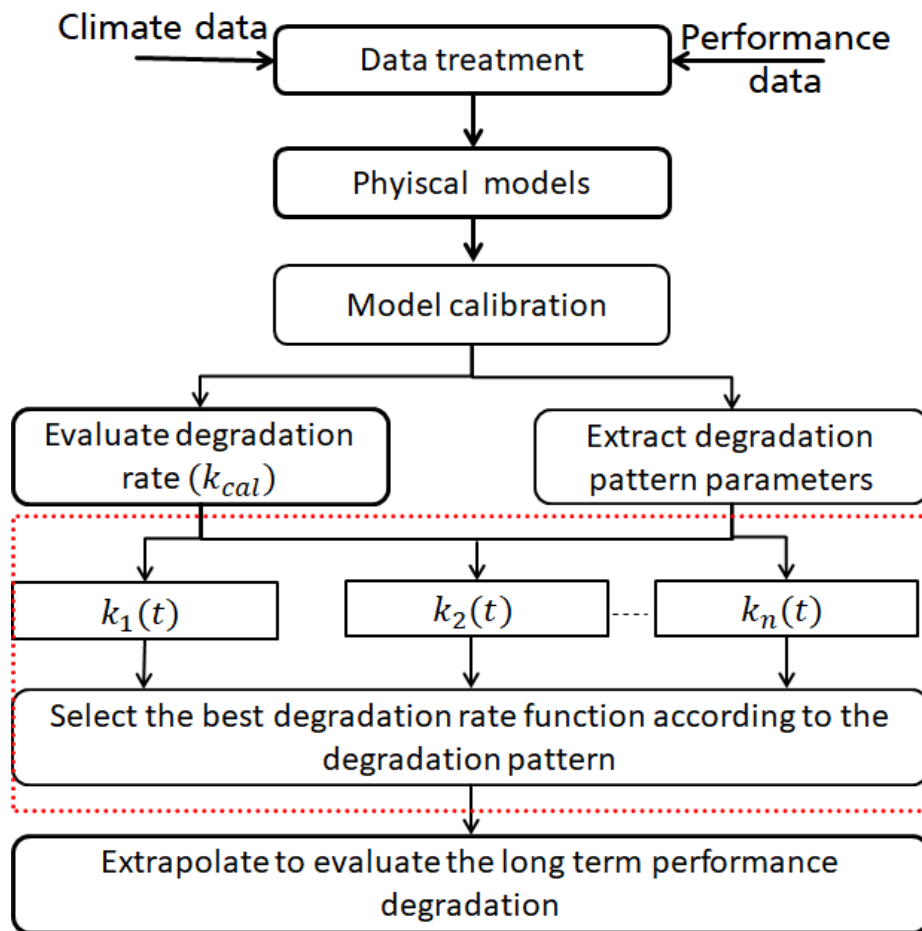


Figure 3.8: Flow chart illustrating the link between the physical and data-driven approach. The red dashed square is the data-driven part, we implement an algorithm to identify the degradation patterns and to select the appropriate rate function

Figure 3.8 illustrate the link between the physical and the data-driven approaches. The fundamental assumption in this link is that, the module experience the same degradation pattern in other geographical locations. This means that the degradation pattern parameters extracted in the training location can be applied in other locations to select the best degradation function for long-term predictions. Therefore, the differences are within the calculated degradation rate at calibration ( $k_{cal}$ ) which is dependent on the climatic stresses of a given location.

# Chapter 4

## Results and Discussion

Table 4.1: Chapter 4 Nomenclatures

Symbols	
$c_i$	clearness index [-]
$E_a$	activation energy [eV]
$k$	degradation factor [1/year]
$FT_{3\%}$	Failure time calculated using -3% degradation [year]
$FT_{full}$	Failure time calculated complete dataset [year]
$k_B$	Boltzmann constant ( $8.62 \times 10^{-5}$ eV/K)
$P_{max}$	power at maximum power point [W]
$R_D$	degradation rate [%/hour]
$Rel_{diff}$	relative difference
$SD_{res}$	residual standard deviation
$T_m$	module temperature [K]
$T_{mm}$	measured module temperature [ $^{\circ}C$ ]
$T_{mp}$	modeled module temperature [ $^{\circ}C$ ]
$(\mu)$	shape parameter [-]
Subscripts	
$cal$	calibration
$h$	hydrolysis
$p$	photo-degradation
$t$	thermo-mechanical
$T$	Total
Abbreviations	
AH	tropical with very high irradiance
AK	tropical with high irradiance
BH	desert with high irradiance
BK	desert with very high irradiance
KGPV	Köppen-Geiger-Photovoltaic
FP	Facebook prophet
MSEP	mean square error of prediction
PR	performance ratio
RUL	remaining usefull lifetime
STC	standard test conditions

In this chapter, the results of the physical model, data-driven model as well as for the hybrid model are presented and discussed respectively.

## 4.1 Results for the physical model

### 4.1.1 Properties of the proposed power degradation function

As already mentioned that, non-linearity of power loss is often observed in the field depending on the module technologies or degradation modes. And also that, the loss in power can take different shapes, for example: exponential-shaped, linear-shaped, steps degradation and saturating power loss over time. Moreover, since energy yield could highly depend on how the performance degradation evolves over time (see figure 4.1b), it is very crucial to choose a degradation model to take into account the different failure patterns. A simplified non-linear power degradation model proposed in this research aims to take into consideration these non-linearity dependencies of power degradation. To do this, a shape parameter  $\mu$  has been introduced to model all the degradation shapes as shown in figure 4.1a.

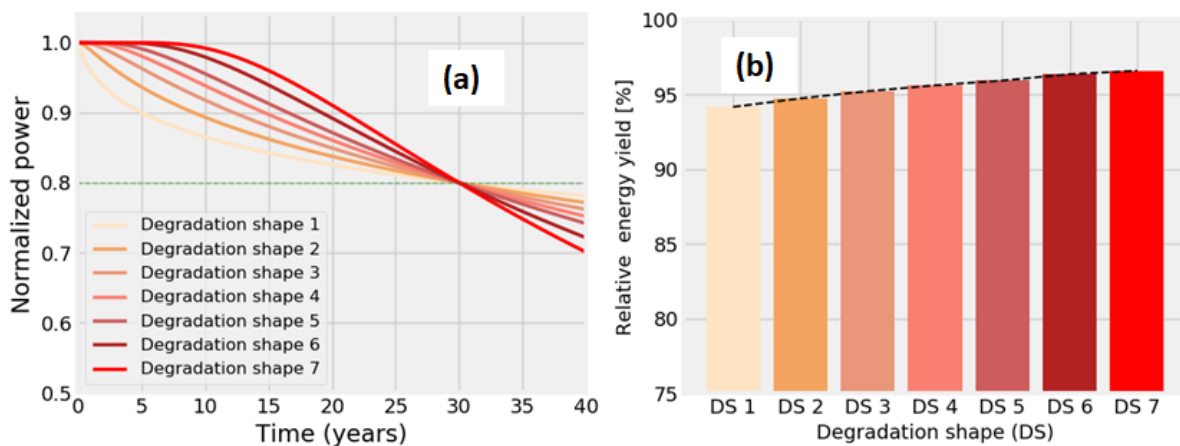


Figure 4.1: A) Optimization of power degradation shapes by altering the shape parameter  $\mu$  and B) Relative energy yield corresponding to the degradation shapes

Figure 4.1a shows the simulated degradation shapes 1-7 corresponding to different values of  $\mu = 0.1, 0.2, 0.3, 0.4, 0.5, 0.8$  &  $1.0$  respectively. On the one hand, when  $\mu = 0.1$  and  $\mu = 0.2$ , one can achieve the commonly observed degradation shape in thin film technologies with a faster degradation at early stages of exposure and followed by stabilization [Jordan et al. \(2017b\)](#). On the other hand, one can expect the degradation shape similar to that when  $\mu = 1.0$  for glass-glass modules if we speculate that for this module design there are less moisture pathways and moisture ingress compared to glass-backsheet modules. Therefore, the moisture induced degradation modes are slower at the earlier stages of the module lifetime. However, as the breathable pathways and drying are also limited, the moisture will accumulate over the years, leading to a dramatic increase in degradation rate.

### 4.1.2 Calibration and validation of the specific degradation rate models

Two basic approaches are applied for the calibration of the different degradation rate models: (a) optimization of model performances and (b) through prior knowledge from previous studies. Optimization of model performance, which compares measured and simulated data, is applied by the help of a built-in nonlinear least-squares solver in the GNU Octave software. Prior knowledge, with the aid of sensitivity analysis, is used as a baseline to select the initial fitting guesses and also as a confirmation that the extracted values are in a meaningful range.

To derive the model parameters, equations 3.2, 3.5 and 3.6 are fitted on experimental data from the indoor accelerated ageing tests at given specific test conditions as presented in chapter 3 table 3.2. The extracted parameters are presented in table 4.2 together with the percentage residual standard deviation ( $SD_{res}$ ) (see equation 3.22). To further ensure a better calibration procedure, in each case the distribution of the residuals is plotted and analysed (to check if the residuals follow a normal distribution). The parameter  $\Gamma$  of the power function in equation (3.10) has been normalized to one and the extracted shape parameter ( $\mu$ ) is 0.7 for hydrolysis, 0.4 for photo- and thermo-mechanical degradation in figure 4.2.

To validate the models, different sets of data measured at different test conditions (see table 4.2) are used and by using the extracted parameters the simulations are compared with the measured data points through evaluation of the mean square error of prediction (MSEP, see equation 3.23) as also presented in table 4.2. The MSEP is also used as a metric to correlate the uncertainties in model calibration with the predictions when compared with the  $SD_{res}$ . For example, a 0.5%  $SD_{res}$  led to 0.025% MSEP for the hydrolysis model, a 1.65%  $SD_{res}$  resulted into 0.216% MSEP for the thermo-mechanical model and 0.19%  $SD_{res}$  led to 0.168% MSEP for the photo-degradation model. Although, there is a correlation of the uncertainties due to model calibration as its evaluated in the thermo-mechanical model, the uncertainties in experimental data sets used for validation can also influence the evaluated mean square error therefore it's also useful to plot and interpret the results basing on the degradation trend. Evaluating a confidence interval of the prediction can also help to analyze the model performance.

Table 4.2: Extracted parameters for the three rate models and the percentage residual standard deviation ( $SD_{res}$ ) as well as the mean square error of prediction (MSEP)

Degradation rate model	Extracted models parameters					
	$A_i$	$E_a$ [eV]	$n$	$X$ & $\Theta$	$SD_{res}$	MSEP
Hydrolysis: Eq(3.2)	6.11e4	0.91	1.90	-	0.5%	0.025%
Photodegradation: Eq(3.5)	1.20e-3	0.43	1.80	0.63	0.2%	0.168%
Thermo-mechanical: Eq(3.6)	9.10e-5	0.40	-	2.24	1.6%	0.216%

Figure 4.2 shows calibration and validation results for the hydrolysis, photo-degradation and thermo-mechanical models (equations 3.2, 3.5 and 3.6) respectively. In black is the measured power for DH 75<sup>0</sup>C/85RH; red is the respective model fit with a violet line at 5000 hours representing the optimized data points. The blue line is the predicted power at DH 85<sup>0</sup>C/85RH, the light blue patch is the 95% prediction confidence interval and in green the measured power at DH 85<sup>0</sup>C/85RH, used for model validation. The vertical lines on measured data points indicate a 2.5% measurement uncertainty. The color usage

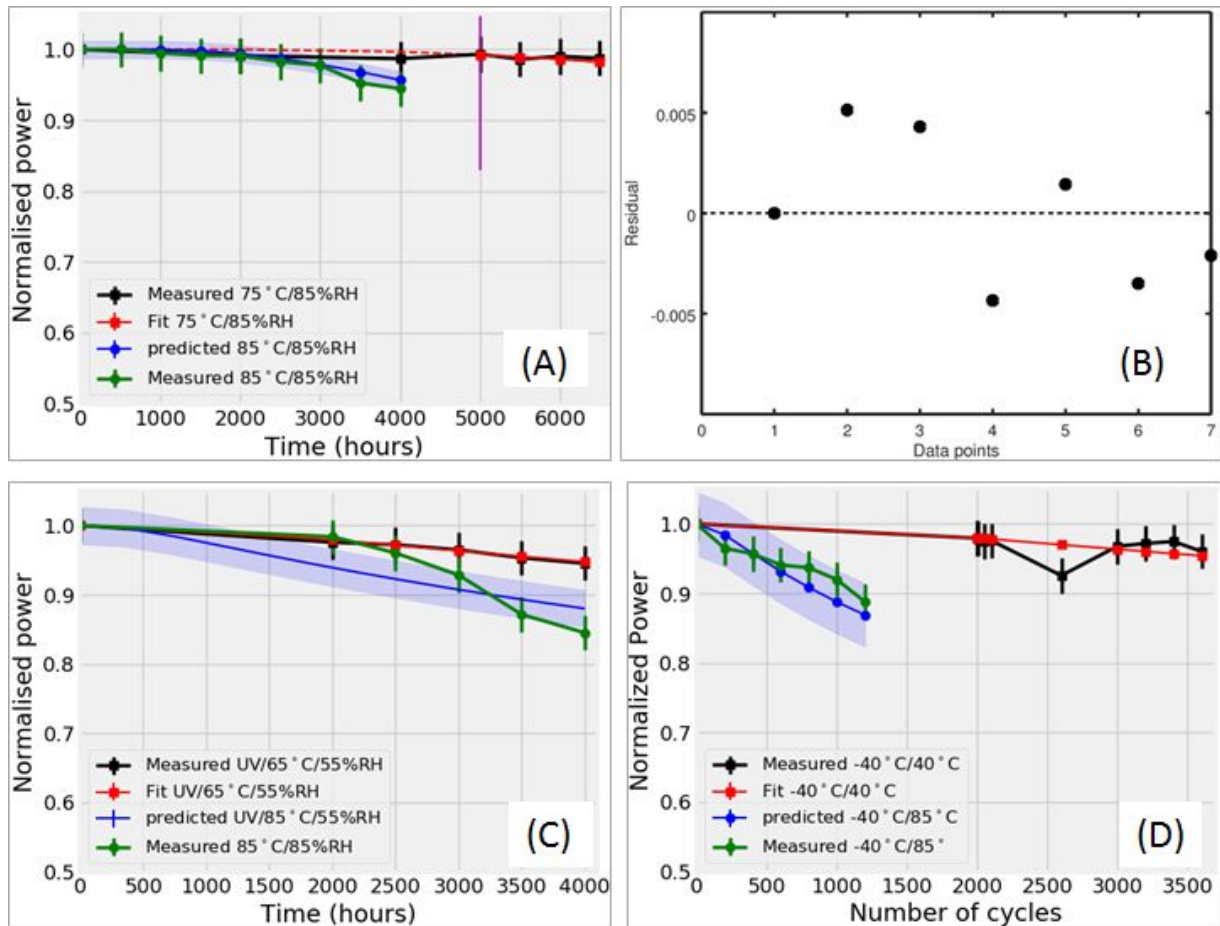


Figure 4.2: A: Hydrolysis model Eq(3.2) calibration and validation, the vertical violet line represents the optimized data points; B: Residual distribution of the fitted data points of the DH test; C: Photo-degradation model Eq(3.5) calibration and validation, and D: Thermo-mechanical model Eq(3.6) calibration and validation. The blue patch is the 95% confidence interval of prediction.

and explanation above are consistent for photo-degradation and thermo-mechanical graphs using respective data sets. For all the models, the predictions are satisfactory and are within a 95% confidence interval. The observable variations could be linked with the measurement uncertainties.

It important to note that, when applying the physical models, the extracted parameters are usually valid only for a particular module type. Meaning that the parameters have to be evaluated when the module type or technology changes.

### 4.1.3 Calibration and validation of the combined degradation rate model

The combined/total degradation rate (equation 3.8) is calibrated using outdoor measurements of Gran Canaria. The dataset of Gran Canaria is selected over Negev and Zugspitze because the module in Gran Canaria has been exposed longer compared to the ones of Negev and Zugspitze, and moreover it shows a clear degradation trend. The extracted model parameters are presented in table 4.3. On calibration, the residual standard deviation is 2.34% and the derived parameters,  $\Gamma = 190$  and  $\mu = 0.19$  for the power degradation

function in equation 3.10.

Table 4.3: Extracted model parameters of the individual rate models using the combined rate model 3.8 and with Gran Canaria data

Extracted models parameters				
Degradation rate model	$A_i$	$E_a$ [eV]	$n$	$X$ & $\Theta$
Hydrolysis: Eq(3.2)	4.91e7	0.74	1.90	-
Photodegradation: Eq(3.5)	71.83	0.45	1.90	0.63
Thermo-mechanical: Eq(3.6)	2.04	0.43	-	2.24

The model is validated by using the derived model parameters to simulate the degradation rates using the climatic datasets of Negev and Zugspitze. By comparing the simulated degradation trend with the measured data (see figure 4.3), the accuracy of the model is verified.

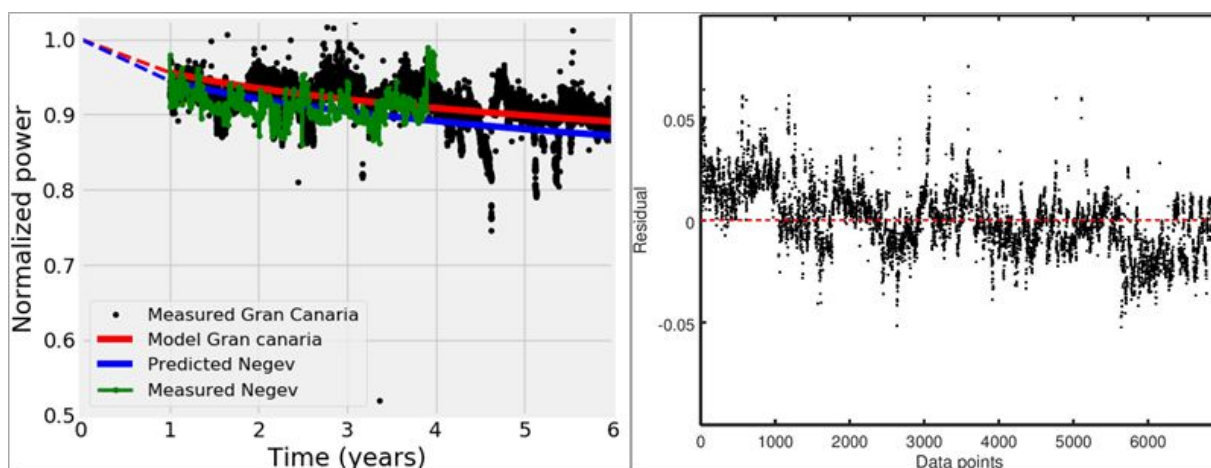


Figure 4.3: Right: Dotted black points are the measured data of Gran Canaria (calibrated dataset); thick red line is the model fit; in green is the measured data of Negev, thick blue line is the model prediction for Negev and the dashed lines indicate normalization to the initial laboratory power values before outdoor exposure respectively. Left: Residual distribution of the calibrated data points.

Figure 4.3 on the right shows the calibrated data of Gran Canaria and the predicted degradation for Negev plotted together with the measured degradation. The alpine predictions were left out to avoid too much information on the graph due to data fluctuations. The outdoor predictions show a good agreement with the measured power degradation.

#### 4.1.4 Degradation rates and lifetime prediction

Depending on the climate a module is installed in, different degradation modes might dominate over the others. Using the proposed degradation models, equations (3.2), (3.5), (3.6), (3.8) and the outdoor derived model parameters, it is possible to predict the dominating degradation precursor and the total degradation rate as well as the failure time from equation (3.11) for any location with known climatic loads. In this section, annual degradation rates of the mc-Si modules were predicted using input climatic loads of Zugspitze, Gran Canaria and Negev as shown in table 4.4.

High thermo-mechanical degradation is predicted for Zugspitze in comparison to Gran Canaria because of high module temperature variations in this climate zone. On the contrary, small degradation due to hydrolysis is predicted in Zugspitze despite the high levels of relative humidity. This could be explained by the low average module temperatures experienced in this region, hence slowing hydrolysis processes and the absolute water vapor concentration. In all cases, high rates are predicted in Negev. This can be explained again by the higher temperatures in this zone that determines the reaction rates for other degradation processes caused by other degradation factors such as hydrolysis by humidity and photo-degradation by UV dose. The predicted failure time defined as a 20% loss in power, show more severe degradation of maximum power output in arid climates where temperatures are higher such as expected. This further confirms the previous studies [Annigoni et al. \(2017\)](#) that temperature could be the primary accelerator of degradation.

Table 4.4: Predicted degradation rates of the mc-Si modules and failure time in the three climatic zones with a 95% lower and upper confidence interval (CI).

Location	Predicted rates and FT					Lower 95% CI (years)	Upper 95% CI (years)
	$R_{Dh}$ (%/year)	$R_{Dp}$ (%/year)	$R_{Dt}$ (%/year)	$R_{DT}$ (%/year)	FT (years)		
Negev	0.169	0.216	0.225	0.74	21.4	16.7	27.1
Gran-Canaria	0.122	0.212	0.104	0.50	31.6	25.0	40.0
Zugspitze	0.043	0.103	0.129	0.3	52.8	42.7	65.0

#### 4.1.5 Comparison of the proposed physical model with other physical model

We compare the predictions of the total degradation rate and failure time using the proposed physical mode and the model proposed by [Bala Subramaniyan et al. \(2018\)](#) in equation (2.39). For meaningful comparison and to avoid any bias, both models are calibrated using the same dataset (from Gran Canaria). Moreover, the model parameters are also derived to be in range with those reported in their paper [Bala Subramaniyan et al. \(2018\)](#). The simulated degradation rates and failure times are as presented in table 4.5. Note that the values of Gran Canaria are perfectly the same because they are the reference calibrated dataset for both models. The comparison is then made on the predictions of the other two locations that is; of Negev and Zugspitze.

The evaluated rates are quite comparable for Negev but show very high difference for Zugspitze. To further analyse the cause of this high discrepancy in the prediction, the sensitivity analysis of the input variables is carried out. Temperature (T), relative humidity (RH) and UV dose bins between (15<sup>0</sup>C-45<sup>0</sup>C), (40%-100%) and (80-120kWh/a/m<sup>2</sup>) respectively are used to generate 500 combinations of T, RH and UV. The sensitivity of the degradation rate with the climatic variables is as shown in figure 4.4.

As shown in figure 4.4, the model according to [Bala Subramaniyan et al. \(2018\)](#) has a higher sensitivity to the input variable especially to the module temperature. At lower or higher values of temperatures, the model overestimates or underestimates the degradation rate respectively and this explains the observed variations in the predictions especially in Zugspitze where the module temperatures are considerably low. The reason to this higher

Table 4.5: Comparison of the proposed model with the model according to [Bala Subramaniyan et al. \(2018\)](#)

Location	Predicted rates and FT			
	$R_{DT}$ [% years] (Proposed) Eq(3.8)	FT [% years] according to Eq(3.11)	$R_{DT}$ [% years] (Subramaniyan) Eq(3.8)	FT [% years] according to Eq(3.11)
Gran Canaria	0.50	31.6	0.50	31.6
Negev	0.74	21.4	0.80	20.0
Zugspitze	0.30	52.8	0.14	113.5

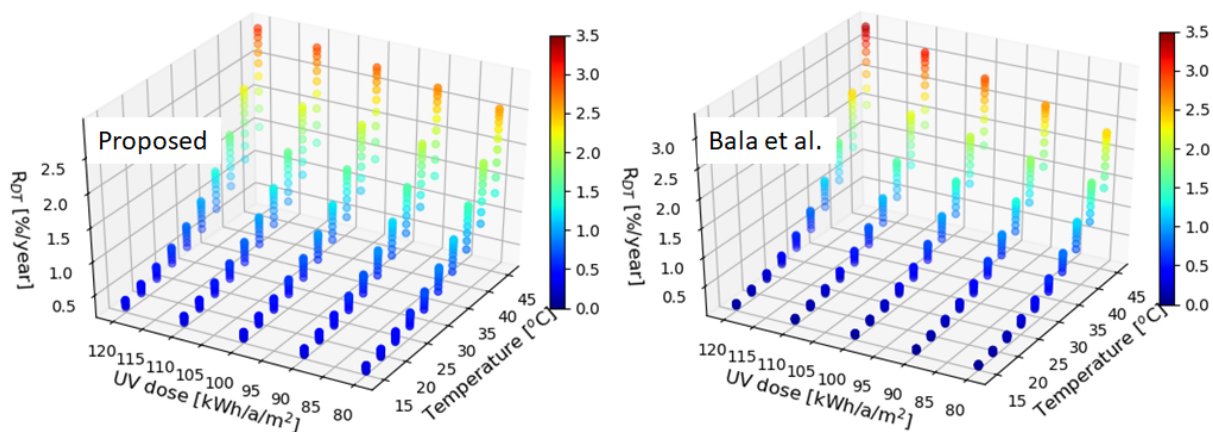


Figure 4.4: Sensitivity analysis of the proposed and the model according to Subramaniyan. Note, each dot represents a value of relative humidity and increases to the bottom.

sensitivity on temperature could be attributed to the model assumption that, all the degradation processes triggered by the combination of the four stresses have the same activation energy. From a physical point of view, this is usually not the case as one can expect different processes to have different kinetics and hence different activation energies. Also, assuming a single activation energy could be too much simplification hence deteriorating the model performance.

#### 4.1.6 Global degradation rates mapping: A global PV degradation risk analysis

The evaluation of the degradation rates dependent on specific degradation processes and the total degradation rate is extend from the three available location to a global scale. The aim is to create a global risk map of the three proposed mechanism and also the total degradation rate. The climate datasets used are extracted, modelled and averaged from the ERA5 reanalysis dataset for the years 2016, 2017 and 2018.

Figures 4.5, 4.6 4.7 and 4.8 show the worldwide degradation rates for hydrolysis, photo-degradation, thermo-mechanical and total degradation respectively. The generated maps are in accordance with the parameters from the studied mono-crystalline modules.

According to the recently proposed Köppen-Geiger-Photovoltaic (KGPV) climate scheme [Ascencio-Vásquez et al. \(2019\)](#), hydrolysis-degradation presents the smallest contribution in almost all the KGPV zones, but is considerable high for the tropical climates AH (trop-

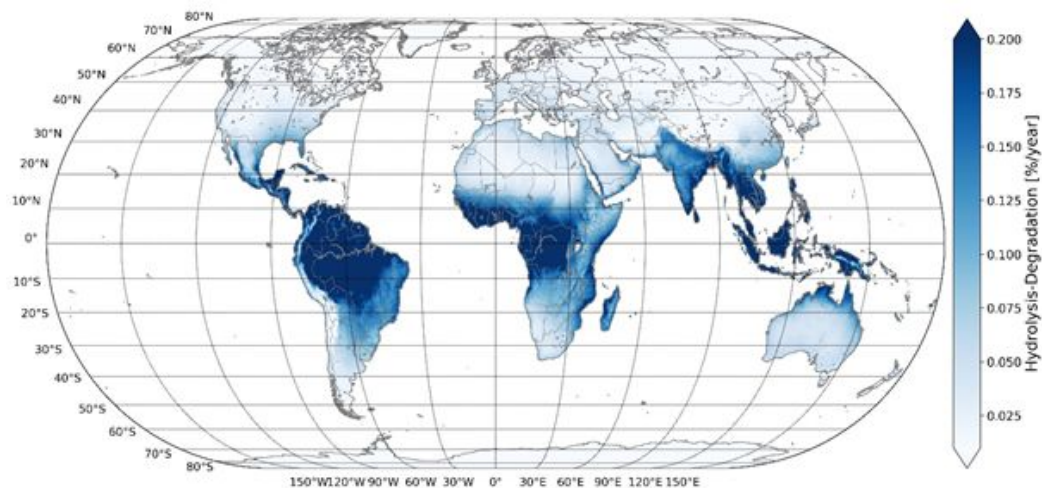


Figure 4.5: Global mapping of hydrolysis degradation rate

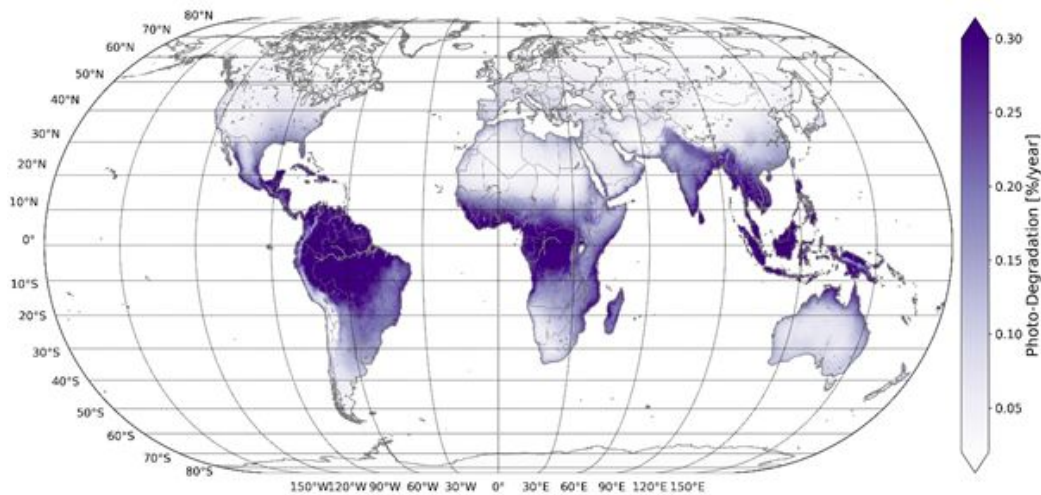


Figure 4.6: Global mapping of photo-degradation rate

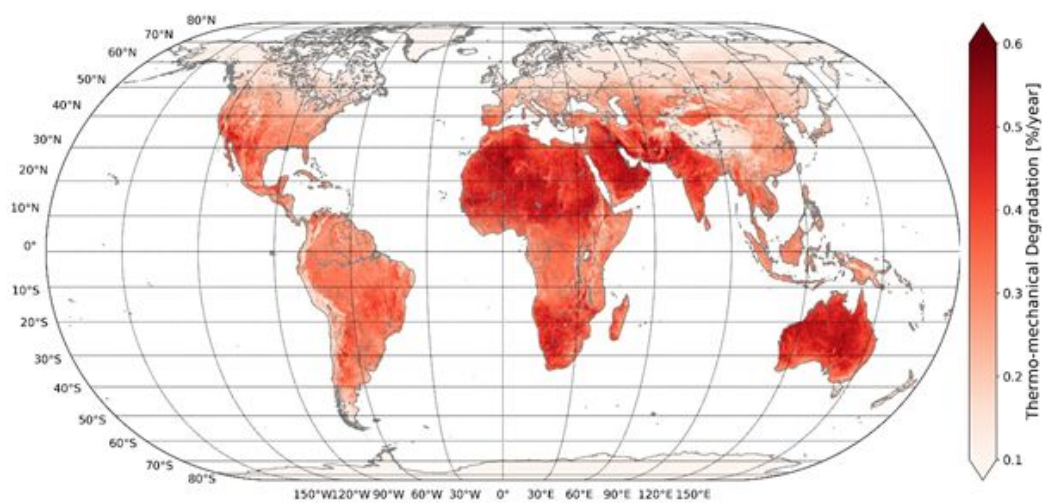


Figure 4.7: Global mapping of thermo-mechanical degradation rate

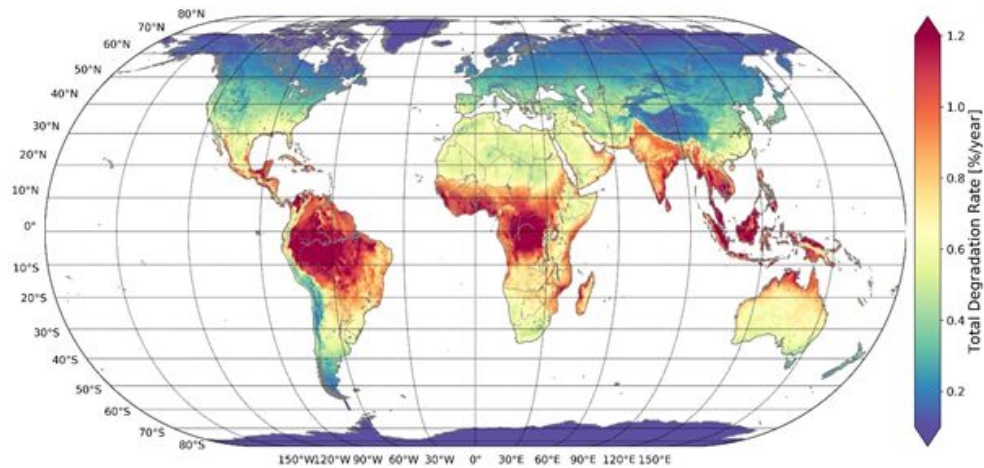


Figure 4.8: Global mapping of total degradation rate

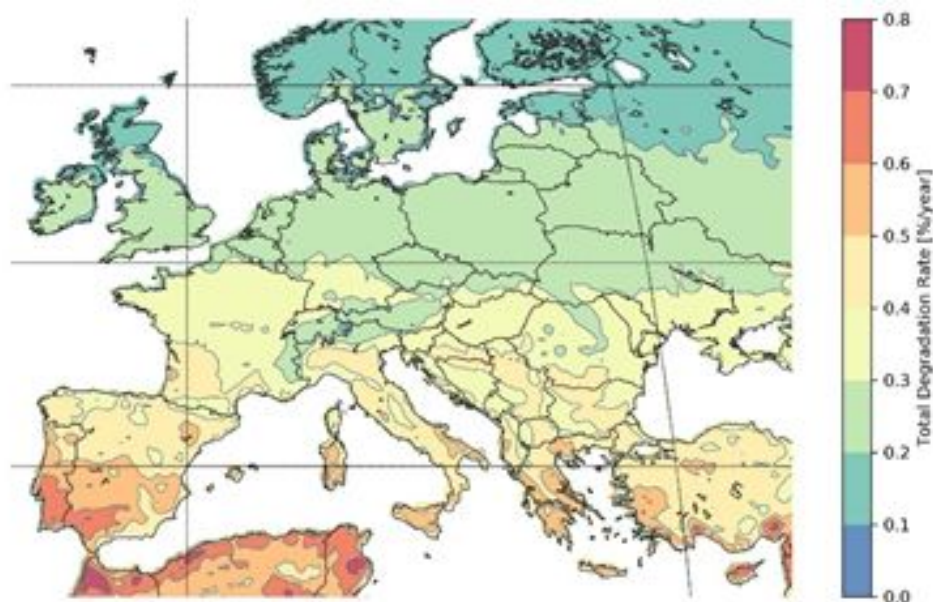


Figure 4.9: European categorization of total degradation rate based on temperature, humidity and UV irradiance for a mono-crystalline silicon PV module.

ical with very high irradiance) and AK (tropical with high irradiance), which zones are related with high precipitation levels (humid areas) and temperature levels. This process can provoke the moisture ingress leading to delamination of polymers or corrosion of solder bonds [Koehl et al. \(2018\)](#).

Photo-degradation has the second-highest contribution to the total degradation rate. This indicator combines the humidity, temperature and UV irradiance impacting the PV module. The impact is similar to the hydrolysis-degradation but higher in terms of absolute values due to the process triggered by UV irradiation. For desert areas, even though the UV irradiation is high, the low humidity in the air decreases the damage of the PV cells due to this mechanism [Ngo et al. \(2016\)](#). The photo-degradation is considerable high in AH (tropical with very high irradiance) and AK (tropical with high irradiance) zones due to the high climatic stresses of all variables (temperature, humidity and UV irradiation). It is surprising that the highest degradation due to photo-degradation was not predicted in the desert with high irradiance (BH) and desert with very high irradiance (BK) climates,

for example in the northern part of Africa where the UV is expected to be higher compared to the tropical regions of central Africa. The reason to this can be attributed to the low values of relative humidity in the desert areas hence lowering the impact of the degradation modes influenced by the combined UV-RH stresses.

Thermo-mechanical degradation exhibits the highest contribution to the total degradation rate in almost all zones. This parameter is affected by the seasonal temperature cycling (the difference between the maximal and minimal temperature of the year) and also the annual average maximum temperature.

The total degradation rates calculated by the combination of the previous three degradation mechanisms is also mapped. In accordance with the literature [Omazic et al. \(2019\)](#), the highest degradation rate is identified in tropical areas (hot and humid). Interestingly, the AK presents lower degradation than the AH, due to lower photo-degradation contribution (related to lower humidity). Globally the highest degradation rates (above 1.4 %/year) are identified in locations next to the equator line. To facilitate the visualization and use of degradation maps, we categorize the locations into bins of 0.2%/year ranging from 0 to 0.8%/year for Europe. The categorized map is shown in figure 4.9. The total degradation rates could reach 0.8%/year in the hottest areas of the south of Spain and Portugal for Europe. In real operating conditions, external degradation factors, such as soiling might increase the degradation rate if taken into account, but the degradation presented here assumes only gradual and non-reversible degradation processes.

#### 4.1.7 Uncertainties evaluation of the physical model

In order to be able to develop reliable predictive models, it makes it crucial to evaluate the different sources of uncertainties that can deteriorate the model performance. Therefore, in this section, the different sources of uncertainties are analyzed and discussed.

##### A. Uncertainties related to data quality

The quality of input data can highly affect the accuracy of the predictions. Here, the impact of data outliers is analysed. The module power measurements were done every five minutes, such high-resolution measurements and the frequently fluctuating environmental conditions outdoors, lead to unavoidable noise even after applying filters and corrections. By using an hourly moving average to minimize the noise in the datasets, the process of model calibration and validation is repeated. The effect of the noise to the derived model parameters as well as on failure time estimation is evaluated. Because the parameters:  $E_a$ ,  $n$ ,  $X$  and of the degradation rates models are very sensitivity, they are assumed constant in this analysis. Therefore, we evaluate the noise effect using the parameter  $\Gamma$  of the power degradation function (3.10). In order to illustrate this effect, the simulations of the failure time for the three location have been repeated using the hourly time-resolution and compared with the five minutes resolution. The MSEP and relative difference in failure time estimation with a five minutes and hourly resolution data are presented in table 4.10. Figure 4.10 shows a plot of the simulated and measured data. Note, the dataset of Gran-Canaria is still used as training or calibration dataset. The residual standard deviation reduced to 2.04% and the derived model parameter reduced to  $\Gamma = 182.3$ .

Although the residual standard deviation improved from 2.23% for 5 minutes resolution to 2.04% for hourly resolution, the improvement did not considerably led to reduction in MSEP. However, it led to a 4.05% relative difference of the predicted failure time. This is

Table 4.6: Percentage mean error in prediction (MSEP) and relative difference of the estimated FT for different data resolutions.

Uncertainties evaluation					
Location	Data Resolution	Parameter $\Gamma$	MSEP [%]	FT [year]	Relative difference
Negev	5 min	190.0	0.0230	21.4	4.05%
	Hourly	182.3	0.0240	20.5	
Zugsptize	5 min	190.0	0.0152	52.8	4.05%
	Hourly	182.3	0.0150	50.7	

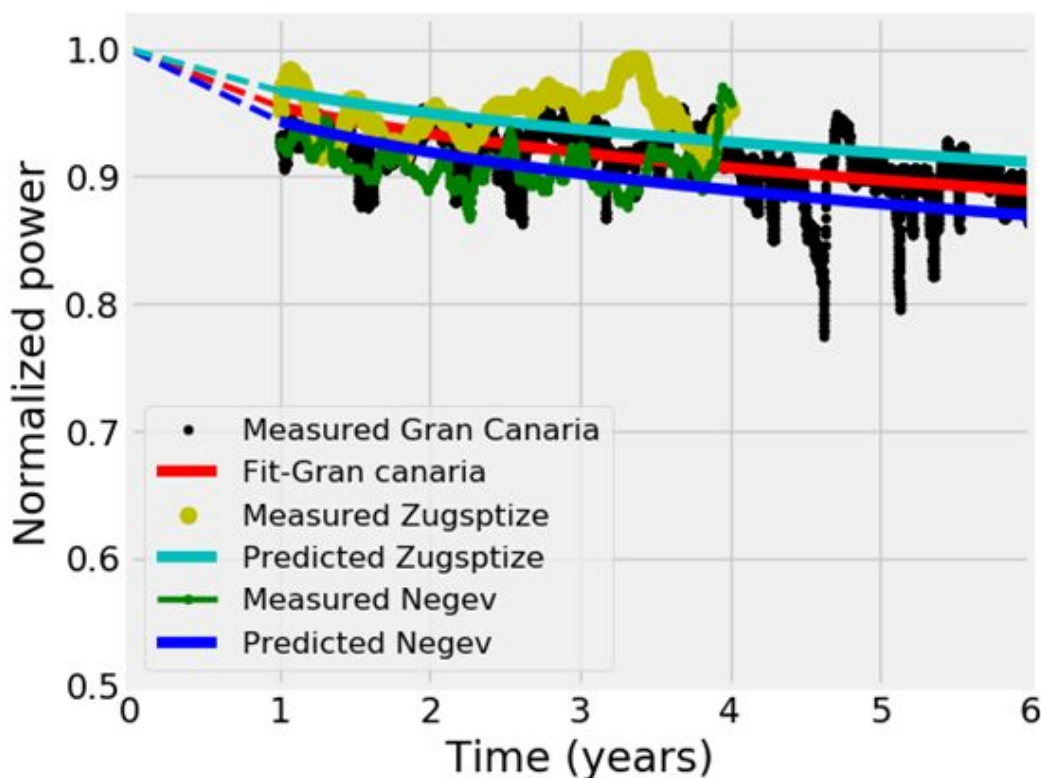


Figure 4.10: Model calibration and validation with hourly resolution

consistent with the observations from indoor results that, the uncertainties in experimental data sets used for validation can also influence the evaluated MSEP.

## B. Uncertainties related to climatic variables evaluation

In most cases, the essential input climate variables (temperature, humidity and UV irradiation) are evaluated from national or private weather services such as EAR5 used in this study to evaluate the global degradation map. The key challenges with these databases is that they are not developed for PV module or systems evaluation. In most cases the required variables such as relative humidity and UV irradiation are not directly measured. Therefore, they have to be evaluated from other variables such as precipitation and global irradiation using specific mathematical models. Indeed, these models are associated with their own uncertainties since they are difficult to calibrate and validate. Indeed, using such calculated parameters poses a question on the absolute values accuracy of the predict

degradation rates or failure time. Moreover, parameters such as ambient temperatures which is widely measured and available are not directly used as model inputs since they have to be converted to module temperature for degradation evaluation. This also influence the evaluated degradation rates and failure time. Since temperature is considered as the main factor that influences the degradation mechanisms, here we demonstrate the uncertainties involved in module temperature evaluation by comparing the predictions of the modeled and measured module temperatures in the three locations.

As can be seen in table 4.7, the relative difference in measured ( $T_{mm}$ ) and modeled ( $T_{mp}$ ) module temperatures can be as high as 47%. Also depending on the location where the module is installed; this difference can lead to as much as 59.3% relative difference between the degradation rate evaluated with the measured module temperatures ( $R_{DT_{mm}}$ ) and the degradation rate evaluated using modeled temperatures ( $R_{DT_{mp}}$ ). One important observation is that, the uncertainties in rates or lifetime prediction due to the uncertainties in module temperatures evaluation, are location dependent. For example, the modeled module temperature showed high uncertainties for Zugspitze as compared to Gran Canaria, on contrary high uncertainties in degradation rates are evaluated for Gran Canaria compared to Zugspitze. This can be explained by the Arrhenius temperature dependence in the degradation rate models. The effect can be clearly explained by the temperature against the degradation rate plot Figure 4.11.

Table 4.7: Comparison of predicted rates and FT using measured and modeled module temperature.

Location	Predicted rates and FT							
	$T_{mm}$ [°C]	$T_{mp}$ [°C]	relative difference	$R_{DT_{mm}}$ [°C]	$R_{DT_{mp}}$ [°C]	$TF_{T_{mm}}$ [years]	$TF_{T_{mp}}$ [years]	relative difference
Negev	36.63	25.35	44.47%	0.75	0.471	33.60	21.09	59.27%
Gran-Canaria	30.12	23.81	26.51%	0.48	0.345	45.80	33.0	38.79%
Zugspitze	4.98	3.65	36.38%	0.23	0.22	71.41	69.22	2.74%

At lower temperature, large variation of temperatures leads to small change in the degradation rate and at high temperatures a small variation in temperature leads to a relatively large change in the degradation rate. Hence, the uncertainties in module temperatures evaluations have a more drastic effect on the accuracy of the predictions in locations with high module operating temperatures.

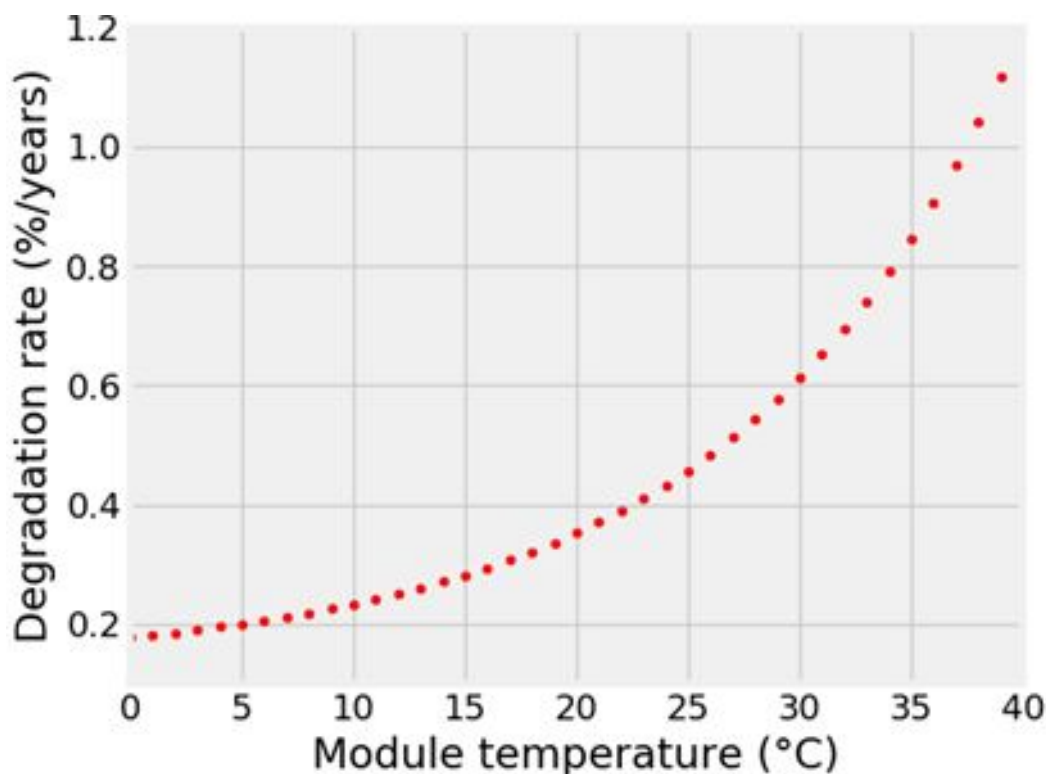


Figure 4.11: Module temperatures against the degradation rate

## 4.2 Results for the data-driven model

### 4.2.1 "Time and degradation pattern" dependent models as well as 3% degradation threshold

To validate the assumptions used in this approach, here the pitfalls of using a constant degradation rate for long-term degradation forecast are illustrated. Also, the dependence of the model on time series degradation patterns is illustrated.

The power degradation function (equation 3.27) is calibrated at different performance degradation intervals (at  $P = -1\%$ ,  $P = -2\%$  and  $P = -3\%$ ). At each interval, a simple extrapolation with a constant degradation rate at calibration ( $k_{cal}$ ) is performed and failure time evaluated. To analyse the dependence on degradation patterns, two of the TISO-modules named TEA5 and TEA6 are used as shown in figure 4.12.

It is clearly visible that although the model fits the data very well at all calibration intervals, the evaluated failure time is very different at each calibration interval. This effect is observed for both modules TEA5 and TEA6. This result demonstrates three aspects: one, a perfectly fitting model does not guarantee better forecast or prediction. Two, a model that assumes a constant degradation factor/rate is not appropriate for long-term PV performance degradation forecast. Three, the model forecast accuracy might highly depend on a specific degradation pattern. This effect is visible in the two modules, for example high discrepancies are visible for the TEA6 module compared to TEA5 module even at similar calibration intervals. Therefore, based on these three observations, the concept of "time and degradation pattern" dependent degradation factor was introduced.

It is also visible that the forecasting accuracy improves as the calibration interval or performance degradation increases, which seems like an obvious observation. However, since the objective is to perform the prediction at the early stages of the module's operation, a 3%

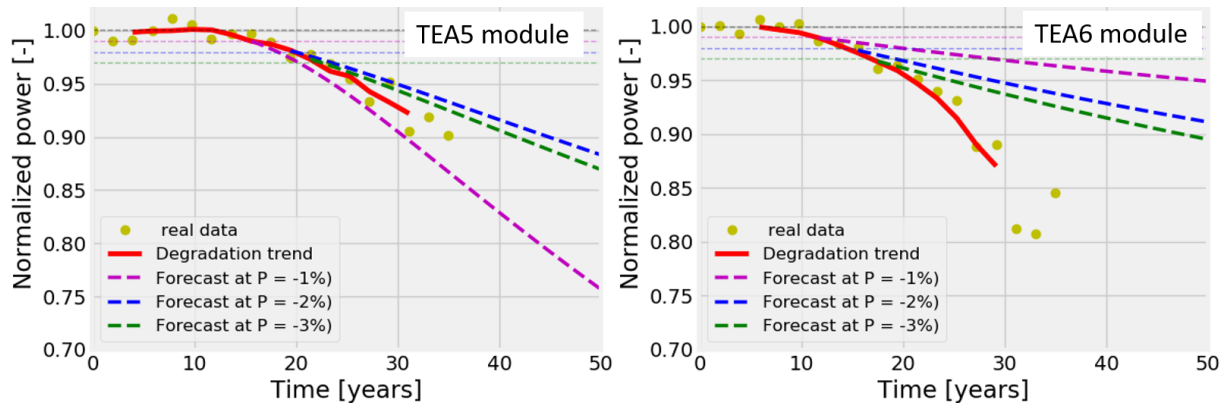


Figure 4.12: Fit and RUL prediction at different percentage power loss of two TISO modules, namely TEA5 and TEA6. The dotted lines represent forecasts at the three calibration intervals

threshold was selected. This threshold was found optimal since it provided good forecasts compared to values less than 3% loss. Moreover, another reason is that in situations where the degradation trend is not monotonically decreasing as in many outdoor datasets, using performance degradation of less than 3% might lead to misinterpretation of degradation with seasonal variation or other performance reducing factors which are reversible. For example, the TEA5-module in figure 4.12 shows that prediction after only 1% performance degradation resulted in under-estimations compared to the measured degradation trend, which is attributed to the variations in the degradation trend due to reversible effects.

## 4.2.2 Model calibration

The power degradation model 3.27 was fitted on measured datasets to extract the model parameters ( $k_{cal}$  and  $\mu$ ). At the same time the degradation pattern parameters  $\Delta P$ ,  $\Delta t$  and  $t_{cal}$  are evaluated. During the calibration process, a total of 7 TISO-modules ( named TEA1, TEA4, TEA6, TEA8, TEA10, TEB1, TEB2) and 2 DKA systems where optimized. From these modules and systems, different failure patterns where extracted by altering the tolerance (which changes the degradation trend). Despite the strong degradation and huge variations in the data points observed for the DKA systems, they are selected for the calibration process because the objective of proposed methodology is to be applicable on a wide set of data distribution.

Figure 4.13 shows an example of one of the TISO-modules (TEA1) with annual measurements for 35 years and one of the DKA systems (Kyocera system) with monthly average values for 9 years, used for model calibration. The extracted parameters are used as the basis to set logical conditions to select which degradation factor model represents better a given degradation pattern. Over 10 logical conditions where achieved to represent the different degradation patterns as presented in table 4.8.

Figure 4.14a shows the 7 TISO-modules used in this study for model calibration. Figure 4.14b is the corresponding change of the degradation factor over time of the 7 modules. It is clearly visible that the rate of degradation factor variation is dependent on the degradation patterns. This is evident for TEA1 module that displays a strong degradation but with a low rate of change of the degradation factor over time. Furthermore, for some degradation patterns like the one of TEA10, a constant degradation factor ( $k = k_{cal}$ ) was sufficient to evaluate the long term degradation. Hence, for such a degradation pattern, it is enough to

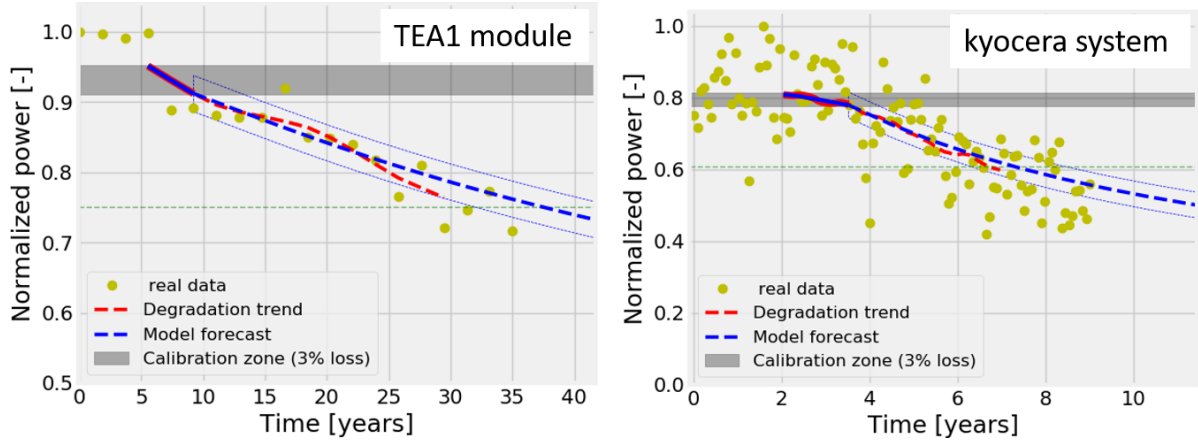


Figure 4.13: TEA1 module (from the TISO-Modules) and Kyocera system (from DKA systems) selected for calibration. In yellow are the measurements and red is the extracted degradation trend and in thick blue line is the model prediction with the 95% confidence interval. The horizontal green dotted line shows the -20% failure threshold of the degradation trend

Table 4.8: Logical conditions for model selection and the corresponding extracted optimization model parameters

Logical conditions	Model	Parameter $y_1$	Parameter $x_1$	Parameter $z_1$
$\mu \leq 0.45$ & $k_{cal} \leq 9.0e-4$	$k_1$	2.0	1.0	1.0
$\mu \geq 0.45$ & $k_{cal} \geq 0.01$	$k_1$	1.0	0.1	1.0
$\mu \leq 0.3$ & $\Delta P \geq 0.01$	$k_1$	1.0	0.1	1.0
$\mu \geq 0.45$ & $\Delta P \geq 0.01$	$k_1$	1.0	1.5	1.0
$\mu \geq 0.55$ & $k_{cal} \leq 0.005$	$k_1$	-	4.0	1.0
$\mu \leq 0.4$ & $\Delta P \leq 0.01$ & $k_{cal} \leq 0.005$	$k_1$	-	4.5	1.0
$\mu \leq 0.35$ & $\Delta P \geq 1.0e-4$ & $t_{cal} \leq 5$	$k_2$	-	-	3.5
$\mu \leq 0.45$ & $\Delta P \leq 1.0e-4$ & $k_{cal} \leq 0.009$	$k_3$	-	0.1	1.0
$k_{cal} \geq 0.01$ & $\Delta P \leq 5.0e-5$ or $\mu \geq 0.45$	$k = k_{cal}$	-	-	-
$k_{cal} \leq 0.013$ & $\Delta P \leq 9.5e-6$ & $\mu \geq 0.43$	$k_3$	-	0.1	0.5
else:	$k_1$	0.0	2.5	1.0

forecast the lifetime by using only the simplified power degradation model e.g. equation 3.10.

### 4.2.3 Validation

The most important and challenging part of all predictive models is the validation process of the models which usually requires different sets of measured data from the ones used in the calibration process. In this study, PV modules and systems with a considerable performance degradation were used to validate the performance of the model. An example is shown in figure 4.15 for Trina and CIGS systems. By comparing the measured trend line and the prediction line, the accuracy of the model was verified.

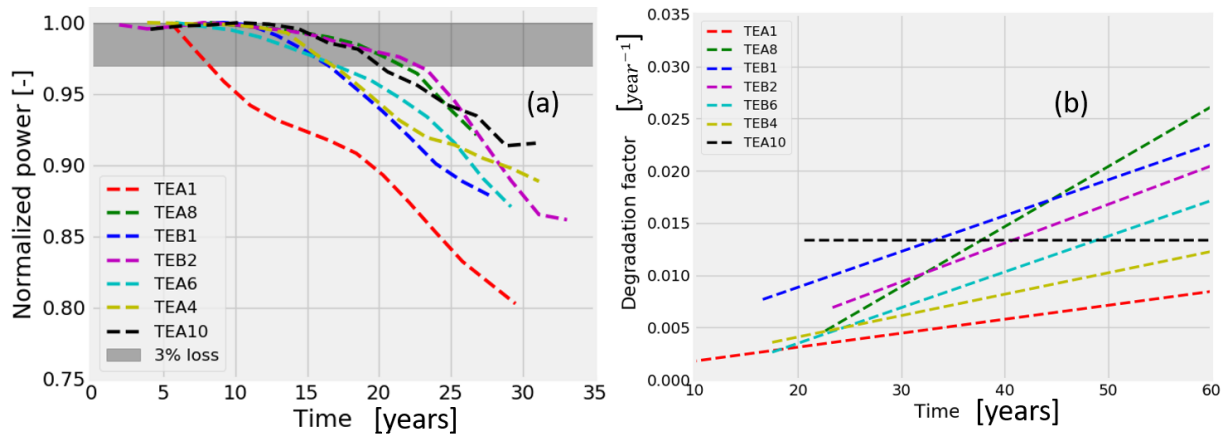


Figure 4.14: A, Different TISO-modules used in model calibration. B, Change of the degradation factor over time of the 7 modules respectively

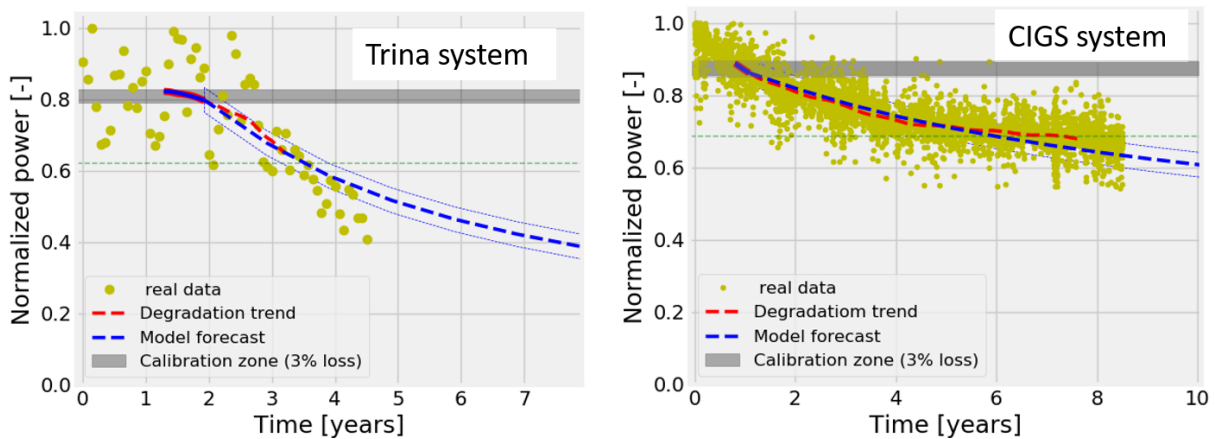


Figure 4.15: Model validation with experimental datasets of Trina (from DKA systems) and CIGS (from Bolzano systems). In yellow are the measurements, in red is the extracted degradation trend and in thick blue line is the model prediction with the 95% confidence interval. The horizontal green dotted line shows the -20% failure threshold of the degradation trend

#### 4.2.4 Model application and comparison with statistical models

The performance of the proposed method is benchmarked against those of two statistical forecasting methods, namely ARIMA and Facebook prophet (FP). The reasons to select these methods is based on a study by Taylor and Letham [Taylor and Letham \(2018\)](#), where the performance of the different statistical models in long-term forecast was compared. In their study, FP was found to be outstanding in comparison with other models. The ARIMA model was characterized with the highest uncertainties. We selected the best and the least performing models to compare the accuracy of the proposed model and to investigate whether the nature of the data under evaluation could affect the models' performance. Moreover, both methodologies are simple to apply and commonly used in different fields. For example, the FP algorithm is implemented in common programming languages such as python and R <sup>1</sup>. The methodology was created as a flexible time series model which is configurable by non-experts. It is based on a decomposable time series model including

<sup>1</sup>The code can be accessed at: <http://https://facebook.github.io/prophet/>

trend, seasonality, holidays (not important for our application) and an error term. The model gives the opportunity to chose linear and logistic time series evolution, the second being suited for the non-linear behavior of PV performance. Furthermore, among the seasonality settings for different time resolutions, yearly seasonality was selected to detect yearly variations in power production due to the seasons of a year. The ARIMA model has free online packages [Hyndman et al. \(2018\)](#) and [Hyndman and Khandakar \(2008\)](#). In this study an auto-arima function which uses the akaike information criterion (AIC) to get the optimal model was used.

Table 4.9: Comparison of ARIMA, Facebook prophet and the proposed model at two prediction intervals. where, mc1 is mc-Si1, mc2 is mc-Si2, 1j is 1j-a-Si1, 3j is 3j-a-Si1, pc1 is pc-Si1, pc2 is pc-Si2, pc3 is pc-Si3 and rib is ribbon1

System	HIT1	mc1	mc2	pc1	pc2	pc3	1j	3j	rib	CdTe1	CIGS1
ARIMA											
FT <sub>3%</sub> [years]	21.4	NA	18.8	10.1	14.2	18.2	16.2	NA	13.8	16.4	NA
RUL <sub>3%</sub> [years]	12.9	NA	10.2	1.6	5.7	9.7	7.8	NA	5.3	7.9	NA
FT <sub>full</sub> [years]	21.2	NA	14.5	NA	22.3	26.5	15.0	NA	21.8	12.5	4.0
RUL <sub>full</sub> [years]	12.8	NA	6.0	NA	13.8	18.0	6.5	NA	13.3	4.0	-4.5
Rel <sub>diff</sub> [%]	0.9	-	22.8	NA	36.3	31.3	36.7	-	21.8	23.8	NA
Facebook prophet											
FT <sub>3%</sub> [years]	34.6	37.8	13.8	9.8	9.5	15.3	15.1	21.0	9.4	14.9	NA
RUL <sub>3%</sub> [years]	26.1	29.3	5.3	1.3	1.0	6.8	6.6	12.5	0.9	6.4	NA
FT <sub>full</sub> [years]	16.7	37.8	14.7	33.1	24.7	18.7	14.9	21.0	24.5	12.8	5.6
RUL <sub>full</sub> [years]	8.2	29.8	6.2	24.7	16.2	10.2	6.4	12.5	16.0	4.2	-2.9
Rel <sub>diff</sub> [%]	51.7	-	6.1	70.3	61.5	18.2	36.9	-	61.6	14.1	NA
Proposed											
FT <sub>3%</sub>	16.5	82.5	17.2	17.8	25.2	25.4	18.7	25.2	25.2	15.8	5.8
RUL <sub>3%</sub> [years]	8.0	74.0	8.7	9.3	16.7	16.9	9.9	16.7	16.7	7.3	-2.7
FT <sub>full</sub> [years]	15.4	82.5	17.2	14.7	24.3	18.8	21.8	25.2	24.3	15.2	6.5
RUL <sub>full</sub> [years]	6.9	74.0	8.7	6.2	15.8	10.3	13.3	16.7	15.8	6.7	-2.0
Rel <sub>diff</sub> [%]	6.7	-	0	17.4	3.6	25.9	14.2	-	3.6	3.8	10.8

The performance evaluation is carried out using the 11 Bolzano system datasets. The comparison of the three models is twofold: first, the models are compared on the lifetime forecast after a small performance degradation interval and second, on the consistence of the forecast at two different forecasting intervals. In the first attempt, the same system input data (normalized and STC irradiance corrected power time series with 3% performance degradation as training data) were tested on ARIMA and FP models. Unfortunately, no meaningful predictions were achieved because the number of calculated change points is greater than the number of observations in the dataset. Instead, the monthly Performance Ratio (PR) was used as the input parameter. The PR sets the actual yield of a PV system in relation with the expected yield at STC conditions [IEC61724-1 \(2017\)](#). For model comparison, the models are calibrated at two different intervals: first, at an interval corresponding to the 3% performance degradation and second, using the entire datasets corresponding to 8.5 years interval. The respective lifetime and RUL forecasts are shown in table 4.9.

Considering a 3% calibration threshold, it is visible that there are high discrepancies as well as unrealistic forecast scenarios (see figure 4.16) for both FP and ARIMA models.

In table 4.9 it is also observed that the failure times are either over- or under-estimated for the ARIMA and Facebook models. The over- and under-estimations can be correlated with the evaluated degradation trend which is influenced by the nature of the dataset as well as the number of data-points. Considering the calibration using the entire dataset, the FP and the proposed model show good agreement in the failure time forecast for most of the systems. This excludes the mc-Si1 system that appeared to be very stable with a performance degradation of less than 2% after 8.5 years. For this system, the proposed model shows an over-estimation of the failure time because the evaluated degradation is too small to achieve optimal calibrations. Comparing the variations in predictions at different calibration intervals, it can be seen that the proposed model displays a good consistency (on average 9.5% relative difference) compared to the other two models that displayed unrealistic scenarios. Although the FP showed a good agreement with the proposed model when calibrated using the entire dataset, it however displayed big variations in lifetime forecast between the two calibration intervals. Overall, the ARIMA model does not perform well in this study since it failed to converge for four systems. The model also tends to overfit the data, hence making it more sensitive to reversible performance reducing events. This is visible when looking at the pc-Si1 system (figure 4.17) where the model failed to converge when calibrated on the entire dataset. This implies that such a model is not useful for performance degradation forecast.

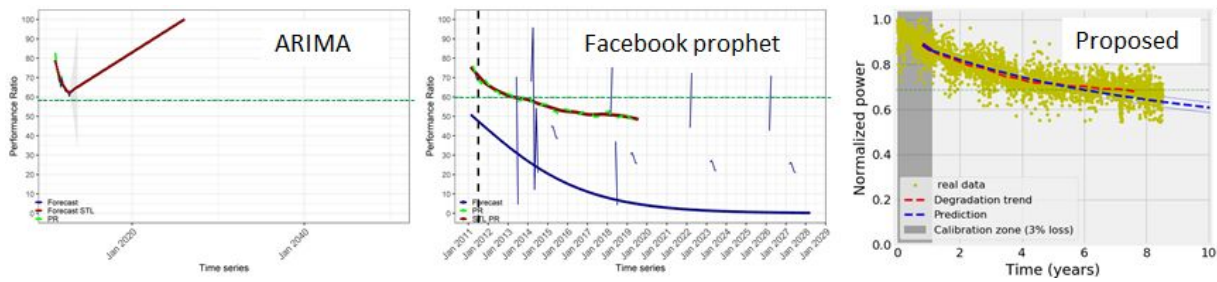


Figure 4.16: ARIMA, Facebook prophet and proposed methods when applied on a CIGS system with fewer data-points using a 3% threshold. The horizontal dotted green line shows the failure time threshold.

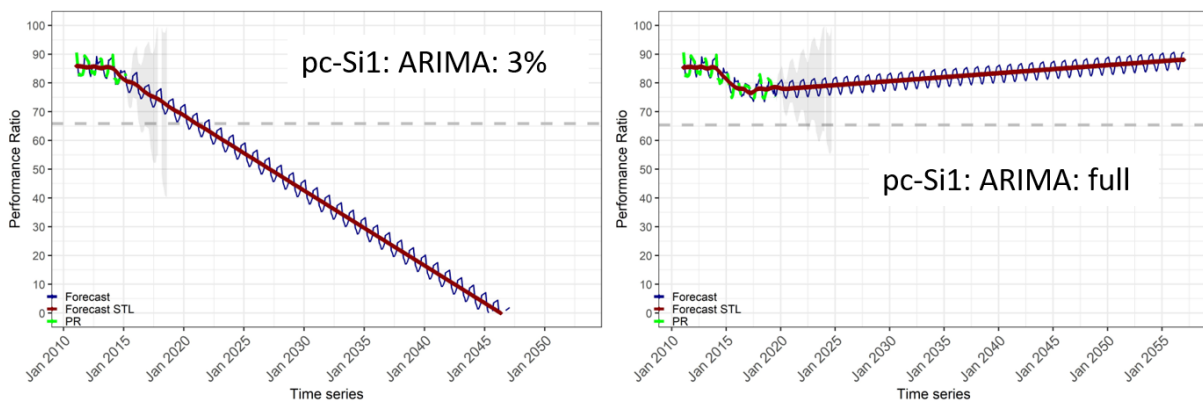


Figure 4.17: Forecast at 3% and entire data-set calibration thresholds using auto-ARIMA model. The figure shows overfitting when calibration is done on the entire dataset.

Considering the calibration using the entire data-sets, the Facebook and the proposed model showed a good agreement in the failure time forecast for most of the systems. This

excludes the mc-Si1 system that appeared to be very stable with a performance degradation of less than 2% after 8.5 years. For this system, the proposed model shows an over-estimation of the failure time because the evaluated degradation is too small to achieve optimal calibrations. Comparing the variations in predictions at different calibration intervals, it can be seen that the proposed model displays a good consistence compared to the other two models. Although the Facebook prophet showed a good agreement with the proposed model when calibrated using the entire data-sets, it however displayed big variations in lifetime forecast between the two calibration intervals. Overall, the ARIMA model showed the under-performance in this study since for over four systems it failed to converge. The model also tends to overfit the data, hence making it more sensitive with performance reducing events that could be reversed. This can be clearly displayed in pc-Si1 system (figure 4.17) where the model failed to converge when calibrated on the entire dataset. This implies, that such a model is not sufficient for performance degradation forecast.

### 4.2.5 Model limits and uncertainties

Although the proposed model has displayed a good performance on a number of PV modules and systems, it is however bound to some limits and uncertainties that could deteriorate the prediction accuracy. The model limits and uncertainties are identified as:

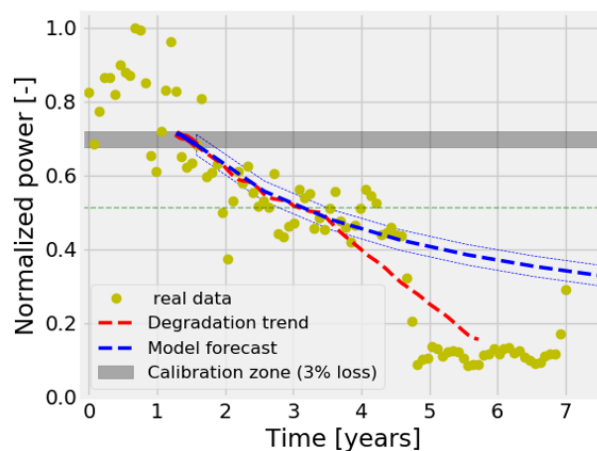


Figure 4.18: System showing a sudden drop in power (around the green box), in blue is the model forecast. The horizontal green dotted line shows the -20% failure threshold of the degradation trend

The model works well when the degradation is gradual and continuous, it cannot forecast events that might lead to dramatic or sudden power losses, such as breakage, fire, or catastrophic failures. For example, figure 4.18 shows one of the DKASC Alice Spring systems; eco-Kinetics-26.5kW-mono-Si-Dual (2010), which experiences a sudden drop in performance. According to the information from the DKA website, this sharp drop in performance was attributed to one PV module in this PV array that was damaged during a windstorm. Hence, the cause is identified as a partial failure of one array string in which this damaged module is connected.

The model is based on degradation patterns; hence it is influenced by the extracted degradation trends. The degradation trend is extracted from time series data by applying

the condition in equation 3.30. Changing the tolerance (tol) value affects the extracted degradation trend as shown in figure 4.19a. Figure 4.19b shows how the calibration as well as the forecast error varies with tol. The RMSE was calculated using equation 3.31 and is converted to percentage.

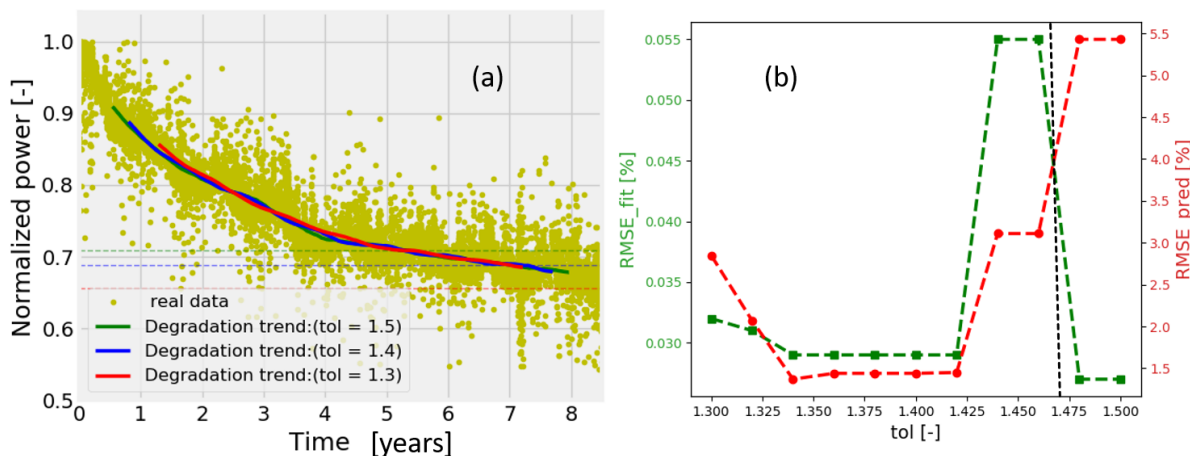


Figure 4.19: A, Variation of the extracted degradation at different values of tol, the horizontal dotted lines show the -20% failure threshold of the degradation trend. B, is the variation of the fitting error (RMSE-fit) and forecast error (RMSE-pred) with different values of tol

According to the evaluated datasets in this study, the value tol and the extracted degradation trend highly depend on the resolution and the outliers in a given dataset. For data sets with a monthly or yearly resolution, the values of tol ranged from 0.9 to 1.25 while datasets with high resolution of 15 minutes, the values were between 1.4 and 1.65. The tolerance factor tol is very useful as it provides a parameter for optimization adapted to the datasets variability unlike the black box automated algorithms.

#### 4.2.6 Assessing the effects of PV modules long-term degradation on lifetime energy yield

To mitigate the financial investment risks for PV systems stakeholders, it is a prerequisite to reliably predict the long-term energy yield. Recently [Reise et al. \(2018\)](#) have reported the different sources of uncertainties in PV systems yield predictions and assessments. A big challenge was on how the degradation effects are taken into account during long-term yield predictions. Indeed, the authors reported that, this is the most unexplored challenge and varies from analyst to analyst. Therefore, in this section we show how the proposed model could be applied to long-term yield predictions to lower the uncertainties associated to long-term performance degradation and hence improve the long-term yield prediction accuracy. Hence we point out that, the scope of the study is limited to analyzing the impact (sensitivity) of degradation to long-term yield prediction and not to propose a model for yield prediction.

The described method is applied to 7 of the TISO modules (TEA1, TEA4, TEA6, TEA8, TEA10, TEB1, TEB2) to extract the degradation trends independent of measurement uncertainties and to forecast the power degradation from a -5% to a 35 years time frame (the current modules age). To expand our analysis, three degradation scenarios; linear with a constant rate, non-linear (proposed but with a constant degradation rate) as

well as non-linear (proposed with a time dependent degradation rate) are assumed. The comparison with a linear approximation is of ultimate importance because it is commonly used during long-term yield evaluation according to Reise et al. (2018). Figure 4.20 shows the results of two of the modules TEA1 and TEA8 that showed the best and the worst forecasts when using the linear approximation.

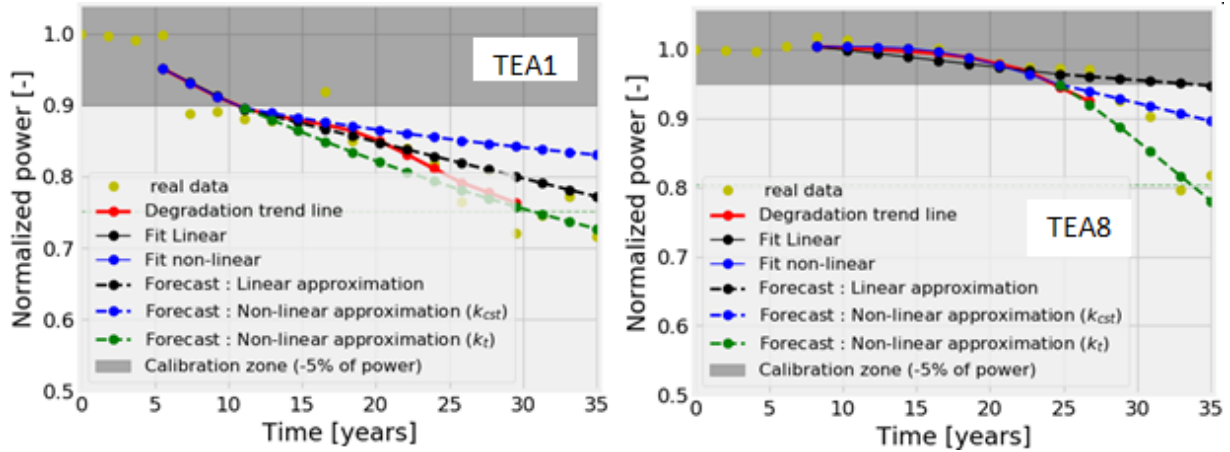


Figure 4.20: (TEA1) and (TEA8) TISO modules that displayed lower and higher uncertainties when long-term predictions are made with a linear approximation (black). The green and blue curves show the forecasts with the non-linear degradation with time dependent rate and with a constant rate respectively. In yellow are the measured data points and in red is the degradation trend

It can be seen that the new approach (non-linear with a time dependent degradation rate) displays consistent results considering the measured data (real data). Since the intended exercise is to assess how this will affect the long-term yield predictions, all the approximations are correlated to the uncertainties in yield evaluations. This was achieved by comparing the relative loss of lifetime energy yield of the measured degradation for the 35 years with the predicted ones as shown in table 4.10. It can be seen that using the proposed long-term degradation method (non-linear with a time dependent rate) reduced the prediction uncertainties to 37.6% on average. Moreover, it is seen that a linear approximation with a constant degradation rate is associated with the highest uncertainties of over 64.7 on average. Indeed, the dependence of the prediction uncertainties to the degradation patterns is clearly visible in the two modules. For module TEA1 with a linear degradation pattern the uncertainty is small compared to module TEA8 with an exponential degradation pattern. Moreover, the residual standard deviation calculated according to equation 3.22, further confirms these discrepancies. Meaning that the linear approximation cannot reliably fit or describe the different degradation patterns observed in the field.

Table 4.11 shows the failure time (defined as the time needed for power to decrease by -20% of the initial value). It is observed that using the proposed method (non-linear approximation with a time dependent rate), consistent failure time forecasts are achieved. On contrary, using a linear as well as a non-linear approximation but with a constant rate, some unrealistic scenarios are predicted for some modules. Indeed these scenarios are correlated with the degradation patterns. These calculations demonstrate that if these scenarios are included in the lifetime yield predictions, they can lead to over estimation of the lifetime yield. Hence the proposed model could provide a solution to improve the lifetime yield accuracy.

Table 4.10: Comparison of evaluated loss in lifetime energy yield in 35 years using the 3 degradation approximation scenarios. Relative uncertainty is calculated according to the measured yield loss

Module name	TEA1	TEA4	TEA6	TEA8	TEA10	TEB1	TEB2
Measured							
Loss of lifetime energy [years]	-19.04	-7.86	-9.07	-6.58	-5.09	-8.87	6.97
Linear							
Loss of lifetime energy [years]	-15.70	-3.38	-0.46	+0.37	-0.29	-5.70	-3.57
Relative uncertainty [%]	17.5	57.0	94.9	105.7	94.3	35.7	48.8
Non-linear with a constant rate							
Loss of lifetime energy [years]	-12.74	-3.84	-1.38	-1.47	-1.21	-6.47	-4.93
Relative uncertainty [%]	33.1	51.1	84.7	78.6	76.2	27.1	29.3
Non-linear with a time dependent rate							
Loss of lifetime energy [years]	-39.7	-16.89	-4.25	-13.55	-2.46	-8.86	-6.81
Relative uncertainty [%]	52.0	53.4	52.8	51.4	51.6	0.1	2.3

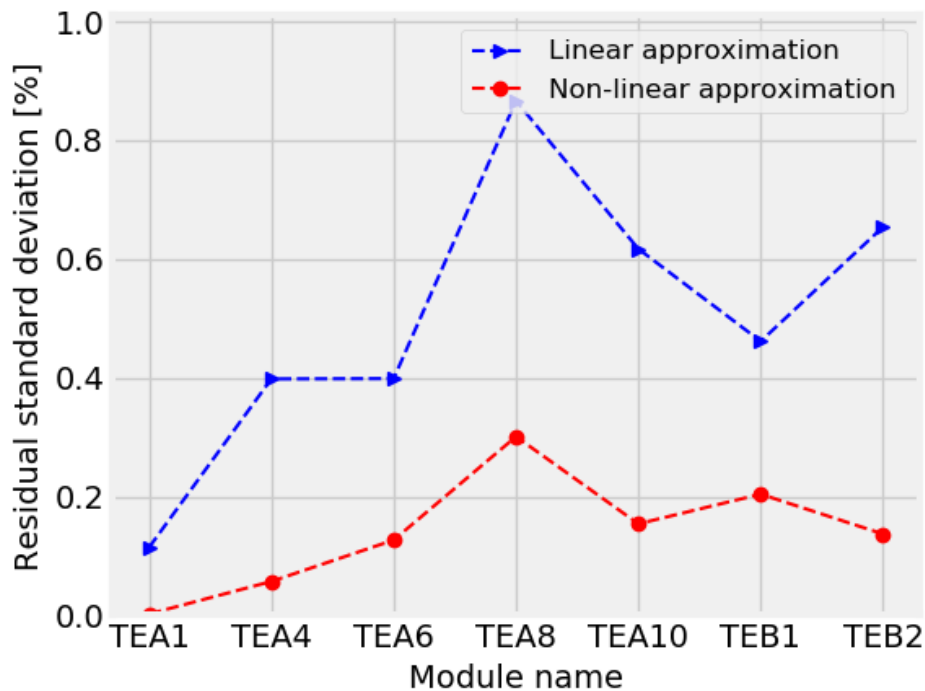


Figure 4.21: Residual standard deviation of the 7 TISO modules fitted at -5% degradation using linear and non-linear models respectively

#### 4.2.7 Simplified User Interface (PVLIFE Toolbox)

After optimizing, testing and further validating our model under different data scenarios, the described approach is embedded into a simplified user interface for PV lifetime forecast called 'PVLIFE toolbox' as shown in figure 4.22. This simplified interface is aimed to be applicable by any user, even without deep knowledge in data analysis. The toolbox has for main buttons; the browse button that allows to enter the data path, the run button

Table 4.11: Comparison of evaluated loss in lifetime energy yield in 35 years using the 3 degradation approximation scenarios. Relative uncertainty is calculated according to the measured yield loss

Module name	TEA1	TEA4	TEA6	TEA8	TEA10	TEB1	TEB2
Linear							
Failure time [years]	38.7	82.7	96.4	123.7	112.0	75.9	116.6
Non-linear with a constant factor							
Failure time [years]	95.0	92.5	82.8	52.8	77.1	73.9	67.1
Non-linear with a time dependent factpr							
Failure time [years]	29.8	33.1	38.0	33.4	44.1	38.8	39.9

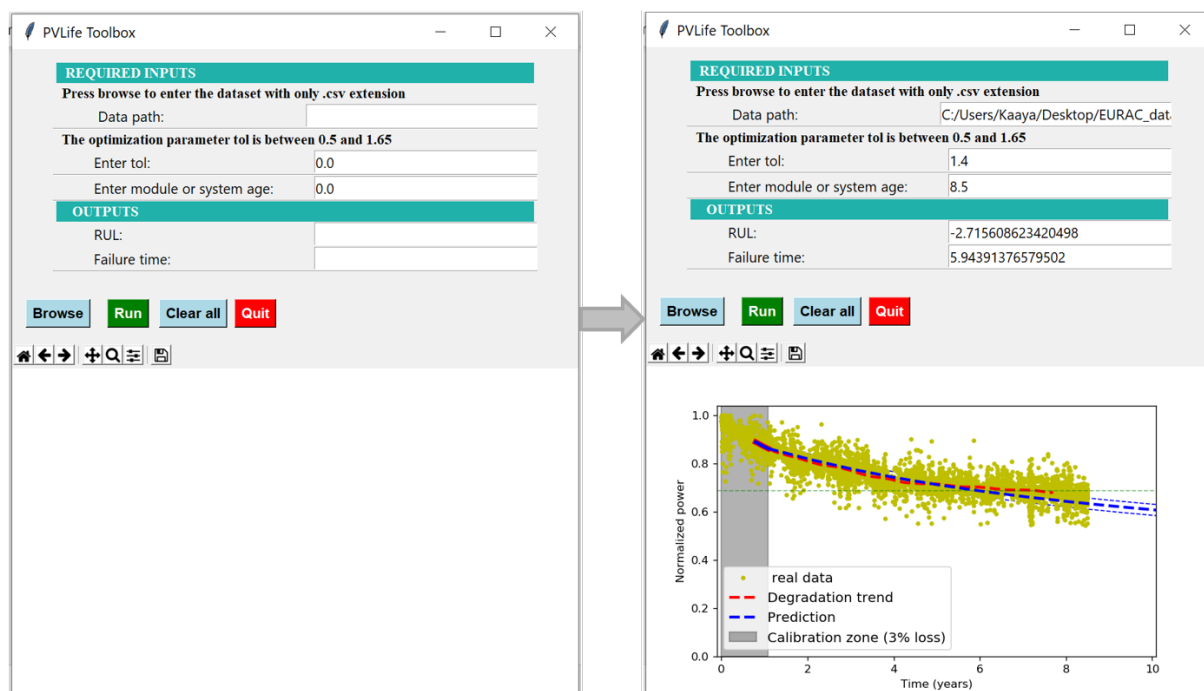


Figure 4.22: PVLife Toolbox, on the left is the layout before simulation and on the right is the layout after simulation

that starts the simulation, the clear button that deletes the current inputs-output to allow entrance of new inputs and the quit button that exits the toolbox. The toolbox has been created using the module Tkinter in python therefore it can run on the python interface.

## 4.3 Results for the hybrid model

### 4.3.1 Application of the hybrid model

After calibration and validation of both the physical and the data-driven methods, both approaches are combined into a hybrid model as described in section 3.3. The hybrid model is then applied to re-calculate the failure time of the three mono-crystalline modules. The results are compared with the one from the physical model as in table 4.12. Figure 4.23 shows the evolution of the degradation trends for the physical as well as the hybrid model. If we base our argument on the module installed on Zugspitze and on the current bill of materials, we can conclude that the predicted failure time with the hybrid method is more probable as compared to the failure time evaluated with only a physical model.

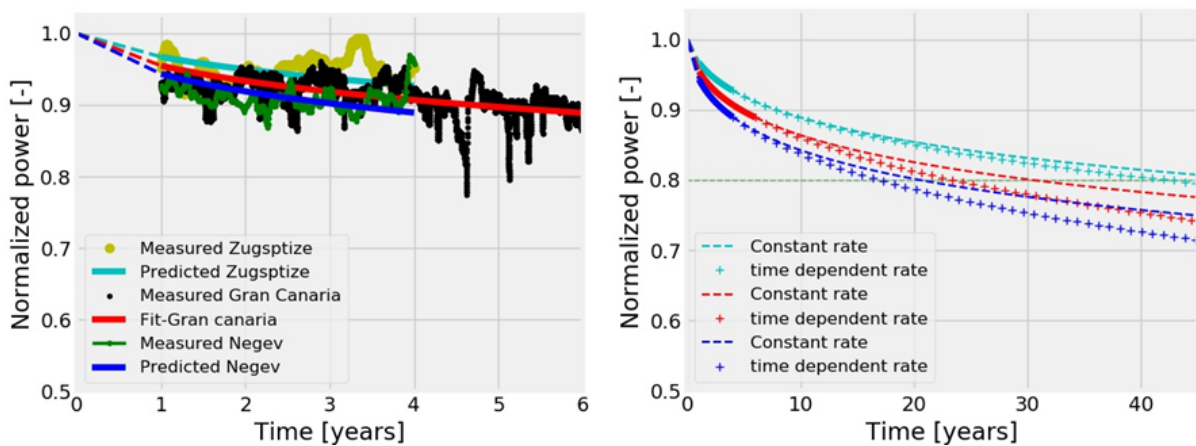


Figure 4.23: On the right: model and measured degradation trend until the time of exposure. On the left: bold lines, measured trend, dotted lines model forecast for with a physical model (using constant rate) and with a hybrid model (using time dependent rate). The colors represent the three climatic locations.

Table 4.12: Comparison of the physical model and the hybrid models

Module Location	Failure time [years]		Relative difference
	Hybrid model	Physical model	
Zugspitze	42.4	52.8	19.7 %
Gran Canaria	23.6	31.6	25.3 %
Negev	17.0	21.4	20.6 %

# Chapter 5

## Conclusion

When exposed in outdoor environment, PV modules as well as systems are affected by continuous cycles of temperature, humidity, irradiation, mechanical stress, and soiling. These environmental factors cause different degradation modes to take place within a PV module and reduce the performance of the system. Therefore, it is necessary to develop diagnostic techniques, lower the performance uncertainty, and predict the behavior of PV systems with higher accuracy. In this research, two main modelling approaches to predict the degradation rates, the failure time and the remaining useful lifetime of PV modules as well as systems have been proposed.

On the one hand, a physical model for quantifying the impact of combined climatic stresses on module maximum power output degradation is proposed. Degradation rate models are proposed and validated with indoor measurements for specific degradation precursors. A combined degradation rate model is developed. The model is calibrated and validated with real field data sets using three identical mono-crystalline modules installed in three climatic zones: maritime, arid and alpine. Severe degradation is predicted in the arid climate characterized by high temperatures. Using EAR5 reanalysis datasets to evaluate the model's input climatic variables, global risk maps of the specific degradation mechanisms and the combined rate model are created. The maps are evaluated based on the studied mono-crystalline modules, and they represent a correlation of different climatic zones to the different degradation mechanisms. For-example, according to the the Köppen-Geiger Photovoltaic (KGPV) climate classification, thermo-mechanical degradation is the harshest for the studied PV module in mostly all climate zones, presenting the highest impact in very high irradiation zones. Photo-degradation and hydrolysis-degradation show similar global spatial distribution, but the first one is higher since it comprises also UV irradiation as a degradation factor. Although, due to the high uncertainty in real degradation rate of PV systems (solar resource, methodology of calculation, quality of operational data, bill-of-materials of PV modules, etc.), the presented maps might not be representative of the actual absolute degradation rates, however, they can be used as a guide to identify possible risk areas in terms of climate stresses.

On the other hand, a data-driven approach is also proposed, the model is aimed to improve the long-term degradation forecasting accuracy using a shorter degradation history. In developing the model, multiple degradation factor models dependent on the degradation patterns as well as time are proposed to describe the different degradation patterns. The data-driven method is based on the monitored degradation and has been calibrated to provide reliable forecast using a short degradation history of only 3%. During the model devel-

opment, a focus is put on data treatment especially on extraction of the degradation trends independent of any reversible performance reducing effect or measurement uncertainties. Therefore, a computer aided approach is proposed to extract the degradation trends from the outdoor data. The model has been validated using different PV module and system datasets with observed long-term degradation. The performance of the proposed model is benchmarked against two statistical methods, namely ARIMA and Facebook prophet, using the time series of 11 experimental PV plants (with different PV technologies). The proposed model displays outstanding performance when forecasts are made after a shorter time compared to the two statistical models which displayed unrealistic forecasts. The model also displays consistent results with a 9.5% average relative uncertainty of the evaluated failure time when forecasts are made at different intervals, which is not the case for the two statistical models. Therefore, the obvious advantages of the proposed model over other data-driven models are that, it is applicable after a small performance degradation of only 3%, which usually can be observed after a short operation time and it is applicable on fewer data points. Another advantage of the proposed approach is that, it is based on a systematic approach for selecting the data and parameters of the models making it applicable for degradation evaluation on a wide range of data distributions. Hence, the models' performance can be well understood and a correlation of different parameters can be achieved, which is not the case for many empirical, data-driven techniques, especially those with a black-box character. Moreover, the model is also applicable to all PV technologies.

On addition, the proposed data-driven model has been applied to assess the effects of long-term degradation to lifetime yield prediction. The assessment has been carried out by assuming three degradation scenarios; linear and non-linear with a constant degradation rate as well as non-linear with a time dependent degradation rate (proposed). Using the latter made it possible to lower the long-term yield prediction relative uncertainty to 37.6% on average compared to 54.4% and 64.7% for a non-linear and linear with a constant degradation rate respectively. Lastly, a 'PVLife toolbox' based on the data-driven algorithms has been developed in this research with a simplified interface to be applicable by any one even without deep knowledge in data analysis.

Finally, the two approach are combined into a hybrid model to achieve a good forecasting accuracy by deploying data-driven algorithms and also to have a physical understanding of the evaluated rates through physical models. The hybrid model has been benchmarked with physical model to evaluate the lifetime of three aforementioned experimental monocrystalline modules and it proves to provide more consistent results. The proposed hybrid model will aid to have more reliable long-term degradation forecast as well as having a physical understanding of the dominating degradation mechanisms influencing the performance degradation. We believe such a model is useful to calculate more reliable leveled cost of energy and thus the economic viability of solar energy as well as to aid in PV materials development that can withstand the different environmental conditions.

# Bibliography

- Annigoni, E., A. Virtuani, M. Cavviccio, G. Friesen, D. Chianese, and C. Ballif (2019). 35 years of photovoltaics: Analysis of the TISO-10-kW solar plant, lessons learnt in safety and performance – Part 2. [38](#)
- Annigoni, E., A. Virtuani, F. Sculati-Meillaud, and C. Ballif (2017, June). Modeling Potential-Induced Degradation (PID) of Field-Exposed Crystalline Silicon Solar PV Modules: Focus on a Regeneration Term. In 2017 IEEE 44th Photovoltaic Specialist Conference (PVSC), pp. 2794–2798. [14](#), [46](#)
- Ascencio-Vasquez, J. (2020). Modelling and worldwide assessment of performance and aging of photovoltaic modules and systems. [77](#), [78](#)
- Ascencio-Vásquez, J., K. Brecl, and M. Topič (2019, October). Methodology of Köppen-Geiger-Photovoltaic climate classification and implications to worldwide mapping of PV system performance. *Solar Energy* 191, 672–685. [38](#), [47](#)
- Bala Subramaniyan, A., R. Pan, J. Kuitche, and G. TamizhMani (2018, September). Quantification of Environmental Effects on PV Module Degradation: A Physics-Based Data-Driven Modeling Method. *IEEE Journal of Photovoltaics* 8(5), 1289–1296. [1](#), [17](#), [19](#), [46](#), [47](#)
- Bosco, N., T. J. Silverman, and S. Kurtz (2016, July). Climate specific thermomechanical fatigue of flat plate photovoltaic module solder joints. *Microelectronics Reliability* 62, 124–129. [17](#)
- Braisaz, B., C. Duchayne, M. Van Iseghem, and K. Radouane (2014, September). PV Aging Model Applied to Several Meteorological Conditions. In 29th PVSEC Proceedings, Amsterdam, pp. 2303–2309. [8](#), [14](#), [15](#), [16](#), [17](#)
- Brownlee, J. (2017, February). Introduction to Time Series Forecasting With Python: How to Prepare Data and Develop Models to Predict the Future. *Machine Learning Mastery*. [37](#)
- Buck, A. L. (1981, December). New Equations for Computing Vapor Pressure and Enhancement Factor. *Journal of Applied Meteorology* 20(12), 1527–1532. [30](#)
- (C3S) (2017). Era5: Fifth generation of ecmwf atmospheric reanalyses of the global climate . copernicus climate change service climate data store. Technical report, <https://cds.climate.copernicus.eu/cdsapp>, Paris. [29](#)
- Cañete, C., J. Carretero, and M. Sidrach-de Cardona (2014, February). Energy performance of different photovoltaic module technologies under outdoor conditions. *Energy* 65, 295–302. [36](#)

- Chen Xiongzi, Yu Jinsong, Tang Diyin, and Wang Yingxun (2011, August). Remaining useful life prognostic estimation for aircraft subsystems or components: A review. In *IEEE 2011 10th International Conference on Electronic Measurement Instruments*, Volume 2, pp. 94–98. 6, 35
- Crommelynck, D. and A. Joukoff (1990, January). A simple algorithm for the estimation of the spectral radiation distribution on a horizontal surface, based on global radiation measurements. *Solar Energy* 45(3), 131–137. 30
- DKASC, A. S. (2019). DKASC, Alice Springs | DKA Solar Centre |, <http://dkasolarcentre.com.au/locations/alice-springs>, 2019-11-08 . 38
- Driemel, A., J. Augustine, K. Behrens, S. Colle, C. Cox, E. Cuevas-Agulló, F. M. Denn, T. Duprat, M. Fukuda, H. Grobe, M. Haeffelin, G. Hodges, N. Hyett, O. Ijima, A. Kallis, W. Knap, V. Kustov, C. N. Long, D. Longenecker, A. Lupi, M. Maturilli, M. Mimouni, L. Ntsangwane, H. Ogihara, X. Olano, M. Olefs, M. Omori, L. Passamani, E. B. Pereira, H. Schmithüsen, S. Schumacher, R. Sieger, J. Tamlyn, R. Vogt, L. Vuilleumier, X. Xia, A. Ohmura, and G. König-Langlo (2018, August). Baseline Surface Radiation Network (BSRN): structure and data description (1992–2017). *Earth System Science Data* 10(3), 1491–1501. 30
- Dunn, L., M. Gostein, and B. Stueve (2013, February). Literature Review of the Effects of UV Exposure on PV Modules. In *NREL PV Module Reliability Workshop*. 16
- Escobar, L. A. and W. Q. Meeker (2007, August). A Review of Accelerated Test Models. arXiv:0708.0369 [stat]. arXiv: 0708.0369. 11, 16, 24
- Faiman, D. (2008). Assessing the outdoor operating temperature of photovoltaic modules. *Progress in Photovoltaics: Research and Applications* 16(4), 307–315. 31
- Gaines, G. B., R. E. Thomas, G. T. Noel, T. S. Shilliday, V. E. Wood, and D. C. Carmichael (1978). Development of accelerated test design for service-life prediction of solar array at Mead, Nebraska. Quarterly report. 17, 18
- Gok, A., D. K. Ngendahimana, C. L. Fagerholm, R. H. French, J. Sun, and L. S. Bruckman (2017, December). Predictive models of poly(ethylene-terephthalate) film degradation under multi-factor accelerated weathering exposures. *PLOS ONE* 12(5), e0177614. 23
- Gu, X., Y. Lyu, L.-C. Yu, C.-C. Lin, and D. Stanley (2015, December). Effect of Intensity and Wavelength of Spectral UV Light on Discoloration of Laminated Glass/EVA/PPE PV Module. In *3rd Atlas-NIST Workshop on PV Materials Durability*. 16
- Hacke, P., S. Spataru, S. Johnston, K. Terwilliger, K. VanSant, M. Kempe, J. Wohlgemuth, S. Kurtz, A. Olsson, and M. Propst (2016, November). Elucidating PID Degradation Mechanisms and In Situ Dark I–V Monitoring for Modeling Degradation Rate in CdTe Thin-Film Modules. *IEEE Journal of Photovoltaics* 6(6), 1635–1640. 14
- Hacke, P., S. Spataru, K. Terwilliger, G. Perrin, S. Glick, S. Kurtz, and J. Wohlgemuth (2015, November). Accelerated Testing and Modeling of Potential-Induced Degradation as a Function of Temperature and Relative Humidity. *IEEE Journal of Photovoltaics* 5(6), 1549–1553. 14

- Halm, A., A. Schneider, V. D. Mihailetschi, L. J. Koduvelikulathu, L. M. Popescu, G. Galbiati, H. Chu, and R. Kopecek (2015, August). Potential-induced Degradation for Encapsulated n-type IBC Solar Cells with Front Floating Emitter. *Energy Procedia* 77, 356–363. [14](#)
- Hattendorf, J., A. Blauaermel, D. Koshncharov, M. C. Koekten, L. Wulff, W.-M. Gnehr, R. Löw, and J. A. Esquivel (2012, October). Potential Induced Degradation in Monocrystalline Silicon Based Modules: An Acceleration Model. In *27th European PVSEC Proceedings*, pp. 3405–3410. [14](#), [15](#)
- Huld, T. and A. M. G. Amillo (2015, June). Estimating PV Module Performance over Large Geographical Regions: The Role of Irradiance, Air Temperature, Wind Speed and Solar Spectrum. *Energies* 8(6), 5159–5181. [30](#), [31](#)
- Hyndman, R. J., G. Athanasopoulos, C. Bergmeir, G. Caceres, L. Chhay, M. O’Hara-Wild, F. Petropoulos, S. Razbash, E. Wang, and F. Yasmeeen (2018). *forecast: Forecasting Functions for Time Series and Linear Models version 8.10 from CRAN*. [57](#)
- Hyndman, R. J. and Y. Khandakar (2008, July). Automatic Time Series Forecasting: The forecast Package for R. *Journal of Statistical Software* 27(1), 1–22. [57](#)
- IEC61724-1 (2017). *Photovoltaic system performance, Part 1: Monitoring*. Geneva, CH: International Electrotechnical Commission;2017. [57](#)
- Jordan, D. and S. Kurtz (2010, June). Analytical improvements in PV degradation rate determination. In *2010 35th IEEE Photovoltaic Specialists Conference*, pp. 002688–002693. ISSN: 0160-8371, 0160-8371. [11](#)
- Jordan, D. C., C. Deline, M. G. Deceglie, A. Nag, G. M. Kimball, A. B. Shinn, J. J. John, A. A. Alnuaimi, A. B. A. Elnosh, W. Luo, A. Jain, M. U. Saleh, H. von Korff, Y. Hu, J.-N. Jaubert, and F. Mavromatakis (2020, January). Reducing Interanalyst Variability in Photovoltaic Degradation Rate Assessments. *IEEE Journal of Photovoltaics* 10(1), 206–212. [1](#)
- Jordan, D. C. and S. R. Kurtz (2013). Photovoltaic Degradation Rates—an Analytical Review. *Progress in Photovoltaics: Research and Applications* 21(1), 12–29. [5](#), [23](#)
- Jordan, D. C., T. J. Silverman, B. Sekulic, and S. R. Kurtz (2017). PV degradation curves: non-linearities and failure modes. *Progress in Photovoltaics: Research and Applications* 25(7), 583–591. [33](#)
- Jordan, D. C., T. J. Silverman, J. H. Wohlgemuth, S. R. Kurtz, and K. T. VanSant (2017a). Photovoltaic failure and degradation modes. *Progress in Photovoltaics: Research and Applications* 25, 318–326. [16](#)
- Jordan, D. C., T. J. Silverman, J. H. Wohlgemuth, S. R. Kurtz, and K. T. VanSant (2017b). Photovoltaic failure and degradation modes. *Progress in Photovoltaics: Research and Applications* 25(4), 318–326. [26](#), [42](#)
- Kempe, M. D. (2006, October). Modeling of rates of moisture ingress into photovoltaic modules. *Solar Energy Materials and Solar Cells* 90(16), 2720–2738. [23](#)

- Kempe, M. D. (2014, June). Evaluation of the uncertainty in accelerated stress testing. In 2014 IEEE 40th Photovoltaic Specialist Conference (PVSC), pp. 2170–2175. ISSN: 0160-8371. [17](#)
- Kempe, M. D., G. Jorgensen, K. Terwilliger, T. J. McMahon, C. E. Kennedy, and T. T. Borek (2007). Acetic Acid Production and Glass Transition Concerns with Ethylene-Vinyl Acetate Used in Photovoltaic Devices. [8](#)
- Kersten, F., F. Fertig, K. Petter, B. Klöter, E. Herzog, M. Strobel, J. Heitmann, and J. W. Müller (2017). System performance loss due to LeTID. [36](#), [37](#)
- Klünter, C., I. Rauschen, K. Reinartz, B. Müller, B. Farnung, and K. Kiefer (2019, October). Degradation in PV Power Plants: Theory and Practice. 36th European Photovoltaic Solar Energy Conference and Exhibition, 1331–1335. [37](#)
- Koehl, M., M. Heck, and S. Wiesmeier (2012, April). Modelling of conditions for accelerated lifetime testing of Humidity impact on PV-modules based on monitoring of climatic data. *Solar Energy Materials and Solar Cells* 99, 282–291. [24](#)
- Koehl, M., M. Heck, and S. Wiesmeier (2018). Categorization of weathering stresses for photovoltaic modules. *Energy Science & Engineering* 6(2), 93–111. [27](#), [49](#)
- Koehl, M., M. Heck, S. Wiesmeier, and J. Wirth (2011, July). Modeling of the nominal operating cell temperature based on outdoor weathering. *Solar Energy Materials and Solar Cells* 95(7), 1638–1646. [27](#)
- Koehl, M., S. Hoffmann, and S. Wiesmeier (2017). Evaluation of damp-heat testing of photovoltaic modules. *Progress in Photovoltaics: Research and Applications* 25(2), 175–183. [23](#)
- Koehl, M., D. Philipp, N. Lenck, and M. Zundel (2009, August). Development and application of a UV light source for PV-module testing. In *Proceedings of SPIE - The International Society for Optical Engineering* 7412. [16](#)
- Kratochvil, J. A., W. E. Boyson, and D. L. King (2004). Photovoltaic array performance model. [31](#)
- Köntges, M., S. Kurtz, C. E. Packard, U. Jahn, K. A. Berger, K. Kato, T. Friesen, H. Liu, M. Van Iseghem, J. Wohlgemuth, D. Miller, M. Kempe, P. Hacke, F. Reil, N. Bogdanski, W. Herrmann, C. Buerhop-Lutz, G. Razongles, and G. Friesen (2014). Review of Failures of Photovoltaic Modules. Report, IEA International Energy Agency. [8](#), [14](#), [26](#), [33](#), [35](#)
- Köntges, M., G. Oreski, U. Jahn, M. Herz, P. Hacke, and K.-A. Weiß (2017). Assessment of photovoltaic module failures in the field : International Energy Agency Photovoltaic Power Systems Programme : IEA PVPS Task 13, Subtask 3 : report IEA-PVPS T13-09:2017. Technical report, International Energy Agency, Paris. [1](#), [6](#)
- Laayouj, N., H. Jamouli, and M. E. Hail (2016, December). Intelligent Prognostic Framework for Degradation Assessment and Remaining Useful Life Estimation of Photovoltaic Module. *Journal of Engineering and Technological Sciences* 48(6), 772–795–795. [32](#)

- Lausch, D., V. Naumann, A. Graff, A. Hähnel, O. Breitenstein, C. Hagendorf, and J. Bagdahn (2014, January). Sodium Outdiffusion from Stacking Faults as Root Cause for the Recovery Process of Potential-induced Degradation (PID). *Energy Procedia* 55, 486–493. [14](#)
- Listou Ellefsen, A., E. Bjørlykhaug, V. Æsøy, S. Ushakov, and H. Zhang (2019, March). Remaining useful life predictions for turbofan engine degradation using semi-supervised deep architecture. *Reliability Engineering & System Safety* 183, 240–251. [32](#)
- Marín, M. L., A. Jiménez, J. López, and J. Vilaplana (1996, July). Thermal degradation of ethylene (vinyl acetate). *Journal of thermal analysis* 47(1), 247–258. [23](#)
- Masuda, A., N. Uchiyama, and Y. Hara (2015, March). Degradation by acetic acid for crystalline Si photovoltaic modules. *Japanese Journal of Applied Physics* 54(4S), 04DR04. [8](#)
- McKay, M. D., J. D. Morrison, and S. C. Upton (1999, March). Evaluating prediction uncertainty in simulation models. *Computer Physics Communications* 117(1), 44–51. [31](#)
- Meyers, B., M. Deceglie, C. Deline, and D. Jordan (2019, November). Signal Processing on PV Time-Series Data: Robust Degradation Analysis without Physical Models. arXiv:1907.09456 [eess]. arXiv: 1907.09456. [1](#), [2](#)
- Miller, D. C., E. Annigoni, A. Ballion, J. G. Bokria, L. S. Bruckman, D. M. Burns, Xinxin Chen, L. Elliott, Jiangtao Feng, R. H. French, S. Fowler, Xiaohong Gu, P. L. Hacke, C. C. Honeker, M. D. Kempe, H. Khonkar, M. Köhl, L.-E. Perret-Aebi, N. H. Phillips, K. P. Scott, F. Sculati-Meillaud, T. Shioda, S. Suga, S. Watanabe, and J. H. Wohlgemuth (2015, June). Degradation in PV encapsulation transmittance: An interlaboratory study towards a climate-specific test. In 2015 IEEE 42nd Photovoltaic Specialist Conference (PVSC), pp. 1–6. ISSN: null. [30](#)
- Moser, D., M. D. Buono, U. Jahn, M. Herz, M. Richter, and K. D. Brabandere (2017). Identification of technical risks in the photovoltaic value chain and quantification of the economic impact. *Progress in Photovoltaics: Research and Applications* 25(7), 592–604. [6](#), [14](#)
- Munoz, M. A., M. C. Alonso-García, N. Vela, and F. Chenlo (2011, September). Early degradation of silicon PV modules and guaranty conditions. *Solar Energy* 85(9), 2264–2274. [16](#)
- Naumann, V., T. Geppert, S. Großer, D. Wichmann, H.-J. Krokoszinski, M. Werner, and C. Hagendorf (2014, January). Potential-induced Degradation at Interdigitated Back Contact Solar Cells. *Energy Procedia* 55, 498–503. [14](#)
- Ndiaye, A., A. Charki, A. Kobi, C. M. F. Kébé, P. A. Ndiaye, and V. Sambou (2013, October). Degradations of silicon photovoltaic modules: A literature review. *Solar Energy* 96, 140–151. [8](#), [23](#)
- Ngo, T., Y. Heta, T. Doi, and A. Masuda (2016, April). Effects of UV on power degradation of photovoltaic modules in combined acceleration tests. *Japanese Journal of Applied Physics* 55(5), 052301. [24](#), [49](#)

- Omazic, A., G. Oreski, M. Halwachs, G. C. Eder, C. Hirschl, L. Neumaier, G. Pinter, and M. Erceg (2019, April). Relation between degradation of polymeric components in crystalline silicon PV module and climatic conditions: A literature review. *Solar Energy Materials and Solar Cells* 192, 123–133. [50](#)
- Pan, R., J. Kuitche, and G. Tamizhmani (2011, January). Degradation analysis of solar photovoltaic modules: Influence of environmental factor. In *2011 Proceedings - Annual Reliability and Maintainability Symposium*, pp. 1–5. ISSN: 0149-144X, 0149-144X. [8](#)
- Park, N., C. Han, and D. Kim (2013, December). Effect of moisture condensation on long-term reliability of crystalline silicon photovoltaic modules. *Microelectronics Reliability* 53(12), 1922–1926. [8](#), [23](#)
- Philipp, D., T. Geipel, P. Gebhardt, A. Schmid, T. Naeem, and E. Fokuhl (2019, October). LeTID - Comparison of Test Methods on Module Level. 36th European Photovoltaic Solar Energy Conference and Exhibition, 816–821. [36](#), [37](#)
- Phinikarides, A., N. Kindyni, G. Makrides, and G. E. Georghiou (2014, December). Review of photovoltaic degradation rate methodologies. *Renewable and Sustainable Energy Reviews* 40, 143–152. [2](#), [6](#)
- Reise, C., B. Müller, D. Moser, G. Belluardo, and P. Ingenhoven (2018, April). Task 13: Uncertainties in PV System Yield Predictions and Assessments. [60](#), [61](#)
- Rizzo, A., A. Cester, M. V. Madsen, F. C. Krebs, and S. A. Gevorgyan (2018). A Novel Algorithm for Lifetime Extrapolation, Prediction, and Estimation of Emerging PV Technologies. *Small Methods* 2(1), 1700285. [33](#)
- Schwingshackl, C., M. Petitta, J. E. Wagner, G. Belluardo, D. Moser, M. Castelli, M. Zebisch, and A. Tetzlaff (2013, January). Wind Effect on PV Module Temperature: Analysis of Different Techniques for an Accurate Estimation. *Energy Procedia* 40, 77–86. [31](#)
- Segado, P. M., J. Carretero, and M. Sidrach-de-Cardona (2015). Models to predict the operating temperature of different photovoltaic modules in outdoor conditions. *Progress in Photovoltaics: Research and Applications* 23(10), 1267–1282. [31](#)
- Sharma, V. and S. S. Chandel (2013, November). Performance and degradation analysis for long term reliability of solar photovoltaic systems: A review. *Renewable and Sustainable Energy Reviews* 27, 753–767. [23](#)
- Sheng, Z., Q. Hu, J. Liu, and D. Yu (2019, January). Residual life prediction for complex systems with multi-phase degradation by ARMA-filtered hidden Markov model. *Quality Technology & Quantitative Management* 16(1), 19–35. [32](#)
- Swanson, R., M. Cudzinovic, D. DeCeuster, V. Desai, J. Jürgens, N. Kaminar, W. Muligan, L. Rodrigues-Barbarosa, D. Rose, D. Smith, A. Terao, and K. Wilson (2005, January). The surface polarization effect in high-efficiency silicon solar cells. pp. 410. [14](#)

- Taubitz, C., M. Kröber, M. Schütze, and M. B. Köntopp (2014, November). Potential Induced Degradation: Model Calculations and Correlation between Laboratory Tests and Outdoor Occurrence. In 29th European PVSEC Proceedings, pp. 2490–2494. [14](#), [15](#)
- Taylor, S. J. and B. Letham (2018, January). Forecasting at Scale. *The American Statistician* 72(1), 37–45. [2](#), [33](#), [56](#)
- Urraca, R., T. Huld, F. J. Martinez-de Pison, and A. Sanz-Garcia (2018, August). Sources of uncertainty in annual global horizontal irradiance data. *Solar Energy* 170, 873–884. [28](#)
- Virtuani, A., M. Caccivio, E. Annigoni, G. Friesen, D. Chianese, C. Ballif, and T. Sample (2019). 35 years of photovoltaics: Analysis of the TISO-10-kW solar plant, lessons learnt in safety and performance—Part 1. *Progress in Photovoltaics: Research and Applications* 27(4), 328–339. [38](#)
- Virtuani, A., D. Strepparava, and G. Friesen (2015, October). A simple approach to model the performance of photovoltaic solar modules in operation. *Solar Energy* 120, 439–449. [37](#)
- Whitfield, K., A. Salomon, S. Yang, and I. Suez (2012, June). Damp heat versus field reliability for crystalline silicon. In 2012 38th IEEE Photovoltaic Specialists Conference, pp. 001864–001870. ISSN: 0160-8371, 0160-8371. [8](#)
- Wohlgemuth, J. H. (2012). Standards for pv modules and components – recent developments and challenges. Presented at the 27th European Photovoltaic Solar Energy Conference and Exhibition, Frankfurt, Germany. [1](#), [23](#)
- Wu, D., J. Zhu, T. R. Betts, and R. Gottschalg (2014). Degradation of interfacial adhesion strength within photovoltaic mini-modules during damp-heat exposure. *Progress in Photovoltaics: Research and Applications* 22(7), 796–809. [23](#)
- Zhang, S., Y. Zhang, and J. Zhu (2018, April). Residual life prediction based on dynamic weighted Markov model and particle filtering. *Journal of Intelligent Manufacturing* 29(4), 753–761. [32](#)
- Zhu, J., M. Koehl, S. Hoffmann, K. A. Berger, S. Zamini, I. Bennett, E. Gerritsen, P. Malbranche, P. Pugliatti, A. D. Stefano, F. Aleo, D. Bertani, F. Paletta, F. Roca, G. Graditi, M. Pellegrino, O. Zubillaga, F. J. C. Iranzo, A. Pozza, T. Sample, and R. Gottschalg (2016). Changes of solar cell parameters during damp-heat exposure. *Progress in Photovoltaics: Research and Applications* 24(10), 1346–1358. [23](#)
- Zorrilla-Casanova, J., M. Piliouguine, J. Carretero, P. Bernaola-Galván, P. Carpena, L. Mora-López, and M. Sidrach-de-Cardona (2013). Losses produced by soiling in the incoming radiation to photovoltaic modules. *Progress in Photovoltaics: Research and Applications* 21(4), 790–796. [36](#)

## **Paper 1.**

Kaaya, M. Koehl, A.P. Mehilli, S. de Cardona Mariano, & K.A. Weiss, "Modeling Outdoor Service Lifetime Prediction of PV Modules: Effects of Combined Climatic Stressors on PV Module Power Degradation". IEEE Journal of Photovoltaics, vol. 9, Issue 4, pp. 1105–1112, July. 2019.

**DOI:** [10.1109/JPHOTOV.2019.2916197](https://doi.org/10.1109/JPHOTOV.2019.2916197)

### **Abstract:**

Photovoltaic modules are exposed to a variety of climatic loads during outdoor operation. Over time, these loads trigger a number of degradation modes within the modules leading to performance loss. This paper quantifies the impact of combined climatic loads on the module's maximum power output using a mathematical approach. Three degradation precursor reactions, namely, hydrolysis, photodegradation, and thermomechanical degradation, are assumed to be necessary for service lifetime prediction. For each reaction, an empirical kinetics model is proposed and validated with indoor test measurements. A generalized model to quantify the effects of combined climatic loads is proposed. The generalized model is calibrated and validated using outdoor test measurements. The model is then applied to predict the annual degradation rates and a 20% performance loss of three identical monocrystalline modules installed in three benchmarking climates: maritime (Gran Canaria, Spain), arid (Negev, Israel), and alpine (Zugspitze, Germany) using real monitored meteorological data. A degradation of 0.74%/year corresponding to 21.4 years operation time was predicted as the highest for an arid environment, compared with 0.50%/year and 0.3%/year degradation for maritime and alpine environments, respectively. The proposed models will find applications in outdoor predictions as well as in the combined stress accelerated tests to develop test designs.

## **Paper 2.**

S. Lindig, I. Kaaya, K.A. Weiss, D. Moser, and M. Topic, "Review of statistical and analytical degradation models for photovoltaic modules and systems as well as related improvements," IEEE Journal of Photovoltaics, vol. 8, Issue. 6, pp. 1773–1786, Nov. 2018.

**DOI:** [10.1109/JPHOTOV.2018.2870532](https://doi.org/10.1109/JPHOTOV.2018.2870532)

### **Abstract:**

In this work, we investigate practical approaches of available degradation models and their usage in photovoltaic (PV) modules and systems. On the one hand, degradation prediction of models is described for the calculation of degradation at system level where the degradation mode is unknown and hence the physics cannot be included by the use of analytical models. Several statistical models are thus described and applied for the calculation of the performance loss using as case study two PV systems, installed in Bolzano/Italy. Namely, simple linear regression (SLR), classical seasonal decomposition, seasonal- and trend-decomposition using Loess (STL), Holt-Winters exponential smoothing and autoregressive integrated moving average (ARIMA) are discussed. The performance loss results show that SLR produces results with highest uncertainties. In comparison, STL and ARIMA perform with the

highest accuracy, whereby STL is favored because of its easier implementation. On the other hand, if monitoring data at PV module level are available in controlled conditions, analytical models can be applied. Several analytical models depending on different degradations modes are thus discussed. A comparison study is carried out for models proposed for corrosion. Although the results of the models in question agree in explanation of experimental observations, a big difference in degradation prediction was observed. Finally, a model proposed for potential induced degradation was applied to simulate the degradation of PV systems maximum power in three climatic zones: alpine (Zugspitze, Germany), maritime (Gran Canaria, Spain), and arid (Negev, Israel). As expected, a more severe degradation is predicted for arid climates.

### **Paper 3.**

J. A-Vásquez, I. Kaaya, K. Brecla, K-A. Weiss and M.Topic, "Global climate data processing and mapping of degradation mechanisms and degradation rates of PV modules". *Energies MDPI*, vol. 12 (24) 4749 Dec 2019.

DOI: <https://doi.org/10.3390/en12244749>

#### **Abstract:**

Photovoltaic (PV) systems are the cheapest source of electricity in sunny locations and nearly all European countries. However, the fast deployment of PV systems around the world is bringing uncertainty to the PV community in terms of the reliability and long-term performance of PV modules under different climatic stresses, such as irradiation, temperature changes, and humidity. Methodologies and models to estimate the annual degradation rates of PV modules have been studied in the past, yet, an evaluation of the issue at global scale has not been addressed so far. Hereby, we process the ERA5 climate re-analysis dataset to extract and model the climatic stresses necessary for the calculation of degradation rates. These stresses are then applied to evaluate three degradation mechanisms (hydrolysis-degradation, thermomechanical-degradation, and photo- degradation) and the total degradation rate of PV modules due to the combination of temperature, humidity, and ultraviolet irradiation. Further on, spatial distribution of the degradation rates worldwide is computed and discussed proving direct correlation with the Köppen-Geiger-Photovoltaic climate zones, showing that the typical value considered for the degradation rate on PV design and manufacturer warranties (i.e., 0.5%/a) can vary  $\pm 0.3\%/a$  in the temperate zones of Europe and rise up to 1.5%/a globally. The mapping of degradation mechanisms and total degradation rates is provided for a monocrystalline silicon PV module. Additionally, we analyze the temporal evolution of degradation rates, where a global degradation rate is introduced and its dependence on global ambient temperature demonstrated. Finally, the categorization of degradation rates is made for Europe and worldwide to facilitate the understanding of the climatic stresses.



# Appendix

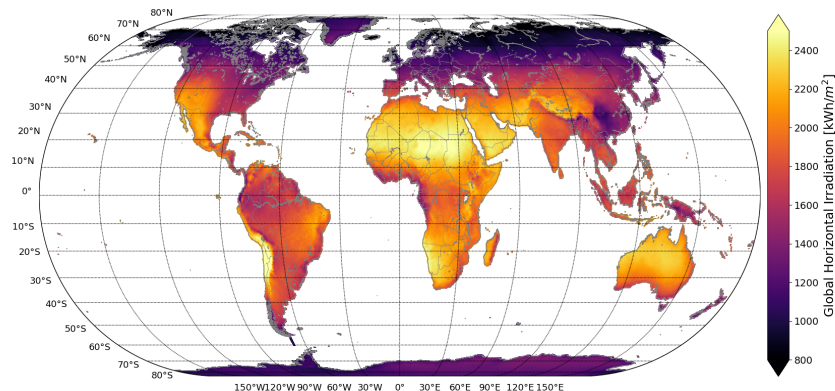


Figure 1: Global horizontal irradiation used to model UV. Since the ambient temperature is proportional to the irradiance levels, the global distribution of ambient temperatures takes the same trend. Figure reprinted from [Ascencio-Vasquez \(2020\)](#). The map is according to EAR5 dataset and of the year 2018

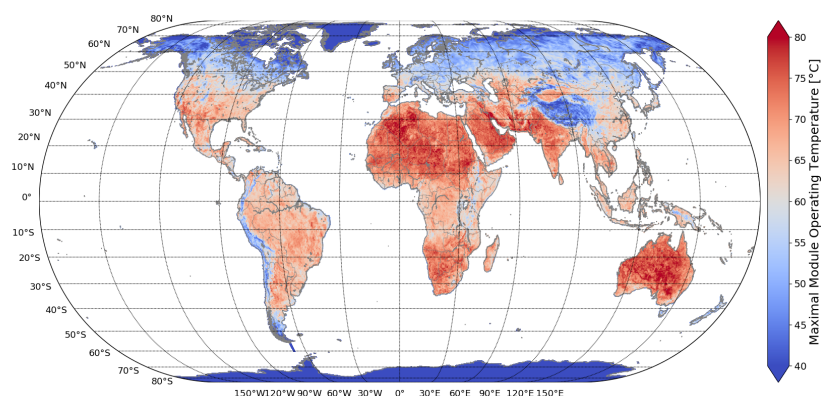


Figure 2: Maximum module temperature distribution worldwide. The module temperature is calculate from the ambient temperature using the Faiman model. Figure reprinted from [Ascencio-Vasquez \(2020\)](#). The map is according to EAR5 dataset and of the year 2018

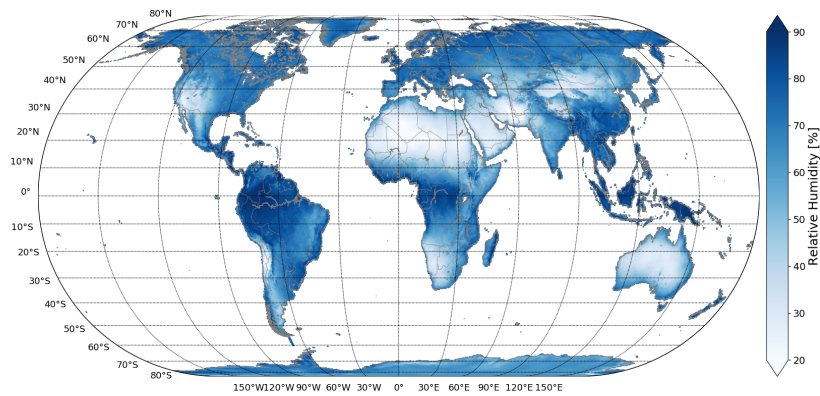


Figure 3: Distribution of relative humidity worldwide. The relative humidity is calculated from the ambient and the dew point temperatures using the Buck's formula. Figure reprinted from [Ascencio-Vasquez \(2020\)](#). The map is according to EAR5 dataset and of the year 2018